Analysis of solitary waves in inhomogeneous systems

Rahmi Rusin

A thesis presented for degree of
Doctor of Philosophy

Department of Mathematical Sciences
University of Essex

July 2020

To the memory of my late father (may Allah bless him with *jannah*) who always encouraged me to keep pursuing higher education

Dedicated to:
My dearest **Herman Bakir** and my mother **Khairumi**

Declaration

The work in this thesis is based on research carried out at the Applied Mathematics Group, Department of Mathematical Sciences, University of Essex, United Kingdom. No part of this thesis has been submitted elsewhere for any other degree or qualification, and it is all my own work, unless referenced, to the contrary, in the text.

Rahmi Rusin
July 2020

Acknowledgements

In the name of Allah, the Most Gracious and the Most Merciful, first and foremost, praise is to the Almighty Allah, who has granted countless blessings so that I have finally been able to accomplish this thesis.

I would like to express my sincere gratitude and appreciation to all those who have contributed to my thesis completion. It is a very challenging journey, and will not be possible without everyone's support. It would be impossible to list all names, but they deserve my sincere and special thanks. Firstly, I would like to express my sincere gratitude to my supervisor Prof. Hadi Susanto for introducing me to this exciting field of mathematical science and for his dedicated help, advice, inspiration, encouragement, and continuous support throughout my Ph.D. studies.

Next, I would like to thank the chair of my supervisory board, Dr. Vanni Noferini, for his support and useful comments. My sincere thanks also go to Dr. Robert Marangell, who provided me an opportunity to work with him and gave access to research facilities during my study visit at the University of Sydney, Australia. I also acknowledge my internal examiner, Dr. Chris Antonopoulos, and my external examiner, Prof. Jonathan Wattis, for insightful comments, helpful questions, and fruitful discussions during my viva examination, which contributed a lot to the thesis corrections.

A special deepest gratitude goes to my better half, Herman Bakir, for his invaluable support and understanding of my goals and aspirations. His unique way of love and support has always been my strength. His patience and sacrifice will remain my inspiration throughout my life. Thank you for believing me that I can do more than I think.

I would like to express my heartfelt gratitude to my late father, M. Rusaini Rusin (may Allah bless him with *jannah*), my loving mother, Khairumi, for her endless prayers and unlimited support. Without them, I would not have been able to complete much of what I have done and become who I am. I would also like to express my sincere gratitude to my parents in law for their kindness; my brothers and their families. Rusin's family will always be in my heart; my brothers and sisters in law and their families. Thank you for all their supports and prayers throughout my studies and my life in general. I also thank my friends and office staff in the Department for their support and cooperation during my studies.

Finally, I gratefully acknowledge financial support from Lembaga Pengelolaan Dana Pendidikan (Indonesia Endowment Fund for Education), Republic of Indonesia. Grant Ref. No: S-5405/LPDP.3/2015.

Abstract

In this thesis, we aim to investigate solitary waves of three nonlinear Schrödinger (NLS)-type models, namely, the NLS equation with an asymmetric double Dirac delta potential, the NLS equation with a Dirac delta potential on star graphs, and the discrete nonlinear Schrödinger (DNLS) equation.

For the first model, we obtain analytic solutions and show the difference between ground states that arise due to symmetric and asymmetric potentials. We find bifurcating asymmetric ground states at a threshold value of solution norm. In contrast to the symmetric case, pitchfork bifurcation no longer exists, and we find a saddle node one instead.

For the second problem, we use coupled mode reduction method to yield conditions for symmetry breaking bifurcations. We notably obtain that the bifurcation is degenerate. There are two distinct asymmetric bifurcating solutions with the same norm. We provide an estimate of the bifurcation point. We also study non-positive definite states bifurcating from the linear solutions. Typical dynamics of unstable solutions are also presented.

Finally, we study the fundamental lattice solitons of the DNLS equation and their stability via a variational method. Using a Gaussian ansatz and comparing the results with numerical computations, we report a novel observation of false instabilities. Comparing with established results and using the Vakhitov-Kolokolov criterion, we deduce that the instabilities are due to the ansatz. In the context of using the same type of ansatzs, we provide a remedy by employing multiple Gaussian functions. The results show that the higher the number of Gaussian functions used, the better the solution approximation.

Publications

1. Chapter 5 in this thesis has been published in:
   R. Rusin, R. Kusdiantara, and H. Susanto. Variational approximations using Gaussian ansatz, false instability, and its remedy in nonlinear Schrödinger lattices. *Journal of Physics A: Mathematical and Theoretical* 51 (47), 475202 (2018)

2. R. Rusin, R. Kusdiantara, and H. Susanto. Variational approximations of soliton dynamics in the Ablowitz-Musslimani nonlinear Schrödinger equation. *Physics Letters A* 383 (17), 2039-2045 (2019)

3. R. Rusin and H. Susanto. Rayleigh-Ritz approximation for the stability of localised waves. *AIP Conference Proceedings* 2192, 060016 (2019)

4. Chapter 3 in this thesis has been published in:
   Rusin, R., Marangell, R. & Susanto, H. Symmetry breaking bifurcations in the NLS equation with an asymmetric delta potential. Nonlinear Dyn 100, 3815–3824 (2020).

5. Chapter 4 in this thesis is under review in:
   R. Rusin and H. Susanto. Dynamics of nonlinear Schrodinger equations with Delta potential on star graphs. Submitted to *Journal of Physics A*, 2019

Contents

List of Figures

Chapter 1

Introduction

Research in this thesis was initiated because of the author's interest in nonlinear waves. Waves are ubiquitous around us. There are various examples of wave motion that we encounter regardless of whether we recognize it or not. Most wave phenomena cannot be explained by linear waves theories. One prominent example is a tsunami, a giant wave caused by earthquakes or volcanic eruptions under the sea [1]. Nonlinear waves as part of nonlinear science not only help us understand the behaviour of the tsunami but also the complexity behind it. Another physical phenomenon that can be clearly explained by nonlinear wave theory is in quantum physics such as light pulse propagation in optical fibers or in Bose-Einstein condensate (BEC) [2].

The nature, properties and behaviour of waves can be studied from several points of view, from simple to a more complex one, from physical or mathematical point of view. Although the study of waves has started since centuries ago, according to

Whitham [3], there is no exact definition that precisely describe the wave phenomena. Although there are several definitions of waves with some restrictions, in general a wave can be described as a disturbance that travels from one location to another with a recognizable velocity of propagation. A common feature of waves in all applications is that they can be described by linear or nonlinear partial differential equations (PDEs). They are called linear and nonlinear waves based on linear and nonlinear equations, respectively.

In a certain PDE describing nonlinear waves, there are several types of solutions. To mention some, there are periodic waves, solitary waves, fronts/kinks and modulated waves as seen in Figure 1.1. A solitary wave is an example of a nonlinear wave which is localised and has a finite energy. It arises in some classes of nonlinear PDEs and has been observed in nature, experiments, and numerical simulations [2, 4].

The study of nonlinear waves started when a solitary wave was first discovered accidentally by John Scott Russell in 1834 when he was surveying the Union Canal near Edinburgh, Scotland. He saw a rounded smooth heap of water which constantly propagated caused by a sudden stop of a fast-moving boat. The smooth and bell-shaped crest was rolling on without change of its shape and speed [5]. Later, he made an experiment in a wave tank and found out that it was very easy to generate such waves. A pulse will turn into a solitary wave or two followed after plunging a block of wood into the water. Unfortunately, for many years Russell's solitary wave, that he called a great wave of translation, was surprisingly neglected until in 1895 Korteweg and de Vries showed that Russell's finding could be described accurately by the equation that is now known as the KdV equation [2, 6]. The belittlement of Russell's idea was because scientists at that time could not accept that a wave with finite amplitude can propagate without change of form as it contradicts the nonlinear shallow water wave theory [7, 8]. In 1965, Zabusky and Kruskal numerically discovered the solitary wave solutions of KdV equation with spatially periodic boundary condition. They found that the initial condition of sine wave evolves into several solitary waves, that later are named as solitons, which propagate with different speeds. They maintain their shapes and velocities except a small phase shift after they collide and pass through each other [4].

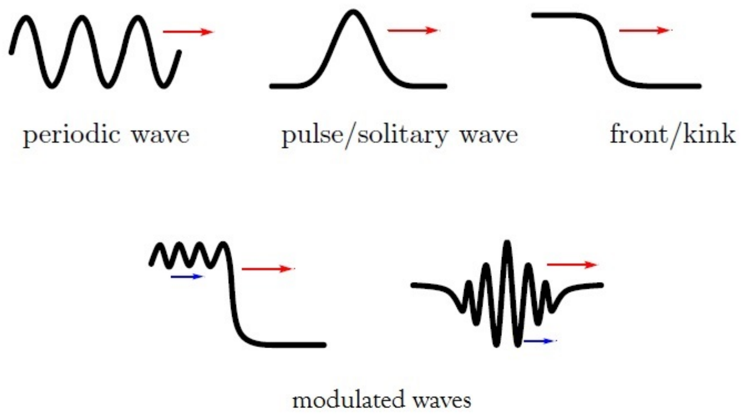

Figure 1.1. Several types of nonlinear waves (taken from [9]).

For mathematicians, the term soliton refers to a specific solitary wave solution of an exact 'ideal' system, i.e. it does not contain nonsolitonic or perturbational effects such as frictional loss mechanisms, external driving forces, and defects. In this thesis, we will use the term solitary wave or soliton interchangeably to refer to a localised finite energy solution of a nonlinear evolution equation. Qualitatively, it results from a balance of dispersion and a nonlinearity after evolution of initial depression [8, 10]. A solitary wave is also defined as a wave propagating at a steady rate without change in shape and speed [11]. Some references use the term nonlinear bound states to refer to solitary wave solutions [2, 7, 12].

Besides KdV, another fundamental equation in the theory of nonlinear waves that admits such solution is the nonlinear Schrödinger (NLS) equation. In this thesis, we study solitary waves in inhomogeneous NLS-type systems namely, one-dimensional NLS equation with asymmetric double Dirac delta potential, one-dimensional NLS equation on a three-edge star graph with a Dirac delta potential in each edge, and a discrete version of one-dimensional NLS equation. These three inhomogeneous systems admit solitary wave solutions. We call the solitary waves for the latter system as discrete solitons.

The NLS equation, as one of the well-known complex nonlinear evolution systems, is a dispersive Hamiltonian system. It appears in various fields of nonlinear science. In nonlinear optics, one notable application is to describe the propagation of electromagnetic pulses in media which are assumed to be Kerr nonlinear [13, 14]. Another important application is to describe the dynamics of Bose-Einstein condensates [14, 15]. As its continuum counterpart, the discrete nonlinear Schrödinger (DNLS) equation is also one of the well-known mathematical models that describes many important (discrete) physical systems [16, 17]. The DNLS equation arises in a wide range of applications in physics, both as a discretization of the continuum counterpart or in its own right as a lattice system [18–20]. Two notable applications are as models of coupled optical waveguides [21] and trapped Bose-Einstein condensates (BECs) in a strong optical lattice [15].

The NLS equation has been shown to be integrable under the inverse scattering transform (IST) since it admits a linear (Lax) pair representation and possesses an infinite number of conservation laws [22–25]. Although the IST method yields an exact solution, it is not explicit and rather complicated to analyse, except for special cases of solutions [19]. On the other hand, the NLS equation with external potentials and the DNLS equation are not integrable [17]. However, it has been observed that solitary wave (or soliton) solutions are present in both systems.

To have a better understanding of the behaviour of a system and its solutions especially from a physical point of view, several different approaches have been used numerically and analytically. The existence of a solitary wave solution is studied by solving the equation for time independent solution, it can be as a stationary (equilibrium) solution or travelling wave. After the solution has been obtained, we can study the dynamics of the system in their long-time behaviour, i.e., as time increases.

Naturally, once solutions are identified, the immediate next question concerns their stability. It is related to a question of what happens with the solutions in long period of time if perturbation occurs. Intuitively, we say that the equilibrium solution is stable if all solutions start close to it will stay close as time goes on. In the case of linear dynamical systems, the stability of an equilibrium solution can be determined by the eigenvalues of the operator. Since the notion of stability is localised near the equilibrium solution, to understand the stability of the nonlinear wave, we can use linearisation around the equilibrium solution and find the (generalisation of the) eigenvalues of the operator. We call these eigenvalues the spectrum of the operator.

Another concept of stability is related to the system. If a small change, which is usually identified by the small change of a parameter value, implies the system changes qualitatively, such as the change in the number of equilibria or the stability of the solution, we say that a bifurcation occurs, and the point where it occurs is called a bifurcation point.

Here, we present three main projects on solitary waves in inhomogeneous systems. The first two projects which appear in Chapter 3 and 4 are on the NLS equation with external potential. The NLS equation with external potential, also known as Gross-Pitaevskii equations, has symmetric ground states. The presence of inhomogeneities of various types affect and usually break the symmetry [26]. A ground state is a positive bound state which has minimum energy [12]. This particularly interesting phenomenon that breaks the symmetry of the solution is called spontaneous symmetry breaking. This phenomenon arises due to the effect of combination between the potential and focusing nonlinearity.

The ground state of physical systems generally follows the symmetry of the external potential that acts on the physical field or wave function. In the presence of nonlinearity, such a rule may be preserved only in the weakly nonlinear regime. With the increase of the nonlinearity strength, spontaneous symmetry breaking can occur, in which case symmetric wave functions no longer represent the ground state.

The solutions are in fact unstable against non-symmetric perturbations through a pitchfork bifurcation.

The concept of spontaneous symmetry breaking in the NLS equation was probably first discussed by Davies [27] in a model that describes interactions of quantum particles through a three-dimensional isotropic potential. The breaking was found in terms of bifurcation of broken rotational symmetry of the ground state. A simpler model in the form of coupled ordinary differential equations (ODEs) exhibiting a symmetry breaking bifurcation was given in [28]. Now the notion of symmetry breaking has been studied in a variety of contexts, such as in particle physics [29], Bose-Einstein condensates [30, 31], metamaterials [32], spatiotemporal complexity in lasers [33], photorefractive media [34], biological slime moulds [35], coupled semiconductor lasers [36] and in nanolasers [37]. All these systems incorporated a double-well potential and the spontaneous breaking of inversion symmetry manifests in a transition to two states that are localised in one of the potential wells and mirror images of each other. Theoretical works on spontaneous symmetry breaking bifurcations include linearly coupled nonlinear Schrödinger equations that admit asymmetric two-component soliton modes [38–42], unstable linearly coupled dark solitons that lead to bosonic Josephson vortices [43–45] and symmetry breaking of linearly coupled vortices [46, 47]. Later works on symmetry breaking in the NLS equation with double well potentials include among others [12, 48–51]. The reader is referred to the book [52] for a recent collection of work on the subject.

In Chapter 3, we investigate the existence and stability of ground states by phase plane analysis approach. We obtain analytical solutions for the NLS equation with asymmetric double Dirac delta potential on the infinite domain. The results show a spontaneous symmetry breaking, and there is a notable difference between ground states and bifurcating solutions that arise due to symmetric and asymmetric double Dirac delta potentials. We start the analysis by considering the symmetric potential case where we find at a threshold value of solution norm asymmetric ground states bifurcate from the symmetric one. The bifurcation in this case is pitchfork. When the wells are asymmetric, we show that the standard pitchfork bifurcation becomes broken, i.e. unfolded, and instead a saddle node type is obtained. Using a geometrical approach, we also establish the instability of the corresponding solutions along each branch in the bifurcation diagram

In Chapter 4, we study the symmetry breaking of the NLS equation with a Dirac delta potential. The interesting part is that our spatial setting is not the standard real space but a star graph. By reducing the system to a finite dimensional system of coupled ODEs, we obtain conditions for a symmetry breaking bifurcation in a symmetric family of states as the propagation constant, that is related to the solution norm, is varied. We obtain that the symmetry breaking bifurcation is degenerate, where subcritical and supercritical-like bifurcations occur from the same point. There are two distinct asymmetric bifurcating solutions with the same norm. We provide an estimate of the bifurcation point. We also study non-positive definite states bifurcating from the linear solutions and present the typical dynamics of a solution when it is unstable.

The equations we address in Chapter 3 and 4 include Dirac delta potentials. This type of narrow potentials interacting with wide solitons gives a point defect to the solutions. In nonlinear optics, the equation describes a soliton propagation in a medium with a point defect or a wide soliton interacting with a much narrower one in bimodal fiber. In BECs, when an impurity of a length-scale much smaller than the healing length exists, the dynamics of a condensate can also be described by such an equation [53–55].

The method used to study solitary waves in Chapter 3 is phase plane analysis. We convert the NLS equation with asymmetric double Dirac delta potential into ODEs to obtain positive standing waves. By simple geometric analysis of the phase plane orbit, we obtain the condition of the instability of the positive standing waves. In Chapter 4, our approach is what we call a coupled mode reduction method. This variational method reduces the problem of infinite dimensional PDEs into finite dimensional ODEs. It utilizes the solution of linearised system to obtain the nonlinear bound states.

In the third project which appears in Chapter 5, we study discrete solitons in one-dimensional DNLS equation and their stability in time, which is analysed also using variational method, called variational approximation (VA) method. The VA is a semi-analytical method that can be used to approximate discrete solitons by choosing an appropriate trial function, usually called ansatz. While the standard

VA for studying discrete soliton in the DNLS equation is an exponential function, here we consider a Gaussian ansatz and later we observe a false instability for the on-site soliton in an interval of coupling constant. Comparing the results with the numerical computation and using Vakhitov-Kolokolov criterion, we conclude that the instability is due to the shape of the ansatz. We obtain the remedy for the false instability by increasing the number of Gaussian functions used. We show that using multiple Gaussian ansatz we have a better approximation of the solutions.

Chapter 2

Theoretical background and literature review

In this chapter, we provide some basic concepts and results from existing studies as the necessary background for the following chapters. This includes some notions in functional analysis, the NLS equation, the NLS with external potential, the DNLS equation, VA method, coupled mode reduction method, spectrum, and stability.

2.1 Functional analysis

In this section, we present theoretical background in functional analysis. The source of theoretical background given in this section is taken from the book by Kapitula and Promislow [56]. The realisation of the abstract idea of some functional analysis notions can be seen in the study of nonlinear waves which will be discussed in the subsequent sections. In many applications including the NLS equation, it is much easier if the working space used is so called Sobolev space as defined in the following definitions.

2.1.1 Sobolev spaces

Definition 2.1.1 (**Banach Space**). *For functions $u : \mathbb{R} \mapsto \mathbb{C}$ define the L^p-norm for any $p \geq 1$,*

$$||u||_p := \left(\int_{\mathbb{R}} |u(x)|^p dx \right)^{1/p}.$$

The L^∞-norm is realized as the $p \to \infty$ limit of the L^p-norm, and is given for smooth functions by $||u||_\infty := \sup_{x\in\mathbb{R}} |u(x)|$. For any $p \geq 1$ the Banach space $L^p(\mathbb{R})$ is given by

$$L^P(\mathbb{R}) := \{u : ||u||_p < \infty\}.$$

Definition 2.1.2 (**Sobolev space**). *A Sobolev space $W^{k,p}(\mathbb{R})$ is defined by*

$$W^{k,p}(\mathbb{R}) := \{u \in L^p(\mathbb{R}) : ||u||_{W^{k,p}} < \infty\}$$

where $W^{k,p}$-norm is defined for differential functions by

$$||u||_{W^{k,p}} := \left(\sum_{j=0}^{k} ||\partial_x^j u||_p^p \right)^{1/p}.$$

The Hilbert spaces, H^k are defined as $H^k := W^{k,2}$. Note that $H^0(\mathbb{R}) = L^2(\mathbb{R})$.

Definition 2.1.3 (**Dense**). *A subset X of a topological space A is called dense (in A) if every point $a \in A$ either belong to X or is a limit point of X i.e., for each $a \in A$ there is a sequence $\{a_j\} \subset X$ such that $||a_j - a|| \to 0$ as $j \to \infty$.*

Definition 2.1.4 (Closed and bounded operator). *Let X, Y be two Banach spaces with norms $\|\cdot\|_X, \|\cdot\|_Y$ respectively, and assume that $Y \subset X$ is dense. Consider linear operator $\mathcal{L}$, with $Y = D(\mathcal{L})$, the domain of $\mathcal{L}$ dense in X and $\mathcal{L} : Y \mapsto X$. We say that a linear operator is closed if for any sequence $\{u_j\} \subset Y$ with*

$$\lim_{j\to+\infty} \|u_j - u\|_X = 0 \quad \textit{and} \quad \lim_{j\to+\infty} \|\mathcal{L}u_j - v\|_X = 0,$$

then we have $u \in Y$ and $\mathcal{L}u = v$. The operator is bounded from Y to X if

$$\sup\{\|\mathcal{L}u\|_X : u \in Y, \|u\|_Y = 1\} < \infty$$

Definition 2.1.5 (Adjoint operator). *Let $\mathcal{L} : Y = D(\mathcal{L}) \subset X \to X$ be a bounded linear operator, where X is a Hilbert space equipped with the inner product $\langle .,. \rangle$. Then the Hilbert-adjoint operator $\mathcal{L}^a$ of $\mathcal{L}$ is the operator $\mathcal{L}^a : D(\mathcal{L}^a) \to Y$ such that for all $u \in X$ and $v \in D(\mathcal{L}^a)$,*

$$\langle \mathcal{L}u, v \rangle = \langle u, \mathcal{L}^a v \rangle .$$

Definition 2.1.6 (Compact operator). *If for each bounded sequence $\{u_j\} \subset Y$ the sequence $\{\mathcal{L}u_j\} \subset X$ has a convergent subsequence, then the operator $\mathcal{L}$ is said to be compact.*

Definition 2.1.7 (Self-adjoint operator). *A bounded linear operator $\mathcal{L} : X \to X$ on a Hilbert Space X is said to be self-adjoint or Hermitian if $\mathcal{L}^a = \mathcal{L}$.*

2.1.2 Spectrum

Definition 2.1.8 (Resolvent and spectrum). *The resolvent set of operator $\mathcal{L}$, $\rho(\mathcal{L})$, is the set of complex numbers $\lambda \in \mathbb{C}$ such that*

(a) $\lambda\mathcal{I} - \mathcal{L}$ *is invertible,*

(b) $(\lambda\mathcal{I} - \mathcal{L})^{-1}$ *is a bounded linear operator.*

where $\mathcal{I}$ *is the identity operator. For* $\lambda \in \rho(\mathcal{L})$ *the operator* $(\lambda\mathcal{I} - \mathcal{L})^{-1}$ *is called the resolvent of* $\mathcal{L}$*. The spectrum of* $\mathcal{L}$ *is the complement of the resolvent set, i.e,* $\sigma(\mathcal{L}) = \mathbb{C} \setminus \rho(\mathcal{L})$*.*

Definition 2.1.9 (Fredholm operator). *The operator* $\mathcal{L}$ *is a Fredholm operator if*

(a) *Kernel of* $\mathcal{L}$*, ker(*$\mathcal{L}$*), is finite-dimensional,*

(b) *Range of* $\mathcal{L}$*, R(*$\mathcal{L}$*), is closed with finite codimension.*

Definition 2.1.10 (Fredholm index). *The Fredholm index of Fredholm operator is defined by*

$$ind(\mathcal{L}) = dim(\ker(\mathcal{L})) - codim(R(\mathcal{L}))$$

Definition 2.1.11 (Spectrum set). *Let X be a Banach space and let* $\mathcal{L} : D(\mathcal{L}) \mapsto X$ *be a closed linear operator with domain* $D(\mathcal{L})$ *dense in X. The spectrum of* $\mathcal{L}$ *is decomposed into the following two sets:*

(a) *The essential spectrum of a Fredholm operator* $\mathcal{L}$*,*$\sigma_{ess}(\mathcal{L})$*, is the set of all* $\lambda \in \mathbb{C}$ *such that either*

- $\lambda\mathcal{I} - \mathcal{L}$ *is not Fredholm, or*
- $\lambda\mathcal{I} - \mathcal{L}$ *is Fredholm, but* $ind(\lambda\mathcal{I} - \mathcal{L}) \neq 0$*.*

(b) *The point spectrum of a Fredholm operator* $\mathcal{L}$ *is the set defined by*

$$\sigma_{pt} = \{\lambda \in \mathbb{C} : ind(\lambda\mathcal{I} - \mathcal{L}) = 0, but\ \lambda\mathcal{I} - \mathcal{L} \text{ is not invertible}\}.$$

The elements of the point spectrum are called eigenvalues of $\mathcal{L}$.

Definition 2.1.12 (Compact perturbation). *The operator $\mathcal{L}$ is a relatively compact perturbation of $\mathcal{L}_0$ if $(\mathcal{L}_0 - \mathcal{L})(\lambda I - \mathcal{L}_0)^{-1} : X \to X$ is compact for some $\lambda \in \rho(\mathcal{L}_0)$*

Theorem 2.1.13 (Weyl essential spectrum theorem). *Let $\mathcal{L}$ and $\mathcal{L}_0$ be closed linear operators in a Banach space X. If $\mathcal{L}$ is a relatively compact perturbation of $\mathcal{L}_0$, then the following properties hold:*

(a) $\lambda I - \mathcal{L}$ is Fredholm if and only if $\lambda I - \mathcal{L}_0$ is Fredholm

(b) ind$(\lambda \mathcal{I} - \mathcal{L})$ = ind$(\lambda \mathcal{I} - \mathcal{L}_0)$

(c) The operators $\mathcal{L}$ and $\mathcal{L}_0$ have the essential spectra.

2.1.3 Sturm-Liouville theory

In this subsection, we provide theory about the point spectrum in the context of Sturm-Liouville theory for second order operator. It is shown that there is one to one correspondence between the ordering eigenvalues and the number of zero for the associated eigenfunctions [56].

Consider a Sturm-Liouville operator

$$\mathcal{L}p := \partial_x^2 p + a_1(x)\partial_x p + a_0(x)p, \tag{2.1}$$

which is defined on $H^2(\mathbb{R})$ with $a_1(x)$ and $a_0(x)$ are smooth functions which decay exponentially to constants $a_1^\pm$ and $a_0^\pm$, respectively as $x \to \pm\infty$, that is

$$\lim_{x\to\pm\infty} e^{\nu|x|} \left|a_1(x) - a_1^\pm\right| = 0 \qquad \text{and} \qquad \lim_{x\to\pm\infty} e^{\nu|x|} \left|a_0(x) - a_0^\pm\right| = 0. \tag{2.2}$$

The operator $\mathcal{L}$ is self-adjoint in the weighted inner product

$$\langle u, v\rangle_\rho = \int u(x)v^*(x)\rho(x)\,dx, \tag{2.3}$$

where * denotes complex conjugation and

$$\rho_\pm := \lim_{x\to\pm\infty} e^{a_1^\pm}\rho(x). \tag{2.4}$$

Theorem 2.1.14. *Consider the associated eigenvalue problem $\mathcal{L}p = \lambda p$ of Sturm-Liouville operator* (2.1) *on the space $H^2(\mathbb{R})$ where the coefficients satisfy* (2.2)*. The point spectrum, $\sigma_{pt}(\mathcal{L})$, consists of a finite number, possibly zero, of simple eigenvalues, which can be enumerated in a strictly descending order $\lambda_0 > \lambda_1 > \cdots > \lambda_N > b := \max\left\{a_0^-, a_0^+\right\}$. For $j = 0, 1, \ldots, N$ the eigenfunction $p_j(x)$ associated with the eigenvalue λ_j can be normalized so that:*

1. *p_j has j simple zeros*
2. *The eigenfunctions are orthonormal in the ρ-weighted inner product.*
3. *The ground-state eigenvalue, if it exists, can be characterized as the supremum of the bilinear form associated to $\mathcal{L}$*

   $$\lambda_0 = \sup_{\|_\rho=1} \langle \mathcal{L}u, u\rangle_\rho\,,$$

   moreover, the supremum is achieved at $u = p_0$, which has no zeros.

2.2 The nonlinear Schrödinger equation

The dimensionless form of the NLS equation is

$$i\Psi_t + \Psi_{xx} + \sigma|\Psi|^2\Psi = 0, \tag{2.5}$$

where $\Psi \in \mathbb{C}$ is a complex valued function of real variables x and $t \in \mathbb{R}^+$. The subscripts indicate derivatives with respect to the variables. The nonlinearity coefficient is denoted by σ where the value can be either $+1$ or -1, indicating the focusing or defocusing nonlinearity, respectively, or in terms of optics, attracting or repelling nonlinearity, respectively. For the next discussion we will focus on solitary waves of the focusing nonlinearity, i.e., $\sigma = 1$.

The NLS equation is a classical field equation which is in the integrable class of nonlinear wave equations. Although several studies have been carried out on the NLS equation before, it started receiving attention after Zakharov and Shabat in 1972 obtained an exact solution using Inverse Scattering Transformation (IST) [57]. The NLS equation (2.5) has solitary wave solutions (also called standing waves) which decay as $x \to \pm\infty$. They have the form $\Psi(x,t) = \psi(x)e^{i\omega t}$, where $\psi(x)$ is time-independent [7]. The function $\psi(x)$ satisfies the stationary equation

$$\psi_{xx} + |\psi|^2\psi - \omega\psi = 0, \tag{2.6}$$

where ω needs to be positive in order to ensure that ψ vanishes at infinity. There exists a unique exact solution of (2.6),

$$\psi(x) = \sqrt{2\omega}\,\mathrm{sech}(\sqrt{\omega}x), \tag{2.7}$$

that satisfies the zero boundary conditions at infinity.

Equation (2.5) is a conservative system which is invariant under some transformations and leads to some conservation laws. Some of the invariances to name but a few are as follows [2, 7, 17, 58]. First, it is invariant under a transformation so called phase or gauge invariance of NLS. It is a transformation $\Psi \to \Psi e^{i\theta}$ where θ is space and time independent. This gauge invariance implies that the wave energy,

$$P = ||\Psi||^2 = \int |\Psi|^2 dx,$$

is conserved. In the context of nonlinear optics, P refers to a beam power.

Since we are interested in solution which decays at infinity, this invariance implies $\psi(x)$ satisfies

$$\psi_{xx} + \psi^3 - \omega\psi = 0, \tag{2.8}$$

The next invariance is a time translation one, which leads to conservation of Hamiltonian [58]

$$H = ||\Psi_x||^2 - \frac{1}{2}||\Psi||^4 = \int \left(|\Psi_x|^2 - \frac{1}{2}|\Psi|^4 \right) dx. \tag{2.9}$$

The system (2.5) is known as Hamiltonian system. Besides Hamiltonian, it also has a Lagrangian structure. The Lagrangian density for the system (2.5) is

$$\mathcal{L} = \frac{i}{2}(\Psi^*\Psi_t - \Psi\Psi_t^*) - |\Psi_x|^2 + \frac{1}{2}|\Psi|^4. \tag{2.10}$$

The partial differential equation (2.5) can be derived from Euler-Lagrange equations, $\delta L/\delta\Psi = 0$

$$\frac{\partial \mathcal{L}}{\partial \Psi} - \partial_x\left(\frac{\partial \mathcal{L}}{\partial \Psi_x}\right) - \partial_t\left(\frac{\partial \mathcal{L}}{\partial \Psi_t}\right) = 0, \tag{2.11}$$

where $\delta L/\delta\Psi$ denotes the Frechet derivative of the Lagrangian $L = \int \mathcal{L}\, dx$. Another invariance which is admitted by (2.5) is Galilean invariance, that is, if $\Psi(x,t)$ is a solution, then $\Psi(x - vt, t)e^{(2ivx - iv^2 t)/4}$ is also solution, where v is an arbritrary velocity parameter. Hence, we can have a moving solitary wave

$$\Psi(x,t) = \psi(x - vt)e^{(2ivx - iv^2 t + i4\omega t)/4}.$$

According to [22], if a system has an infinite number of constants of motion or conservation laws, then it is integrable. The solution behaviour of an integrable system can be analyzed from its exact solutions. Unfortunately, most physical systems are governed by non-integrable nonlinear equations. For example, the NLS equation with external potential which we will discuss in the following subsection.

2.2.1 The NLS equation with a Dirac delta potential

The NLS with external potential which is also known as Gross-Pitaevskii equation

$$i\Psi_t + \Psi_{xx} + |\Psi|^2\Psi - V(x)\Psi = 0, \tag{2.12}$$

can be considered as a perturbed system of (2.5). If $V(x) = -\delta(x - a)$, the bound states of (2.12) satisfy

$$\psi_{xx} - \omega\psi + \psi^3 + \delta(x - a)\psi = 0. \tag{2.13}$$

A Dirac delta function, $\delta(x-a)$, named after Paul Dirac, a 20th-century mathematical physicist (1902–1984), is defined as [59]

$$\delta(x-a) = \begin{cases} 0, & \text{for } x \neq a, \\ \infty, & \text{for } x = a. \end{cases}$$

It is not really a function, it is a limiting function of a sequence of concentrated pulses. We can consider it as a concentrated source or impulse force at $x = a$. One important property of the Dirac delta function is that it has unit area,

$$\int_{-\infty}^{\infty} \delta(x-a)\, dx = 1,$$

and another property is that it is the derivative of the Heaviside unit step function $H(x-a)$,

$$H(x-a) = \begin{cases} 0 & \text{for } x < a \\ 1 & \text{for } x > a. \end{cases}$$

Equation (2.12) describes the interaction of a wide soliton with a narrow potential. The Dirac delta potential gives a defect at $x = a$ to the unperturbed soliton solution. Therefore, the existence of an explicit expression for the soliton profile can be obtained easier compared with one with general linear potential. One can refer to paper [53] to study the instability of bound states of NLS with a Dirac delta potential.

The stationary solution of (2.13) can be constructed from the stationary solution of the unperturbed system (2.8) on each side of the defect. At $x = a$, the solution should satisfy the condition of continuity, $\psi(a^+) = \psi(a^-)$, and the appropriate jump condition in the first derivative, that is $\psi_x(a^+) - \psi_x(a^-) = -\psi(a)$. A nonlinear bound state admitted by Equation (2.13) is

$$\psi(x) = \sqrt{2\omega}\,\mathrm{sech}\left(\sqrt{\omega}|x| + \tanh^{-1}\left(\frac{1}{2\sqrt{\omega}}\right)\right). \tag{2.14}$$

The solutions (2.7) and (2.14) are shown as red-dashed lines and blue-solid lines, respectively in Figure 2.1.

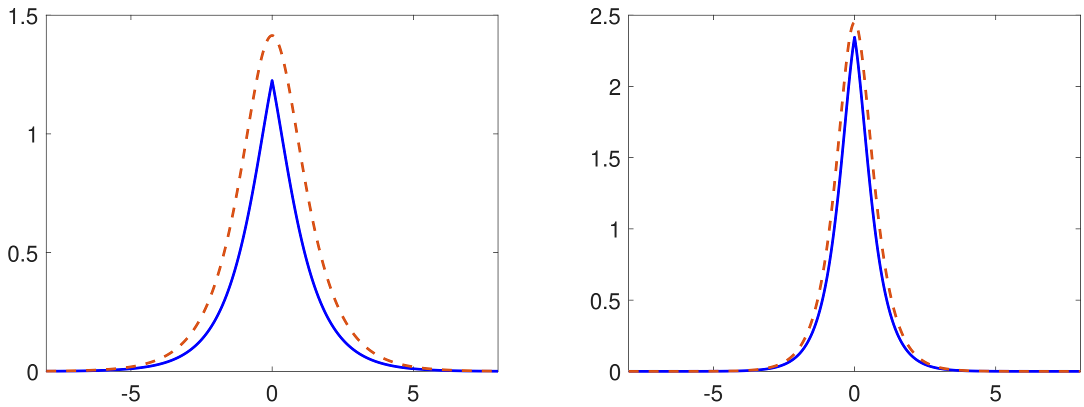

(a) **(b)**

Figure 2.1. Solutions of (2.8) and (2.13) in red-dashed lines and blue-solid lines, respectively for $a = 0$ and (a) $\omega = 1$ and (b) $\omega = 3$.

2.2.2 The NLS equation on star graphs

In this section, we present the result of the NLS equation on star graphs from [26, 60, 61]. We consider the configuration of a star graph $\mathcal{G}$ in its simplest form. It is a metric graph that consists of N half lines with common vertex, usually at the origin. The Schrödinger dynamics are associated with Hilbert space $L^2(\mathcal{G}) = \bigoplus_{k=1}^{N} L^2(\mathbb{R}^+)$. The vector function $\overline{\Psi} \in L^2(\mathcal{G})$ will be of the form $\overline{\Psi} = (\Psi^{(1)}, \Psi^{(2)}, \cdots, \Psi^{(N)})^T$ and norm of Ψ is defined as

$$||\overline{\Psi}|| = \left(\sum_{k=1}^{N} ||\Psi^{(k)}||^2_{L^2(\mathbb{R}^+)} \right)^{1/2}.$$

The NLS on star graph can be defined by posing NLS on each edge of the star graph,

$$i\Psi_t^{(k)} + \Psi_{xx}^{(k)} + |\Psi^{(k)}|^2 \Psi^{(k)} = 0, \tag{2.15}$$

where the upper indices $k = 1, \cdots, N$, label the different branches of the system and the subscripts indicate derivatives with respect to the variables.

The bound states of (2.15) satisfy

$$\Psi_{xx}^{(k)} + (\Psi^{(k)})^3 - \omega \Psi^{(k)} = 0,\ k = 1, 2, \cdots, N.$$

We choose the boundary condition at the origin

$$\sum_{k=1}^{N} \Psi_x^{(k)}(0,t) = \alpha \Psi^{(1)}(0,t), \quad \Psi^{(1)}(0,t) = \cdots = \Psi^{(N)}(0,t). \tag{2.16}$$

Parameter α gives different physical interpretation of the boundary conditions at the origin [26, 60], i.e. for $\alpha < 0$ we have a deep attractive potential well, while $\alpha > 0$ we have potential barrier at the origin. The special case is for $\alpha = 0$, which is called the free Kirchoff boundary condition. One can refer to paper by Adami et.al [62] for the global well-posedness of the dynamics in a star graph with some boundary conditions at the vertex.

The standing waves of NLS on three-edge and four edge star graph can be seen in Figure 2.2.

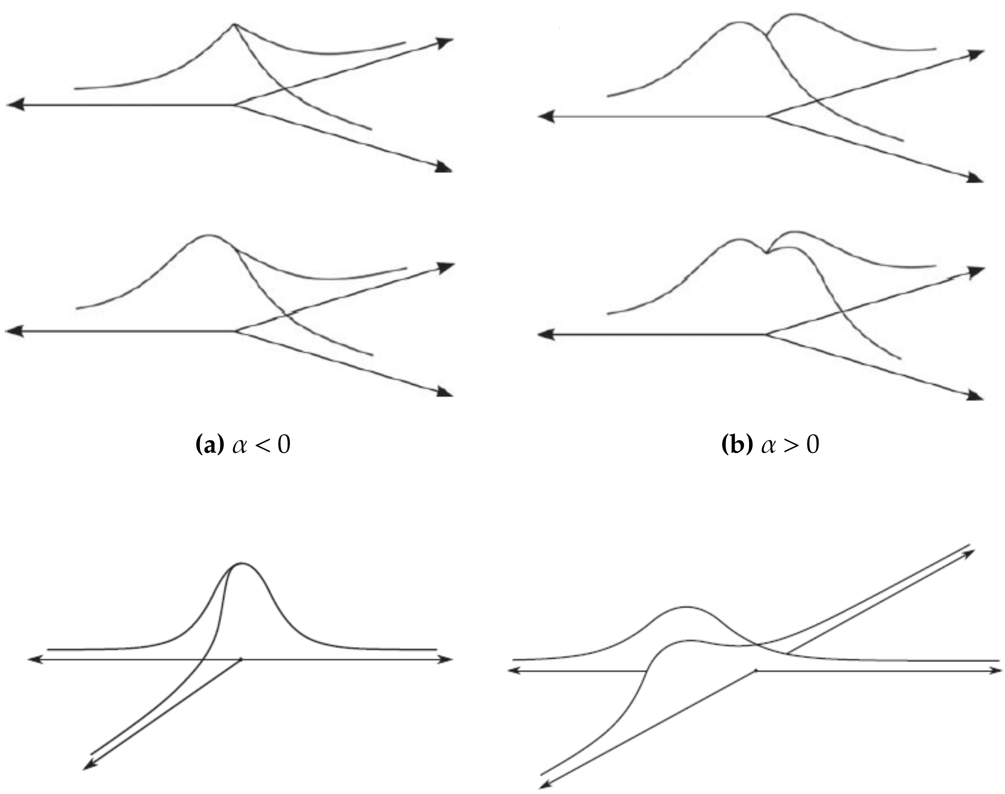

(a) $\alpha < 0$ (b) $\alpha > 0$

(c) $\alpha = 0$

Figure 2.2. Examples of bound states on star graph (taken from [26, 60]).

2.2.3 The discrete nonlinear Schrödinger equation

In this section, we consider the one-dimensional (spatially) Discrete Nonlinear Schrödinger (DNLS) equation

$$i\frac{d\Psi_n}{dt} + c(\Psi_{n+1} - 2\Psi_n + \Psi_{n-1}) + |\Psi_n|^2\Psi_n = 0, \quad n \in \mathbb{N}, \tag{2.17}$$

where Ψ_n is a complex-valued function of time t at site n, $c > 0$ is the strength of the coupling between adjacent sites which is also called as the dispersion coefficient, and ω is the propagation constant.

Equation (2.17) is also a conservative system and can be derived from the Lagrangian

$$L = \sum_{n=-\infty}^{\infty} \left[i\left(\Psi_n^* \frac{d\Psi_n}{dt} - \Psi_n \frac{d\Psi_n^*}{dt} \right) - \frac{c}{2} |\Psi_n - \Psi_{n-1}|^2 + \frac{1}{2} |\Psi_n|^4 \right]. \tag{2.18}$$

Note that if we take $c = 1/(\Delta x)^2$, then (2.17) can be seen as a finite difference approximation of (2.5). In the case c tends to zero i.e., the limit of zero coupling (anti-integrable or anti-continuum limit), the solution of Equation (2.17) is

$$\Psi_n = \sqrt{\omega_n} e^{i(\omega_n t + \alpha_n)}, \tag{2.19}$$

with phase α_n and frequency ω_n.

Assume that the stationary solution of Equation (2.17) is of the form $\Psi_n = \psi_n e^{-i\omega t}$ with $\psi_n \in \mathbb{R}$. The solutions are given by these time-periodic solutions of the DNLS equation. Upon substitution of the steady state solutions into the DNLS equation, it yields the stationary equation

$$\omega \psi_n = c(\psi_{n+1} - 2\psi_n + \psi_{n-1}) + \psi_n^3. \tag{2.20}$$

Equation (2.20) admits two fundamental discrete solitary waves, which interchangeably will also be called discrete solitons, that can be continued all the way from the uncoupled limit $c \to 0$ to the continuous limit $c \to \infty$. The two solutions are on-site and inter-site discrete solitons, which are also usually referred to as Sievers-Takeno (ST) and Page (P) mode, respectively. The two modes become degenerate in the continuous limit $c \to \infty$. In the case c tends to zero, we have that the solution of Equation (2.20) is then $\psi_n = 0$ or $\psi_n = \pm\sqrt{\omega}$.

In the following section we discuss two variational methods used for finding approximate solutions, namely the variational approximations (VA) and the coupled mode reduction method.

2.3 Variational methods

2.3.1 Variational approximations

The VA method is frequently used in solving nonlinear evolution equations [63, 64]. The VA reduces the infinite dimension of the problem into a finite one by introducing a trial function, usually called ansatz, that involve a finite number of parameters describing the dominant characteristics of the solution. This method is usually used for a conservative system, where the dynamics is governed by the system having a Lagrangian formulation which leads to a conserved energy. By substituting the ansatz into the Lagrangian, one will obtain an effective Lagrangian that is a function of the variational parameters introduced in the ansatz. Using Euler-Lagrange principle, the critical values of the parameters can be found by solving the associated variational equations.

As mentioned earlier, Equation (2.20) admits discrete solitons and now we want to approximate the solutions using VA method. The Lagrangian of Equation (2.20) is of the form

$$L = \sum_{n=-\infty}^{\infty} \frac{1}{2}(\omega + 2c)\psi_n^2 - \frac{1}{4}\psi_n^4 - \frac{c}{2}(\psi_{n+1} + \psi_{n-1})\psi_n. \tag{2.21}$$

We observe that Equation (2.20) is an equivalent equation for the Lagrangian (2.21). We introduce the 'soliton-like' ansatz as approximation of the discrete soliton of the stationary equation (2.20)

$$\psi_n^{\mathrm{ST}} = A_1 e^{-a_1|n|}, \tag{2.22}$$

$$\psi_n^{\mathrm{P}} = A_2 e^{-a_2|n-\frac{1}{2}|}, \tag{2.23}$$

where ψ_n^{ST} denotes soliton in ST-modes (on-site soliton) and ψ_n^{P} in P-modes (inter-site soliton), A_1, a_1, A_2, a_2 are variational parameters to be determined [65]. Substituting these ansatz to the Lagrangian yields the effective Lagrangians

$$L_{\mathrm{eff}}^{\mathrm{ST}} = -\frac{1}{4}A_1^2\Big(-2(2c+\omega) + 8c\cosh a_1 + (A_1^2 - 4c - 2\omega)\cosh 2a_1\Big)\operatorname{csch} 2a_1, \tag{2.24}$$

$$L_{\mathrm{eff}}^{\mathrm{P}} = -\frac{A_2^2\Big(-8c\cosh^3 a_2 + (8c\sinh a_2 + 8c)\cosh^2 a_2 - (8\sinh a_2 + 4)\cosh a_2 + A_2^2\Big)}{8\sinh a_2 \cosh a_2}. \tag{2.25}$$

Each of the effective Lagrangian is a function of variational parameters. By variational principle, we can find the variational parameters A_1, a_1, A_2, a_2 by solving the following Euler-Lagrange equations which are also called variational equations

$$\frac{\partial L_{\mathrm{eff}}^{\mathrm{ST}}}{\partial A_1} = \frac{\partial L_{\mathrm{eff}}^{\mathrm{ST}}}{\partial a_1} = 0 \quad \text{and} \quad \frac{\partial L_{\mathrm{eff}}^{\mathrm{P}}}{\partial A_2} = \frac{\partial L_{\mathrm{eff}}^{\mathrm{P}}}{\partial a_2} = 0. \tag{2.26}$$

Substituting back the values of the parameters obtained from (2.26) to (2.22) and (2.23), we can then obtain an approximate solution of (2.20). Figure 2.3 shows the profiles of on-site and inter-site solitons for several values of c. We can see that the obtained approximations are quite close to the numerical results. We have

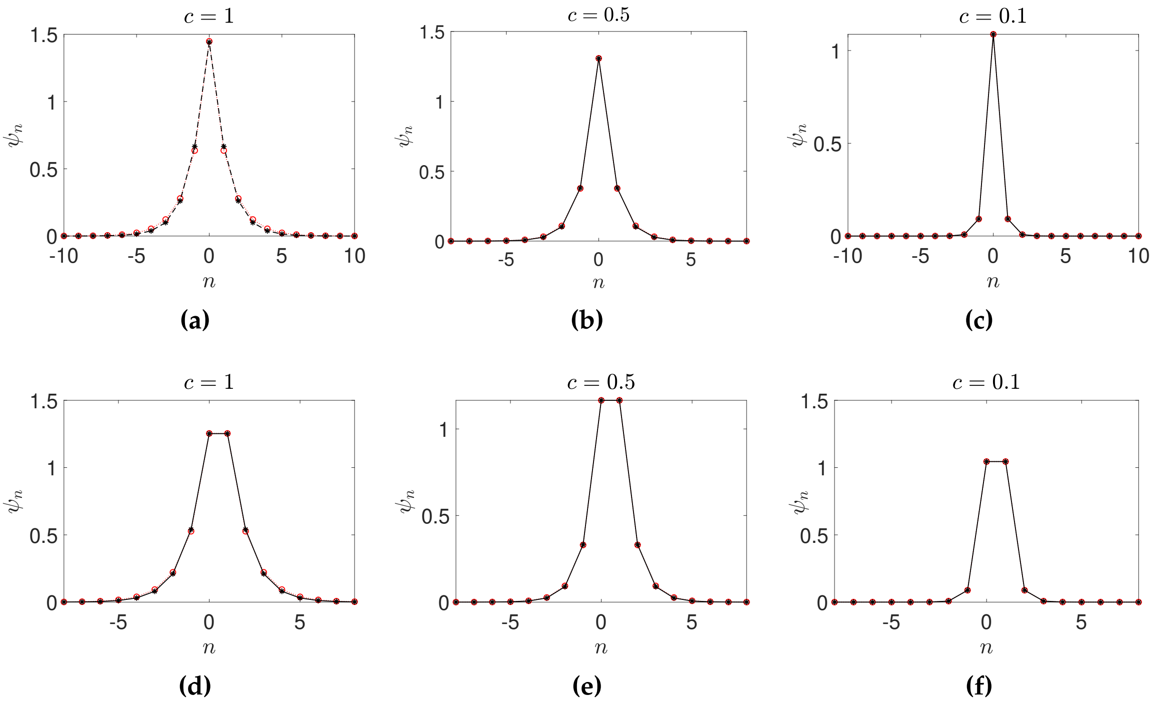

Figure 2.3. Profiles on-site (a-c) and inter-site (d-f) discrete solitons of (2.20) for different values of c as indicated. Stars and circles are numerical computations and approximations, respectively.

shown that to obtain variational equations (2.26) using the VA method we need the Lagrangian of the system. Next, we will show how we obtain variational equations of a system without knowing its Lagrangian in the following subsection.

2.3.2 Variational approximations for discrete lattices

Following [66], we consider a discrete differential equation of the form

$$i\frac{d\Psi_n}{dt} = f_V(\Psi_n, \Psi_n^*) + f_{NV}(\Psi_n, \Psi_n^*), \tag{2.27}$$

where $\Psi_n(t)$ is a complex function of time and Ψ_n^* is its conjugate. We write the right hand side of (2.27) in two parts: the variational part f_V and the non variational part f_{NV}. If the equation is conservative, then $f_{NV} = 0$, and there is a Lagrangian function

$$L = \sum_{n=-\infty}^{\infty} \mathcal{L}(\Psi_n, \frac{d\Psi_n}{dt}, \Psi_n^*, \dot{\Psi}_n^*), \tag{2.28}$$

that yields Equation (2.27) from the relation

$$\frac{\partial L}{\partial \Psi_n^*} - \frac{d}{dt}\left(\frac{\partial L}{\partial \dot{\Psi}_n^*}\right) = i\frac{d\Psi_n}{dt} - f_V(\Psi_n, \Psi_n^*). \tag{2.29}$$

Let Φ_n be the chosen ansatz containing a finite number of parameters to be determined, x_j, for $j = 1, 2, \cdots, N$, and they are functions of t. The calculation upon the substitution of the ansatz to the infinite sum (2.28) yields an effective Lagrangian L_{eff}, which contains the variational parameters and their derivatives with respect to t. This gives us the variational equations

$$\frac{\partial L_{\text{eff}}}{\partial x_j} - \frac{d}{dt}\left(\frac{\partial L_{\text{eff}}}{\partial (dx_j/dt)}\right) = 0, \tag{2.30}$$

which can be solved for x_j's.

Now, we consider the case when $f_{NV} \neq 0$. Recall that,

$$\begin{aligned}
\frac{\partial L_{\text{eff}}}{\partial x_j} &= \frac{\partial L_{\text{eff}}}{\partial \Phi_n^*}\frac{\partial \Phi_n^*}{\partial x_j} + \frac{\partial L_{\text{eff}}}{\partial \Phi_n}\frac{\partial \Phi_n}{\partial x_j} \\
&= 2\text{Re}\left(\sum_{n=-\infty}^{\infty}\left(i\frac{d\Phi_n}{dt} - f_V + \frac{d}{dt}\left(\frac{\partial \mathcal{L}}{\partial(d\Phi_n^*/dt)}\right)\right)\frac{\partial \Phi_n^*}{\partial x_j}\right).
\end{aligned}$$

On the other hand, since the ansatz Φ_n is assumed to satisfy Equation (2.27), then

$$\frac{\partial L_{\text{eff}}}{\partial x_j} = 2\text{Re}\left(\sum_{n=-\infty}^{\infty}\left(f_{NV} + \frac{d}{dt}\left(\frac{\partial \mathcal{L}}{\partial(d\Phi_n^*/dt)}\right)\right)\frac{\partial \Phi_n^*}{\partial x_j}\right).$$

Note that in the two last equations, L is restricted to the space where the ansatz is defined. Combining them, we obtain the equation

$$\text{Re}\left(\sum_{n=-\infty}^{\infty} i\frac{d\Phi_n}{dt}\frac{\partial \Phi_n^*}{\partial x_j}\right) = \text{Re}\left(\sum_{n=-\infty}^{\infty}(f_V + f_{NV})\frac{\partial \Phi_n^*}{\partial x_j}\right). \tag{2.31}$$

The equivalence of Equation (2.31) for spatially continuous and linear Schrödinger equations is known as the Dirac-Frenkel-MacLachlan variational principle [67, 68] (see also [69, 70] that give a near-optimality result for variational approximations, by providing error bounds in terms of the distance of the exact wave function to the approximation manifold).

2.3.3 Coupled mode reduction method

The coupled mode reduction method is another type of variational method that can be used to approximate solutions of NLS. The idea is to obtain the nonlinear bound states by exploiting the linear states. First, we solve the linearised system of the nonlinear evolution equation and take the basis of the eigenspace. We set as an ansatz for the nonlinear bound state the linear combination of the basis of the linear states. The coefficient is taken as the variational parameter. In other words, we project the nonlinear bound states onto the linear state space. By neglecting the terms containing the continuous spectrum, we convert the infinite dimensional problem to ordinary differential equations of finite dimension which is a Hamiltonian system with conserved Hamiltonian and l^2 invariant. This method is analog to the VA method, when we substitute the ansatz into the Lagrangian. We obtain the same variational equations as those from VA method [49].

After solutions are obtained, the next question is to determine their stability. We will discuss linear stability using linearisation in Section 2.4.

2.4 Stability

Stability theory refers to an analysis of the behaviour of equilibria under small perturbations of initial conditions and the behaviour of the near solutions of equilibrium manifolds. We introduce the following definition of orbital stability [7, 58, 71]

Definition 2.4.1. *A solitary wave $\tilde{\psi}e^{i\omega t}$ of* (2.5)*, is orbitally stable if for any $\varepsilon > 0$ there exists a $\delta(\varepsilon) > 0$ such that if $||\psi(x,0) - \tilde{\psi}|| < \delta$ then*

$$\inf_{\theta\in\mathbb{R}, y\in\mathbb{R}} ||\psi(x,t) - \tilde{\psi}(x+y)e^{i\theta}|| < \varepsilon$$

for all t.

Intuitively, the above definitions say that the concept of stability is using the concept of limit that allows phase shifts and translations. A solitary wave is called stable if the perturbed solution, which is a solution in the neighbourhood of the solitary wave will stay close when time is increasing. It is called asymptotically stable if it is stable and the perturbed solution approaches it when time goes to infinity.

In general, it is not an easy task to determine the stability of nonlinear waves, but we can analyse them by perturbation theory such as linearisation of the system about the equilibrium.

2.4.1 Linear stability

We will discuss linear stability using the NLS equation with external potential (2.12)

$$i\Psi_t + \Psi_{xx} + |\Psi|^2\Psi - V(x)\Psi = 0, \tag{2.32}$$

where we assume $V(x)$ is a function which decays at infinity.

We assume that Equation (2.32) has an equilibrium, $\tilde{\psi}$. The behaviour of solutions Ψ in the neighbourhood of $\tilde{\psi}$ can be seen by using linearisation of the system about $\tilde{\psi}$. We use the linearisation ansatz

$$\Psi(x,t) = \left(\tilde{\psi}(x) + \mu\left(\xi(x) + i\eta(x)\right)e^{\lambda t}\right)e^{i\omega t},\ \mu \ll 1$$

where $\tilde{\psi}(x)$ is the equilibrium solution. Upon substitution this ansatz to (2.5) and considering terms linear in μ will lead to the eigenvalue problem

$$\begin{aligned} \lambda\xi &= -\eta_{xx} + \omega\eta - \tilde{\psi}^2\eta + V(x)\eta, \\ \lambda\eta &= \xi_{xx} - \omega\xi + 3\tilde{\psi}^2\xi - V(x)\xi. \end{aligned} \tag{2.33}$$

By setting

$$\begin{aligned} \mathcal{L}_- &= \frac{d^2}{dx^2} - \omega + \tilde{\psi}^2 - V(x), \\ \mathcal{L}_+ &= \frac{d^2}{dx^2} - \omega + 3\tilde{\psi}^2 - V(x), \end{aligned}$$

system (2.33) can be rewritten as

$$\lambda \begin{pmatrix} \xi \\ \eta \end{pmatrix} = \begin{pmatrix} 0 & -\mathcal{L}_- \\ \mathcal{L}_+ & 0 \end{pmatrix} \begin{pmatrix} \xi \\ \eta \end{pmatrix} = \mathcal{L} \begin{pmatrix} \xi \\ \eta \end{pmatrix} \tag{2.34}$$

Equation (2.34) is an eigenvalue problem for (2.5) and λ is called the spectral parameter. Since $\mu \ll 1$, i.e., we consider a sufficiently small neighbourhood, the dynamics of the nonlinear system (2.5) is governed by the obtained eigenvalue problem which is a linear system with infinite dimension. The dynamics of the linear system is used to determine the stability of the nonlinear solitary waves. Therefore we call this as a linear stability of the solitary waves. It is determined by solving the eigenvalue problem (see book by Kapitula and Promislow [56] and Jianke Yang [2] for the details). The set of all λ satisfying the eigenvalue problem is called the spectrum for the solitary wave. It consists of point (discrete) spectrum (which we have known as eigenvalues) and continuous or essential spectrum. The spectrum contains information about the stability and behaviour of the solutions

The eigenvalue problem (2.34) always has $\lambda = 0$ as an eigenvalue. Since $\mathcal{L}_+\tilde{\psi} = 0$, then $\tilde{\psi}$ is the eigenvector corresponding to zero eigenvalue with multiplicity at least 2. If λ is an eigenvalue with its corresponding eigenfunction $(\xi,\eta)^T$, then $-\lambda$ is also an eigenvalue with its corresponding eigenfunction $(-\xi,\eta)^T$. Also, since operator $\mathcal{L}_+$ and $\mathcal{L}_-$ are self-adjoint, then λ^* is also an eigenvalue with its corresponding eigenfunction $(\xi^*,\eta^*)^T$. Hence, the eigenvalues of $\mathcal{L}$ come in pairs or quadruples due to the fact that if λ is an eigenvalue, so are $-\lambda, \lambda^*$ and $-\lambda^*$.

Definition 2.4.2. *The equilibrium solution $\tilde{\psi}$ is spectrally stable if its linearisation $\mathcal{L}$ satisfies $\sigma(\mathcal{L}) \cap \{\lambda \in \mathbb{C} : Re(\lambda) > 0\} = 0$, i.e, there is no spectrum in the open right-half of the complex plane. Otherwise, the wave is spectrally unstable.*

Now, we want to find the essential spectrum of (2.34). The essential spectrum can be obtained by considering $\mathcal{L}_+$ and $\mathcal{L}_-$ in the limit $x \to \pm\infty$ which yields that each linear operator $\mathcal{L}_+$ and $\mathcal{L}_-$ has a limit of $\frac{d^2}{dx^2} - \omega$ [56]. Writing it as 4×4 first order ODEs,

$$\begin{pmatrix} \xi_1 \\ \xi_2 \\ \eta_1 \\ \eta_2 \end{pmatrix}_x = \begin{pmatrix} 0 & 1 & 0 & 0 \\ \omega & 0 & \lambda & 0 \\ 0 & 0 & 0 & 1 \\ -\lambda & 0 & \omega & 0 \end{pmatrix} \begin{pmatrix} \xi_1 \\ \xi_2 \\ \eta_1 \\ \eta_2 \end{pmatrix}, \tag{2.35}$$

the characteristic polynomial of the coefficient matrix is

$$y^4 - 2\omega y^2 + \lambda^2 + \omega^2 = 0. \tag{2.36}$$

The corresponding eigenfunction is of the form $\approx (c_1, c_2)^T e^{ikx}$, where k is a wavenumber, and c_1, c_2 constants. Substituting $y = ik$, and solving the equation for λ, we obtain the essential spectrum is two line segments on the imaginary axis, $\lambda = \pm i(k^2 + \omega)$, k is real.

For the DNLS equation, we use the linearisation ansatz $\Psi_n(t) = (\tilde{\psi}_n + \mu\epsilon_n)e^{-i\omega t}$ with $\mu \ll 1$. Substituting this ansatz to the DNLS equation yields

$$i\frac{d\epsilon_n}{dt} = c(\epsilon_{n+1} - 2\epsilon_n + \epsilon_{n-1}) + 2\tilde{\psi}_n^2\epsilon_n + \tilde{\psi}_n^2\epsilon_n^* - \omega\epsilon_n + O(\mu) \tag{2.37}$$

and neglecting the $O(\mu)$, we will have

$$i\frac{d\epsilon_n}{dt} = c(\epsilon_{n+1} - 2\epsilon_n + \epsilon_{n-1}) + 2\tilde{\psi}_n^2\epsilon_n + \tilde{\psi}_n^2\epsilon_n^* - \omega\epsilon_n. \tag{2.38}$$

Writing $\epsilon_n = (\eta_n + i\xi_n)e^{\lambda t}$ and plugging it into the last equation, we obtain

$$\begin{aligned} \lambda\xi_n &= \omega\eta_n - c\Delta\eta_n - 3\tilde{\psi}_n^2\eta_n \\ \lambda\eta_n &= -\omega\xi_n + c\Delta\xi_n + \tilde{\psi}_n^2\xi_n. \end{aligned} \tag{2.39}$$

Therefore, we have the eigenvalue problem

$$\begin{pmatrix} 0 & \omega - c\Delta - \tilde{\psi}_n^2 \\ -\omega + c\Delta + 3\tilde{\psi}_n^2 & 0 \end{pmatrix}\begin{pmatrix} \xi_n \\ \eta_n \end{pmatrix} = \lambda\begin{pmatrix} \xi_n \\ \eta_n \end{pmatrix}, \tag{2.40}$$

where $\Delta\eta_n = \eta_{n+1} - 2\eta_n + \eta_{n-1}$.

Equation (2.40) is an eigenvalue problem for (2.32). The dynamics of the nonlinear system (2.32) is governed by the obtained eigenvalue problem which is also a linear system with infinite dimension. We see that $\lambda = 0$ is also an eigenvalue. On the other hand, the essential spectrum consists of all λ which is purely imaginary. This is because the essential spectrum can be obtained by substituting $(c_1, c_2)^T e^{ikn}$ for $n \to \pm\infty$.

2.4.2 Vakhitov-Kolokolov criterion

If the solitary wave is positive, we can determine the instability using the Vakhitov-Kolokolov (VK) criterion [2, 58, 72]

Theorem 2.4.3 (VK Criterion [2]**).** *The ground state solitary wave of* (2.5) *is linearly unstable if and only if* $\frac{dP}{d\omega} < 0$. *When it is unstable, there exists a single unstable eigenvalue which is purely real.*

The reader can see [2] for the proof of the theorem.

2.4.3 Bifurcations

As discussed in Chapter 1, bifurcations are the qualitative changes in the dynamics of a system as parameters are varied. Bifurcation points are the parameters at which they occur. One way to represent the bifurcation is using so called a bifurcation diagram. It depicts the dependence on parameters for the qualitative structure of the system. Usually a solid and dashed line is used for stable and unstable fixed points, respectively. There are several types of bifurcations, we will present some of them. The discussion is mainly taken from [73]. We consider a first-order differential equation which depend on parameter r

$$\frac{d\mathbf{x}}{dt} = f(\mathbf{x}, r) \tag{2.41}$$

The fixed points, or equilibrium points, for (2.41) are given by $f(\mathbf{x}_0, r) = 0$. Generally, the fixed points $\mathbf{x}_0$ depends on parameter r.

2.4.3.1 Saddle-node bifurcations

Saddle-node bifurcation is a type of bifurcation where two fixed points coalesce and then annihilate. Bifurcation diagram in Figure 2.4a depicts an example of the saddle-node bifurcation in one dimensional system of (2.41). We can see that there are two fixed points for $r < 0$, one unstable and the other one stable, as r increases they collide at bifurcation point $x = 0$ and disappear when $r > 0$.

2.4.3.2 Transcritical bifurcations

When there is an exchange of fixed points stabilities as the parameter is varied, a transcritical bifurcation occurs. The typical bifurcation diagram for transcritical bifurcation is shown in Figure 2.4b. We can see that for $r < 0$, there are two fixed points and after the bifurcation point, $r = 0$, they switch their stabilities, from stable to unstable, vice versa.

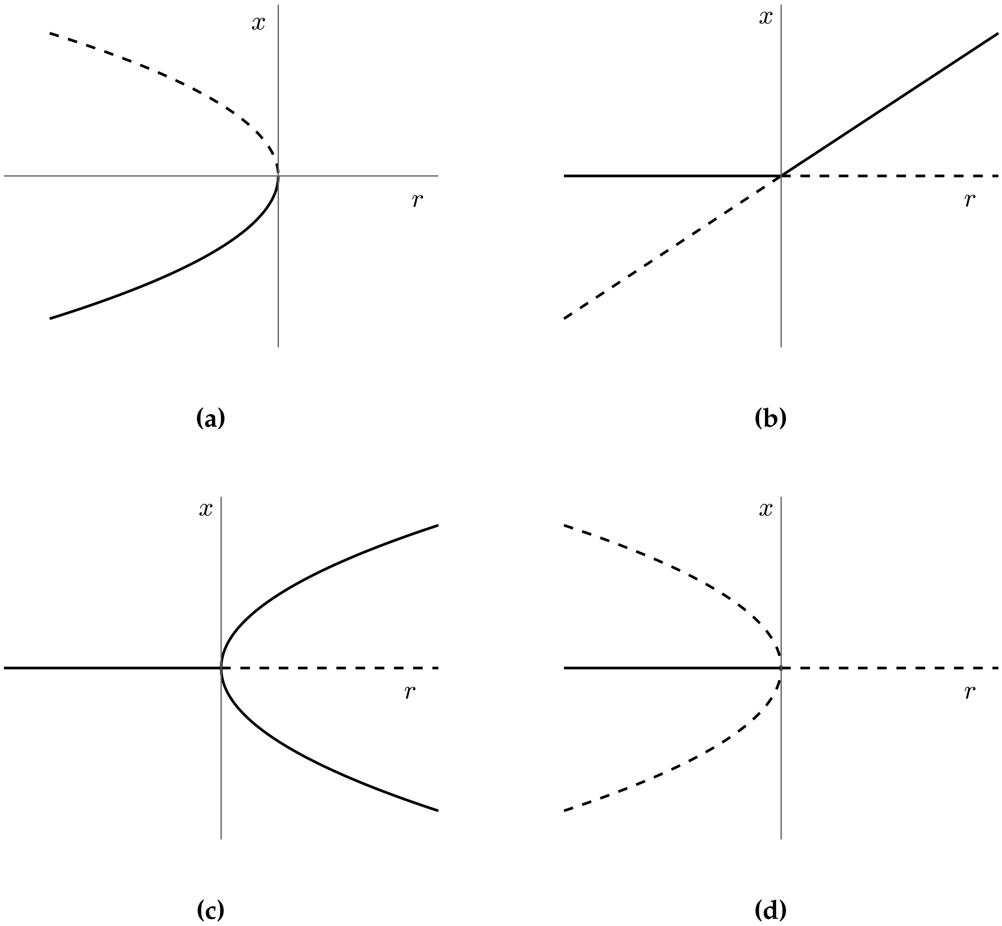

Figure 2.4. One dimensional bifurcation diagram for (a) supercritical and (b) subcritical pitchfork bifurcations.

2.4.3.3 Pitchfork bifurcations

The next type of bifurcation is a pitchfork bifurcation where it is characterized by symmetrically appear and disappear of the fixed points. There are two types of pitchfork bifurcation. The first one is the supercritical pitchfork bifurcation as shown in Figure 2.4c. There is only one fixed point when $r < 0$, and it is stable. When $r = 0$, there is still one fixed points and it becomes unstable when $r > 0$. Also, there is a symmetric pair of stable fixed points appear on the either side of $r = 0$.

The second type of pitchfork bifurcation is subcritical. It can be described by its bifurcation diagram depicted in Figure 2.4d. For $r < 0$, one fixed point is stable, and there are two unstable fixed points. As r increases, the fixed points collide at $r = 0$, and then appear as a single unstable fixed points.

Chapter 3

Symmetry breaking bifurcations in the NLS equation with an asymmetric delta potential

In this chapter, we consider the NLS equation with an asymmetric double Dirac delta potential and study the effect of the asymmetry in the bifurcation, particularly the spontaneous symmetry breaking. An interesting result was presented in [74], on a systematic methodology, based on a two-mode expansion and numerical simulations, of how an asymmetric double well potential is different from a symmetric one. It was demonstrated that, contrary to the case of symmetric potentials where symmetry breaking follows a pitchfork bifurcation, in asymmetric double wells the bifurcation is of the saddle node type.

However, different from [74], our present work provides a rigorous analysis of the bifurcation as well as the linear stability of the corresponding solutions using a geometrical approach, following [12] on the symmetric potential case (see also [75–77] for the approach).

Since the system is autonomous except at the defects, we can analyse the existence of the stationary standing waves using phase plane analysis, or also called phase portrait analysis. We convert the second order differential equation into a pair of first order differential equations with matching conditions at the defects. In the phase plane, the solution which we are looking for will evolve first in the unstable manifold of the origin, and at the first defect it will jump to the transient orbit, and again evolves until the second defect, and then jumps to the stable manifold to flow back to the origin. We also present the analytical solutions that are piecewise continuous functions in terms of hyperbolic secant and Jacobi elliptic function. We analyse their instability using geometric analysis for the solution curve in the phase portrait.

The chapter is organised as follows. In Section 3.1, we present the mathematical model and set up the phase plane framework to search for the standing wave. In Section 3.2, we present the linear states of the system. In Section 3.3, we discuss the geometric analysis for the existence of the nonlinear bound states and show that there is a symmetry breaking of the ground states. Then, the stability of the states obtained are analysed in Section 3.4, where we show the condition for the stability in terms of the threshold value of 'time' for the standing wave evolving between two defects. In Section 3.5, we present our numerics to illustrate the results reported previously. Finally, we summarise the work in Section 3.6

3.1 Mathematical model

We consider the one-dimensional NLS equation

$$i\Psi_t(x,t) + \Psi_{xx}(x,t) + |\Psi(x,t)|^2\Psi(x,t) - V(x)\Psi(x,t) = 0, \tag{3.1}$$

where $\Psi \in \mathbb{C}$ is a complex-valued function of the real variables t and x. The asymmetric double potential $V(x)$ is defined as

$$V(x) = -\delta(x+L) - \epsilon\delta(x-L), \quad 0 < \epsilon \leq 1, \tag{3.2}$$

where L is a positive parameter. We consider solutions which decay to 0 as $x \to \pm\infty$, $\Psi(x,t) = \psi(x)e^{i\omega t}$. The system conserves the squared norm $P = \int_{-\infty}^{\infty} |\Psi(x,t)|^2\, dx$ which is known as the optical power in the nonlinear optics context, or the number of atoms in Bose-Einstein condensates.

Standing waves of (3.1) satisfy

$$\psi_{xx} - \omega\psi + \psi^3 - V(x)\psi = 0, \tag{3.3}$$

The stationary equation (3.3) is equivalent to

$$\psi_{xx} = \omega\psi - \psi^3 \tag{3.4}$$

for $x \neq \pm L$ with matching conditions:

$$\psi(\pm L^+) = \psi(\pm L^-), \quad \psi_x(\pm L^+) - \psi_x(\pm L^-) = -\tilde{V}_\pm \psi(\pm L), \tag{3.5}$$

with $\tilde{V}_- = 1$ and $\tilde{V}_+ = \epsilon$.

Our aim is to study the ground states of (3.1), which are localised solutions of (3.3) and determine their stability. We will apply dynamical system approach by analysing the solutions in the phase plane. However, before proceeding with the nonlinear bound states, we will present the linear states of the system in the following section.

3.2 Linear states

In the limit $\psi \to 0$, Equation (3.3) is reduced to the linear system

$$\psi_{xx} - \omega\psi - V(x)\psi = 0, \tag{3.6}$$

which is equivalent to the system $\psi_{xx} = \omega\psi$ for $x \neq \pm L$ with the matching conditions (3.5).

The general solution of (3.6) is given by

$$\psi(x) = \begin{cases} e^{\sqrt{\omega}(x+L)}, & x < -L, \\ Ae^{-\sqrt{\omega}(x+L)} + Be^{\sqrt{\omega}(x+L)}, & -L < x < L, \\ Ce^{-\sqrt{\omega}(x-L)}, & x > L. \end{cases} \tag{3.7}$$

Using the matching conditions, the function (3.7) will be a solution of the linear system when $A = 1 - 1/2\sqrt{\omega}, B = 1/2\sqrt{\omega}$, and $C = (e^{-2L\sqrt{\omega}}\left(2\sqrt{\omega}e^{4L\sqrt{\omega}} - e^{4L\sqrt{\omega}} + 1\right))/2\sqrt{\omega}$, and ω satisfies the transcendental relation

$$L = \frac{1}{4\sqrt{\omega}} \ln\left(-\frac{\epsilon}{\left(2\sqrt{\omega}-1\right)\left(\epsilon - 2\sqrt{\omega}\right)}\right). \tag{3.8}$$

This equation determines two bifurcation points of the linear states ω_0 and ω_1. We obtain that the eigenfunction with eigenvalue ω_0 exists for any L, while the other one only for $L \geq (1+\epsilon)/2\epsilon$. For $L \to \infty$, $\omega_0 \to 1/4$ and $\omega_1 \to \epsilon^2/4$. We illustrate Equation (3.8) in Figure 3.1. Positive solutions that are non-trivial ground states of the system will bifurcate from ω_0, while from ω_1, we should obtain a bifurcation of 'twisted' mode which is not addressed in the present work.

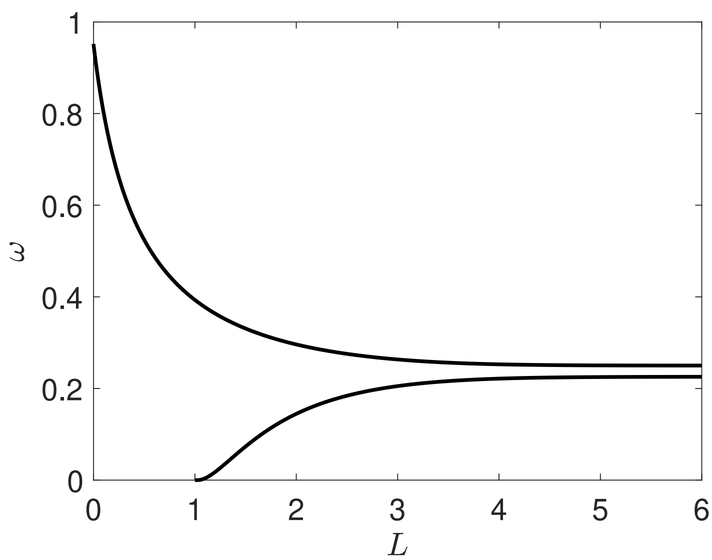

Figure 3.1. The eigenvalues ω as a function of L from (3.8) for $\epsilon = 0.95$. The upper curve is ω_0.

3.3 Nonlinear bound states

To study nonlinear standing waves (bound states), we convert the second order differential equation (3.3) into first order equations. For $x \neq \pm L$, let $u = \psi, y = \psi_x$

$$\begin{aligned} u_x &= y, \\ y_x &= \omega u - u^3, \end{aligned} \tag{3.9}$$

with the matching conditions

$$u(\pm L^+) = u(\pm L^-), \quad y(\pm L^+) - y(\pm L^-) = -\tilde{V}_\pm u(\pm L). \tag{3.10}$$

Without lost of generality, we consider only $u > 0$. The evolution away from the defects is determined by the autonomous system (3.9) and at each defect there is a jump according to the matching conditions (3.10).

3.3.1 Phase plane analysis

System (3.9) has equilibrium solutions $(0,0)$ and $(\sqrt{\omega}, 0)$ and the trajectories in the phase plane are given by (see Appendix B)

$$y^2 - \omega u^2 + \frac{1}{2}u^4 = E. \tag{3.11}$$

In the following we will discuss how to obtain bound states of (3.1) which decay at infinity. In the phase plane, a prospective standing wave must begin along the global unstable manifold W^u of $(0,0)$ because it must decay as $x \to -\infty$. The unstable manifold W^u is given by

$$W^u = \left\{ (u, y) | y = \sqrt{\omega u^2 - \frac{1}{2} u^4}, 0 \leq u \leq \sqrt{2\omega} \right\}.$$

The potential (3.2) will imply two defects in the solutions. After some time evolving in the unstable manifold (in the first quadrant), the solution will jump vertically at the first defect at $x = -L$ according to matching condition (3.10). For a particular value of ω, the landing curve for the first jump follows

$$J(W^u) = \left\{ (u, y) | y = \sqrt{\omega u^2 - \frac{1}{2} u^4} - u \right\}.$$

At the first defect, the solution will jump from the homoclinic orbit to an inner orbit as the transient orbit. Let the value of E for the orbit be $\hat{E} \in \left(-\frac{1}{2}\omega^2, 0\right)$. If we denote the maximum of u of the inner orbit as a, then the value for a in this orbit is

$$\hat{a} = \sqrt{\omega + \sqrt{\omega^2 + 2\hat{E}}}.$$

Denote the value of the solution at the first defect as u_1, then it satisfies

$$u_1^2 - 2u_1 \sqrt{\omega u_1^2 - \frac{1}{2} u_1^4} = \hat{E}, \tag{3.12}$$

which can be re-written as a cubic polynomial in u_1^2,

$$(u_1^2)^3 + \left(\frac{1}{2} - 2\omega\right)(u_1^2)^2 - \hat{E} u_1^2 + \frac{\hat{E}^2}{2} = 0.$$

Using Cardan's method (see Appendix A) to solve the polynomial, we obtain u_1 as function of $\hat{E}$, i.e., for $\omega < 1/4$, there is no real solution, while for $\omega > 1/4$, there are two real valued u_1 given by

$$
\begin{aligned}
u_1^{(1)} &= \left(\frac{1}{3}\left(2\omega - \frac{1}{2}\right) + \frac{2}{3}\sqrt{3\hat{E} + \left(\frac{1}{2} - 2\omega\right)^2} \cos\theta \right)^{1/2}, \\
u_1^{(2)} &= \left(\frac{1}{3}\left(2\omega - \frac{1}{2}\right) - \frac{2}{3}\sqrt{3\hat{E} + \left(\frac{1}{2} - 2\omega\right)^2} \sin\left(\frac{\pi}{6} - \theta\right) \right)^{1/2},
\end{aligned}
\tag{3.13}
$$

where

$$\theta = \frac{1}{3}\cos^{-1}\left(\frac{-54\hat{E}^2 + 18\hat{E}(4\omega - 1) + (4\omega - 1)^3}{\left(12\hat{E} + (1-4\omega)^2\right)^{3/2}} \right).$$

For a given $\omega > 1/4$, the landing curve of the first jump is tangent to the transient orbit, i.e., $u_1^{(1)} = u_1^{(2)}$, for $\hat{E} = \bar{E}_1$, with

$$\bar{E}_1 = \frac{1}{27}\left(36\omega - \sqrt{(12\omega + 1)^3} - 1\right).$$

After completing the first jump, the solution will then evolve for 'time' $2L$ according to system (3.9). The 'time' $2L$ is the length of time for a solution flow from the first defect until it reaches the second defect, and it will satisfy

$$2L = \int_{u_1}^{u_2} \frac{1}{\pm\sqrt{\omega u^2 - u^4/2 + \hat{E}}}\, du, \tag{3.14}$$

where $2L = L_1 + L_2$, with L_1 is the time from $x = -L$ to $x = 0$ and L_2 is the time from $x = 0$ to $x = L$. For $\epsilon = 1, L_1 = L_2 = L$. The result of the integration of the right hand side of (3.14) will be in the form of an elliptic integral of the first kind.

When the solution approaches $x = L$, the solution again jumps vertically in the phase plane according to the matching condition (3.10). The set of points that jumps to the stable manifold W^s is

$$J^{-1}(W^s) = \left\{ (u,y) | y = -\left(\sqrt{\omega u^2 - \frac{1}{2}u^4} - \epsilon u \right) \right\}. \tag{3.15}$$

Let u_2 be the value of the solution at the second defect. The matching condition (3.10) gives

$$\epsilon^2 u_2^2 - 2\epsilon u_2 \sqrt{\omega u_2^2 - \frac{1}{2}u_2^4} = \hat{E}, \tag{3.16}$$

which can also be re-written as a cubic polynomial in u_2^2,

$$u_2^6 + \left(\frac{\epsilon^2}{2} - 2\omega \right) u_2^4 - \hat{E} u_2^2 + \frac{\hat{E}^2}{2\epsilon^2} = 0. \tag{3.17}$$

Using a similar argument, the solution exists only for $\omega > \epsilon^2/4$, where in that case the solutions are given by

$$\begin{aligned} u_2^{(1)} &= \left(\frac{1}{3}\left(2\omega - \frac{\epsilon^2}{2} \right) + \frac{1}{3}\sqrt{12\hat{E} + (\epsilon^2 - 4\omega)^2} \cos\theta \right)^{1/2}, \\ u_2^{(2)} &= \left(\frac{1}{3}\left(2\omega - \frac{\epsilon^2}{2} \right) - \frac{1}{3}\sqrt{12\hat{E} + (\epsilon^2 - 4\omega)^2} \sin\left(\frac{\pi}{6} - \theta \right) \right)^{1/2}, \end{aligned} \tag{3.18}$$

where

$$\theta = \frac{1}{3}\cos^{-1}\left(-\frac{54\hat{E}^2 + 18\hat{E}\left(\epsilon^4 - 4\omega\epsilon^2\right) + \epsilon^2\left(\epsilon^2 - 4\omega\right)^3}{\epsilon^2\left(12\hat{E} + (\epsilon^2 - 4\omega)^2\right)^{3/2}} \right).$$

Similar for the first jump, the landing curve of the second jump is tangent to the transient orbit, i.e., $u_2^{(1)} = u_2^{(2)}$, for $\hat{E} = \bar{E}_2$, with

$$\bar{E}_2 = \frac{1}{27}\left(36\epsilon^2\omega - \sqrt{\epsilon^2(12\omega + \epsilon^2)^3} - \epsilon^4 \right).$$

For a given value of $\bar{E}_1$ and $\bar{E}_2$, they correspond to certain values of L, say $\bar{L}_1$ and $\bar{L}_2$. These values will be used in determining the stability of the solution which will be discussed later in Section 3.4. For fixed L and ϵ, we can obtain $\hat{E}$ upon substitution of (3.13) and (3.18) to (3.14) as function of ω, and therefore we can obtain positive-valued bound states for varying ω.

We present in Figure 3.2 and Figure 3.3 nonlinear bound states of our system for $L = 1$ for $\epsilon = 1$ and $\epsilon = 0.95$, respectively. We show the solution profiles in the physical space and in the phase plane on the left and right panels, respectively. We also calculate squared norms P of the solutions for varying ω. We plot them in Figure 3.4. The solid and dashed lines represent the stable and unstable solutions, respectively, which will be discussed in Section 3.4.

As mentioned at the end of Section 3.2, indeed standing waves of positive solutions bifurcate from the linear mode ω_0. For $\epsilon = 1$, as ω increases, there is a threshold value of the parameter where a pitchfork bifurcation appears. This is a symmetry breaking bifurcation. Beyond the critical value, we have two types of standing waves, i.e., symmetric and asymmetric states. There are two asymmetric solutions that are mirror to each other. Later in Section 3.4, we will see that the symmetric state becomes unstable beyond the critical value and the appearing asymmetric one becomes the stable solution.

When we consider $\epsilon = 0.95$, it is interesting to note that the pitchfork bifurcation becomes broken, i.e. unfolded. The branch of asymmetric solutions splits into two branches and that of symmetric ones breaks into two parts. The upper part of the symmetric branch gets connected to one of the asymmetric branches through a turning point.

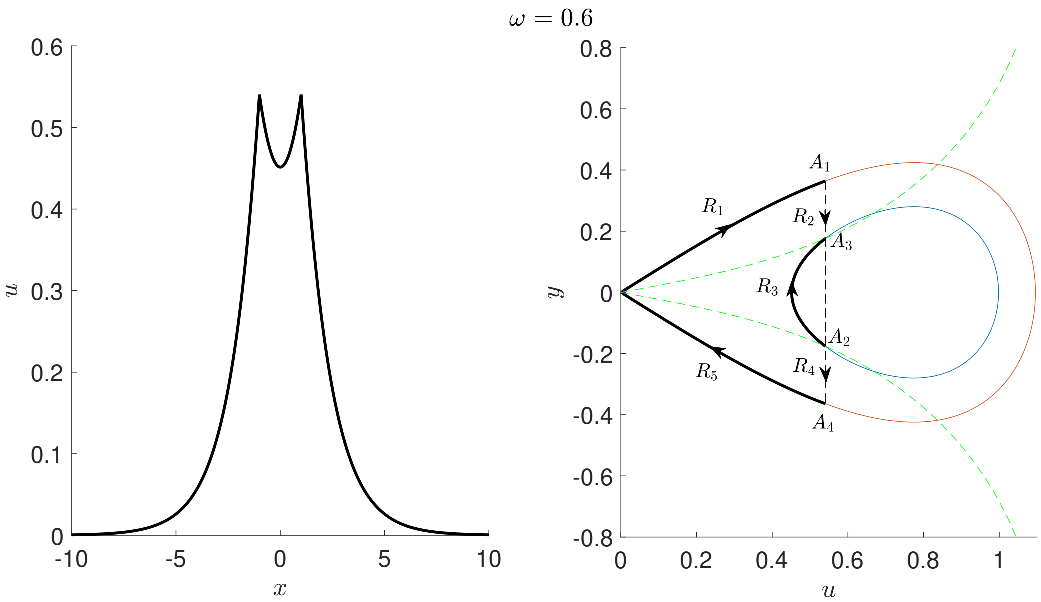

(a)

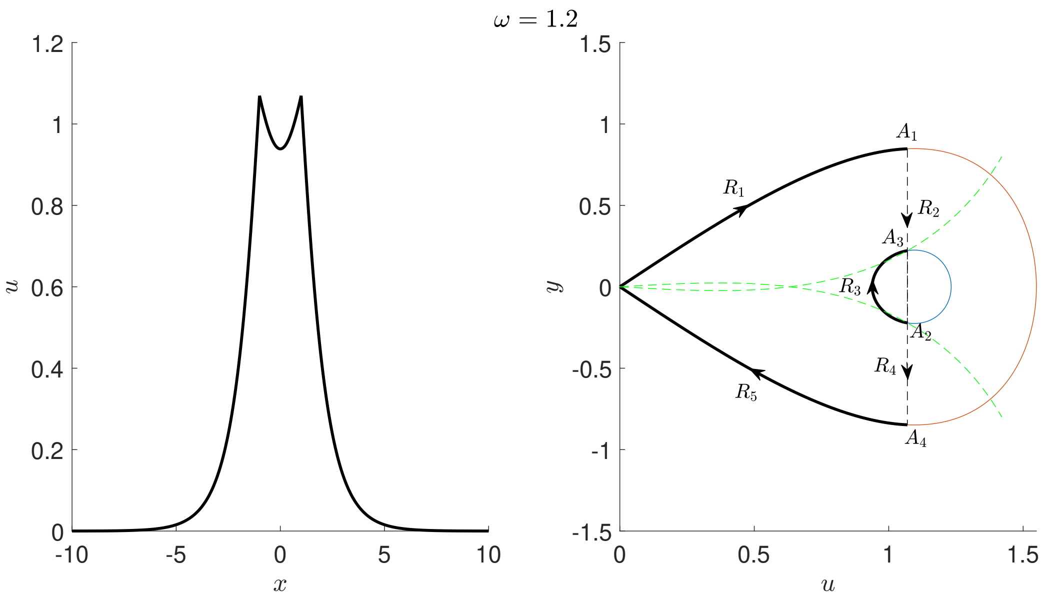

(b)

Figure 3.2. Localised standing waves of the system for $L = \epsilon = 1$ with various values of ω with u_1 and u_2 given by (a) $u_1^{(2)}$ and $u_2^{(2)}$, (b) $u_1^{(1)}$ and $u_2^{(1)}$, (c) $u_1^{(2)}$ and $u_2^{(1)}$, (d) $u_1^{(1)}$ and $u_2^{(2)}$, respectively.

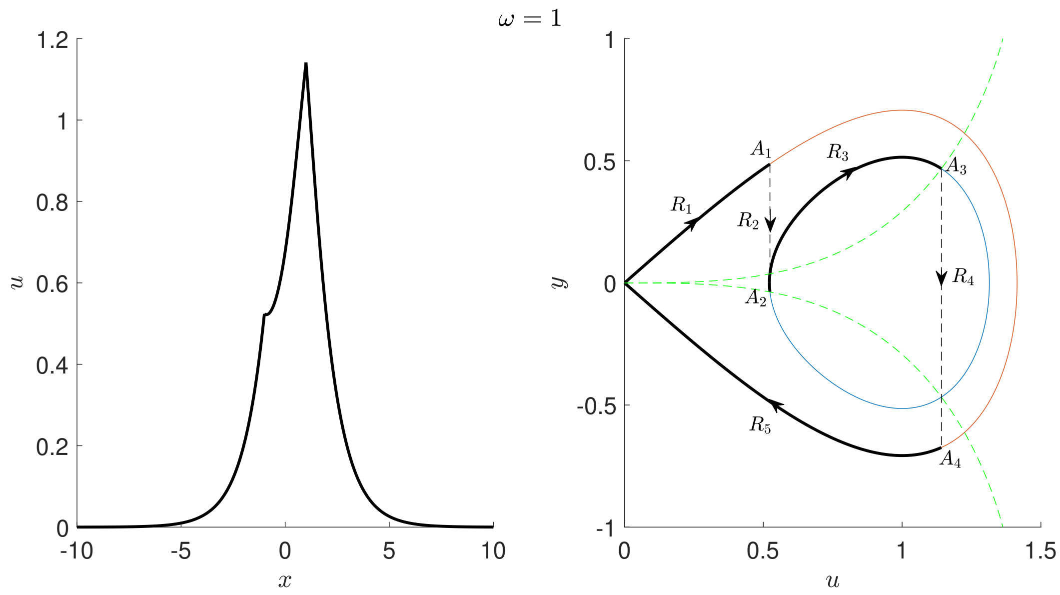

(c)

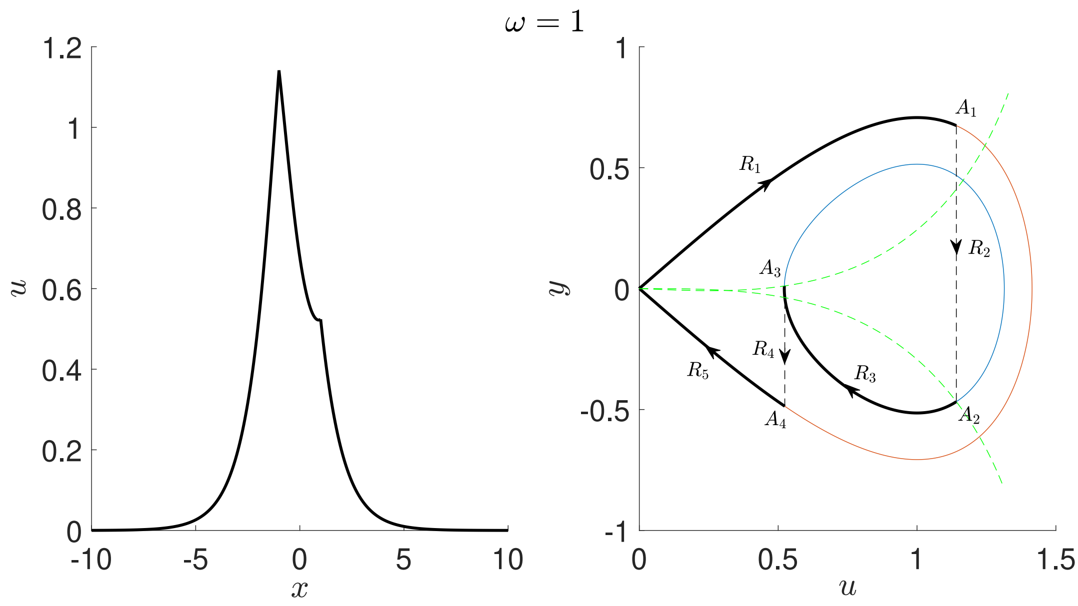

(d)

Figure 3.2. (Continued)

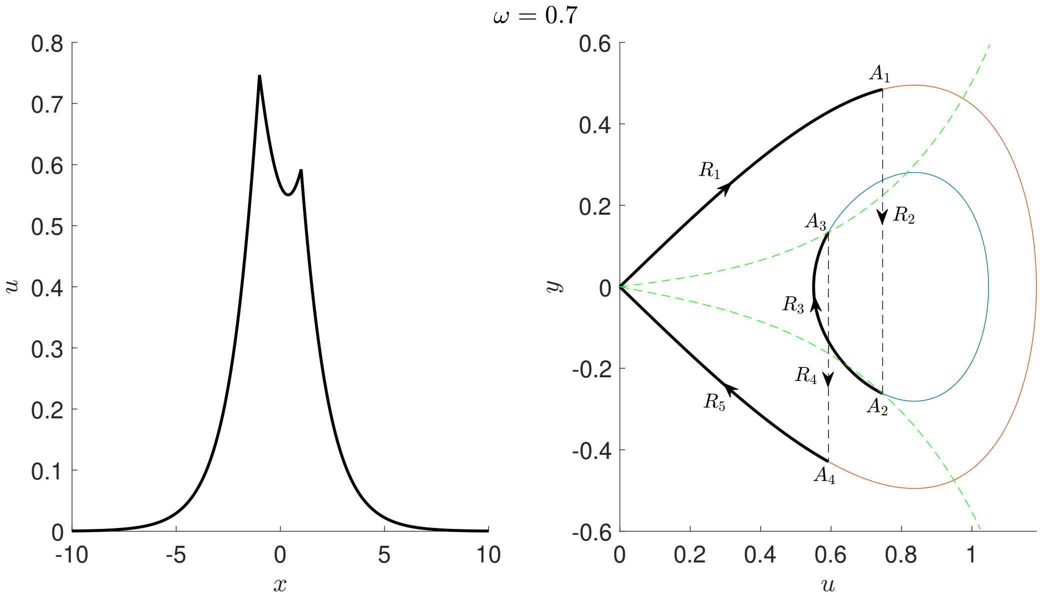

(a)

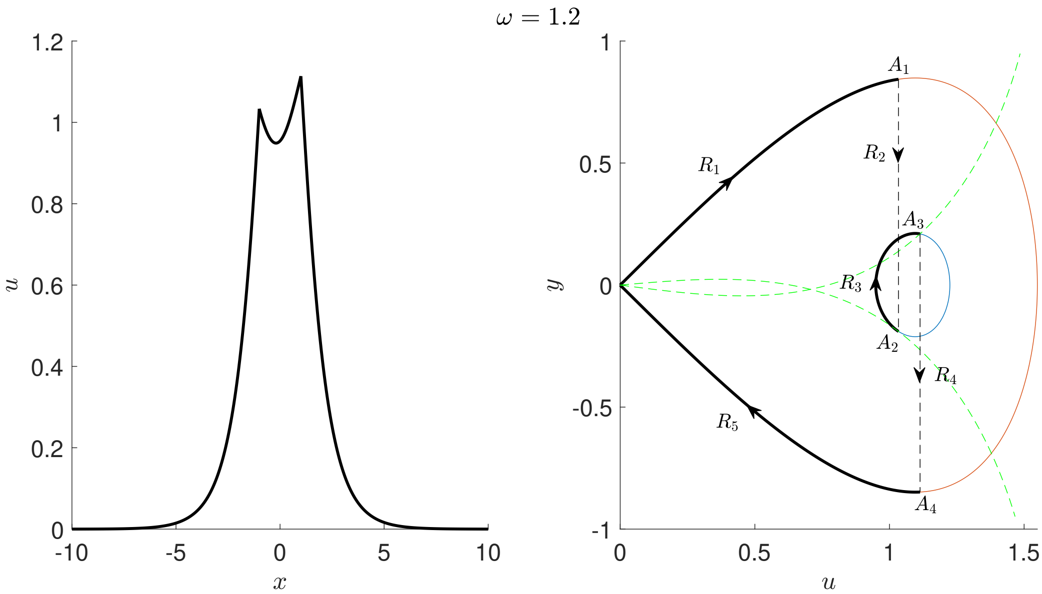

(b)

Figure 3.3. The same as Figure 3.2, but for $\epsilon = 0.95$ with u_1 and u_2 given by (a) $u_1^{(1)}$ and $u_2^{(2)}$, (b) $u_1^{(1)}$ and $u_2^{(1)}$, (c) $u_1^{(2)}$ and $u_2^{(1)}$, (d) $u_1^{(1)}$ and $u_2^{(2)}$, respectively.

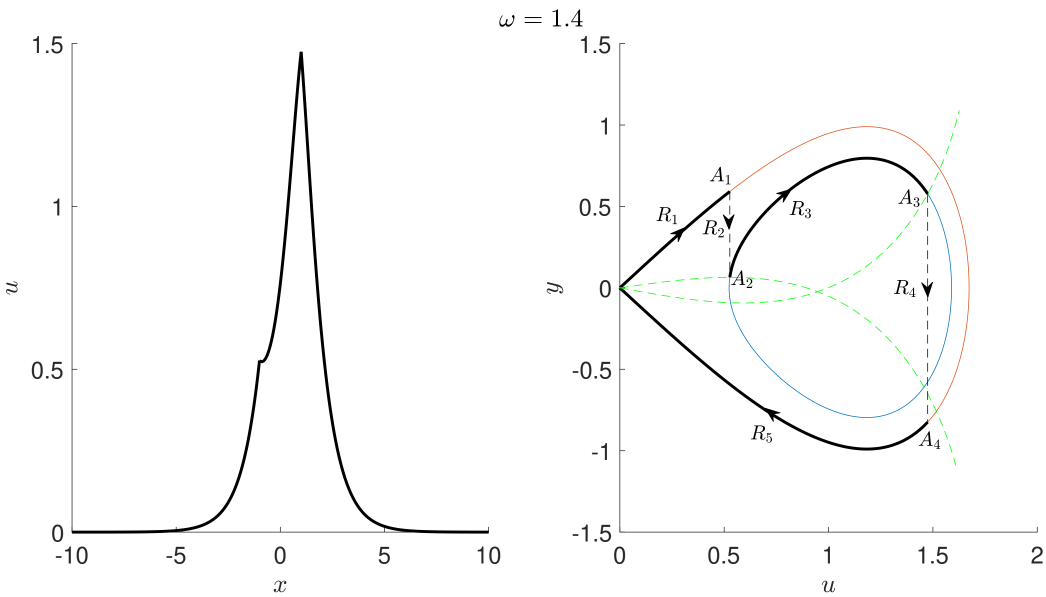

(c)

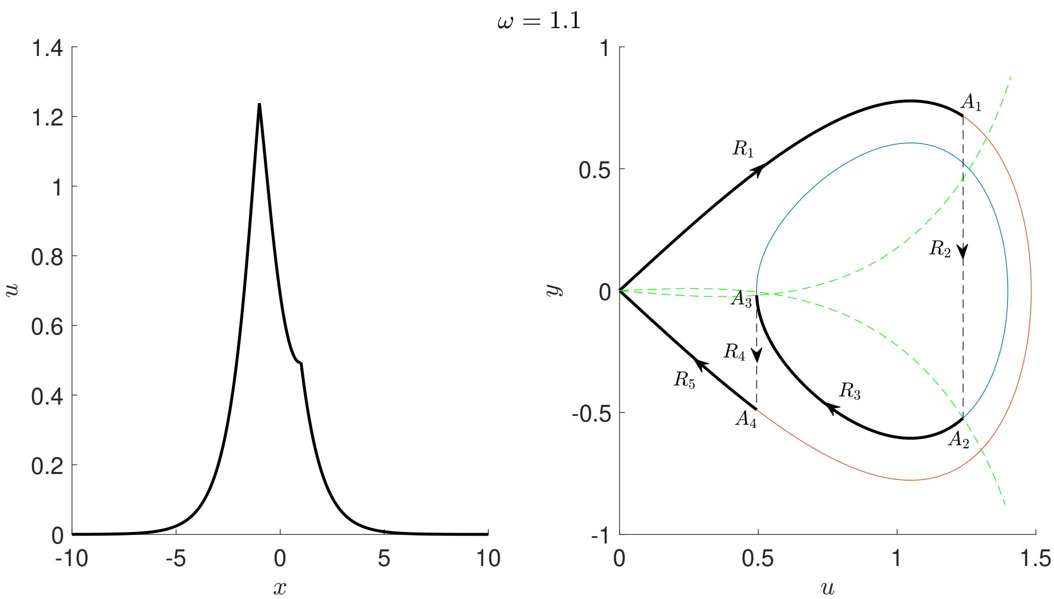

(d)

Figure 3.3. (Continued)

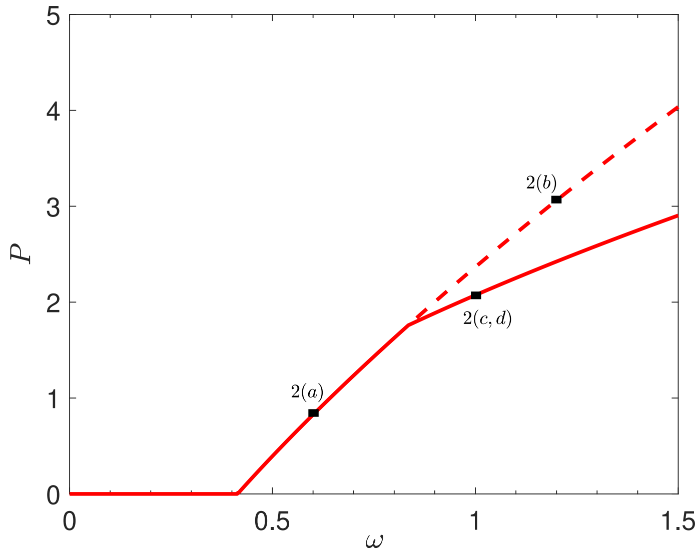

(a)

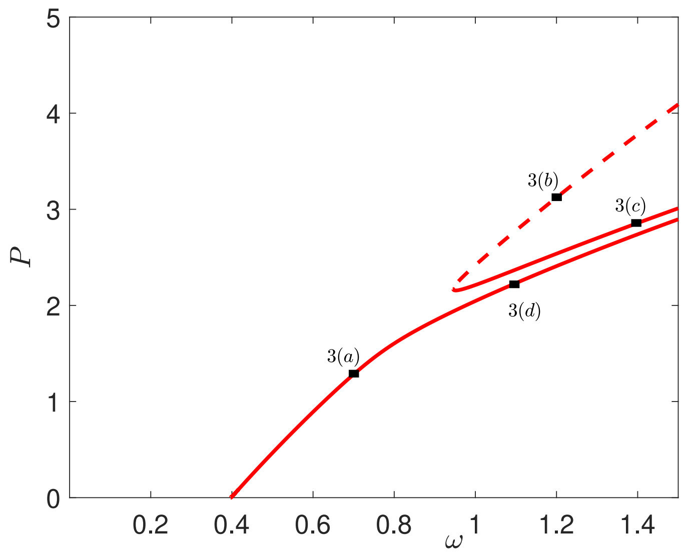

(b)

Figure 3.4. Bifurcation diagrams of the standing waves. Plotted are the squared norms as a function of ω for $L = 1$, and (a) $\epsilon = 1$, (b) $\epsilon = 0.95$.

Using our phase plane analysis, we can determine the critical value of ω where the bifurcation occurs. The critical value ω_c as function of $\hat{E}$ can be determined implicitly from the condition when the two roots of u_1 (3.13) merge, i.e.,

$$\hat{E} = \frac{1}{27}\left(36\epsilon^2\omega - \sqrt{\epsilon^2(12\omega+\epsilon^2)^3} - \epsilon^4\right). \tag{3.19}$$

Substituting this expression into the integral equation (3.14), we can solve it numerically to give us the critical ω for fixed L and ϵ. For $\epsilon = 1$, we obtain that $\omega_c \approx 0.8186$ and for $\epsilon = 0.95$ we have $\omega_c \approx 0.945$ which agree with the plot in Figure 3.4.

3.3.2 Explicit expression of solutions

The solutions plotted in Figure 3.2 and Figure 3.3 can also be expressed explicitly as piecewise continuous functions in terms of Jacobi elliptic function, $\mathrm{dn}(rx,k)$. The autonomous system (3.9) has solution

$$h(x) = a\,\mathrm{dn}(rx,k)$$

with $r(a,\omega) = \frac{a}{\sqrt{2}}$ and $k(a,\omega) = \frac{2(a^2-\omega)}{a^2}$ (see Appendix B). Note that for $a = \sqrt{2\omega}$ we have the homoclinic orbit $h(x) = \sqrt{2\omega}\,\mathrm{sech}(\sqrt{\omega}x)$. Therefore, the analytical solution of (3.3) is

$$u(x) = \begin{cases} \sqrt{2\omega}\,\mathrm{sech}(\sqrt{\omega}(x+\xi_1)), & \text{for } x < -L, \\ a\,\mathrm{dn}(r(x+\xi_2),k), & \text{for } -L < x < L, \\ \sqrt{2\omega}\,\mathrm{sech}(\sqrt{\omega}(x+\xi_3)), & \text{for } x > L, \end{cases} \tag{3.20}$$

where the constants ξ_1, ξ_2, and ξ_3 can be obtained from

$$\begin{aligned}
\xi_1 &= \frac{1}{\sqrt{\omega}}\,\mathrm{sech}^{-1}\left(\frac{u_1}{\sqrt{2\omega}}\right) + L,\\
\xi_2 &= \frac{1}{r}\mathrm{dn}^{-1}\left(\frac{u_1}{a}, k\right) + L,\\
\xi_3 &= \frac{1}{\sqrt{\omega}}\,\mathrm{sech}^{-1}\left(\frac{u_2}{\sqrt{2\omega}}\right) - L.
\end{aligned} \tag{3.21}$$

The value of u_1 and u_2 are the same as those discussed in Section 3.3.1. Note that the Jacobi elliptic function is doubly-periodic. We therefore need to choose the constants ξ_2 carefully such that the solution satisfies the boundary conditions (3.5).

3.4 Stability

After we obtain the standing waves, we will now discuss their stability by solving the corresponding linear eigenvalue problem. We linearise (3.1) about a standing wave solution $\tilde{u}(x)$ that has been obtained previously using the linearisation ansatz $\Psi = \left(\tilde{u}(x) + \delta(pe^{\lambda t} + q^* e^{\lambda^* t})\right)e^{i\omega t}$, with $\lambda \in \mathbb{C}$, and $\delta \ll 1$. Considering terms linear in δ leads to the eigenvalue problem

$$\lambda \begin{pmatrix} p \\ q \end{pmatrix} = \begin{pmatrix} 0 & -\mathcal{L}_- \\ \mathcal{L}_+ & 0 \end{pmatrix} \begin{pmatrix} p \\ q \end{pmatrix} = N \begin{pmatrix} p \\ q \end{pmatrix} \tag{3.22}$$

where

$$\begin{aligned}
\mathcal{L}_- &= \frac{d^2}{dx^2} - \omega + \tilde{u}^2(x) - V(x),\\
\mathcal{L}_+ &= \frac{d^2}{dx^2} - \omega + 3\tilde{u}^2(x) - V(x).
\end{aligned}$$

A solution is unstable when $\mathrm{Re}(\lambda) > 0$ for some λ and is linearly stable otherwise.

We will use dynamical systems method and geometric analysis to determine the stability of the standing waves. Let P be the number of positive eigenvalues of $\mathcal{L}_+$ and Q be the number of positive eigenvalues of $\mathcal{L}_-$, then we have the following theorem [75].

Theorem 3.4.1. *If* $P - Q \neq 0$ *or* 1, *there is a real positive eigenvalue of the operator* N.

Using the Sturm-Liouville Theorem (Theorem 2.1.14), P and Q can be determined by considering solutions of $\mathcal{L}_+ p = 0$ and $\mathcal{L}_- q = 0$, respectively. The system $\mathcal{L}_- q = 0$ is satisfied by standing wave $u(x)$, then Q is the number of zeros of standing wave $u(x)$. Since we only consider positive solutions, then $Q = 0$. By the Theorem 3.4.1, to prove that the standing wave is unstable, we only need to prove that $P \geq 2$. The system $\mathcal{L}_+ p = 0$ is the variational equation for (3.9) where we can interpret that $\mathcal{L}_+$ evolves the tangent vector under the flow. As P is the number of zeros of a solution to the variational equation along $u(x)$, then P can be interpreted as the number of times the tangent vector initially from the origin, $(u, y) = (0, 0)$, crosses the verticality. The tangent vector crosses the verticality means that its slope changes from negative to positive or vice versa, i.e., it will crosses the vertical line (the line parallel to $y-$axis).

Let $\mathbf{p}(u, y)$ be a tangent vector to the outer orbit of the solution at the point (u, y) in the phase portrait, and let $\mathbf{q}(u, y)$ be a tangent vector to the inner orbit at the point (u, y).

$$\mathbf{p} = \begin{pmatrix} y \\ \\ \omega u - u^3 \end{pmatrix} = \begin{pmatrix} \pm\sqrt{\omega u^2 - \frac{1}{2}u^4} \\ \\ \omega u - u^3 \end{pmatrix},$$

and

$$\mathbf{q} = \begin{pmatrix} \hat{y} \\ \\ \omega u - u^3 \end{pmatrix} = \begin{pmatrix} \pm\sqrt{\omega u^2 - \frac{1}{2}u^4 + \hat{E}} \\ \\ \omega u - u^3 \end{pmatrix}.$$

Let F be the flow, so $F(\mathbf{s})$ is the image of $\mathbf{s}$ under the flow (together with the matching conditions at the defects). We count the number of times the tangent vector started from the origin, say $\mathbf{b}(u, y)$, crosses the vertical as its initial point moves along the orbit as x increases. The variational flow preserves the orientation of the vector tangent [76], if there are two vectors tangent to the phase space at (u, y), then the sign of the cross product of the two vectors is unchanged under the flows. Since vector $\mathbf{b}$ is no longer tangent to the orbit due to its defects, we will use each of the corresponding tangent vectors as the bound of the solution as it evolves. We will split the orbit into five regions. Let A_1,A_2,A_3, and A_4 denote the point (u_1, y_1), $(u_1, y_1 - u_1)$, $(u_2, \epsilon u_2 + y_2)$, and (u_2, y_2), respectively, with $y_1 = \sqrt{\omega u_1 - \frac{1}{2}u_1^4}$ and $y_2 = -\sqrt{\omega u_2 - \frac{1}{2}u_2^4}$. The first region labelled by R_1 is for $x < -L$. On the phase plane, it starts from the origin until point A_1. The second region, R_2, is when $x = -L$, i.e. when the solution jumps at the first time from A_1 to A_2. The third region, R_3, is when $-L < x < L$ where the differential equation (3.9) takes the tangent vector from A_2 to point A_3. The fourth region, R_4, is when $x = L$ where the solution jumps for the second time, it jumps from A_3 to A_4, and last region, R_5, is for $x > L$ where the vector will be brought back to the origin.

Let $n_i, i = 1, 2, \ldots, 5$, denote the number of times $\mathbf{b}$ passes through the verticality in the ith region. In the following, we will count n_i in each region. The tangent vector solves the variational flow

$$
\begin{aligned}
q_{1,x} &= q_2, \\
q_{2,x} &= q_1 - 3\tilde{u}^2 q_1,
\end{aligned}
\tag{3.23}
$$

where $\tilde{u}$ is the stationary solution.

3.4.1 Trajectories in R_1 (the case where $x < -L$)

At the first region, we will count n_1. It is the region when **b** starts from the origin and moves along the homoclinic orbit until it reaches the first defect at A_1. The trajectories are labelled by R_1 in Figure 3.2 and Figure 3.3. At this region, the direction of **b** at (u, y) is

$$\tan\theta = \frac{\omega u - u^3}{y} = \frac{\omega - u^2}{\sqrt{1 - \frac{1}{2}u^2}}.$$

The sign of $\tan\theta$ depends on the sign of $\omega - u^2$. For $u < \sqrt{\omega}$, $\tan\theta > 0$, and for $u > \sqrt{\omega}$, the sign is opposite. Since $y > 0$, **b** points up right in the first quadrant of the plane for the first case, and it points down right in the fourth quadrant for the latter. Therefore, for both cases, the angle must be acute, $0 < |\theta| < \frac{\pi}{2}$. In this part, $n_1 = 0$. In what follows we will refer to θ as *the angle of* **b**.

3.4.2 Trajectories in R_2 (the case where $x = -L$)

Next, we will count how many times **b** passes through the vertical when it jumps from A_1 to A_2. The vector **b** at A_2 is

$$\mathbf{b}(A_2) = \begin{pmatrix} y_1 \\ \omega u_1 - u_1^3 - y_1 \end{pmatrix}$$

and its direction is $\tan\theta_2 = \tan\theta_1 - 1$ with θ_i the direction of **b** in region i. It implies that at the first defect, the vector **b** jumps through a smaller angle and larger angle for $L_1 < \bar{L}_1$ and $L_1 > \bar{L}_1$, respectively. After the jump, **b** is tangent to the landing curve $J(W^u)$ but no longer tangent to the orbit of the solution. For $L_1 = \bar{L}_1$, after the jump **b** will be tangent to the transient orbit but in opposite direction. For all cases, **b** does not pass through the vertical. So, up to this stage, $P = n_1 + n_2 = 0$. The trajectories are labelled by R_2 in Figure 3.2 and Figure 3.3.

3.4.3 Trajectories in R_3 (the case where $-L < x < L$)

Vector $\mathbf{b}(A_2)$ now moves along the flow following Equation (3.9) to point $\mathbf{b}(A_3)$. The variational flow (3.23) will preserve the orientation of vector **b** with respect to the tangent vector of the inner orbit, so **q** gives a bound for **b** as it evolves. After the first jumping, vector **b** points towards into the center (or the concave side) of the inner orbit for $L_1 < \bar{L}_1$, and it will point down and out the inner orbit for $L_1 > \bar{L}_1$. On the other hand, for $L_1 = \bar{L}_1$, the landing curve $J(W^u)$ is tangent to the inner orbit to which

b jumps, so **b** is still tangent to the orbit but now pointing backward. Comparing vector **b** with the vector $\mathbf{q}(A_3)$, then up to this point $n_3 = 0$ or 1. The trajectories are labelled by R_3 in Figure 3.2 and Figure 3.3.

3.4.4 Trajectories in R_4 (the case where $x = L$)

In this region, we will count how many times **b** crosses the vertical when it jumps from A_3 to A_4, i.e., when $\mathbf{b}(A_3)$ is mapped to $\mathbf{b}(A_4)$. In this region labelled by R_4 in Figure 3.2 and Figure 3.3, the tangent vector at A_3, $\mathbf{q}(A_3)$, will be mapped to $F(\mathbf{q}(A_3))$ which has smaller angle, and the jump does not give any additional crossing of the verticality, therefore $n_4 = 0$

3.4.5 Trajectories in R_5 (the case where $x > L$)

In this region, again the vector will move along the flow following the differential equation back to the origin. We will observe how the landing curve $J^{-1}(W^s)$ intersecting the inner orbit yields an additional vertical crossing or not. First, we look at the case $L_1 < \bar{L}_1$, at the second defect the vector **b** still points to the transient orbit. We can see that **b** is lower than the vector that is taken to the curve W^s which is tangent to $J^{-1}(W^s)$, i.e. **b** has a larger angle. Comparing these two vectors, in this region, there will be no additional crossing to the vertical.

Now, for the case $L_1 \geq \bar{L}_1$, if $L_2 > \bar{L}_2$ at the second defect, vector **b** is pointing out the transient orbit and compare to the vector that is tangent to $J^{-1}(W^s)$, **b** has a smaller angle. After the jump, the flow pushes it to cross the verticality, so in

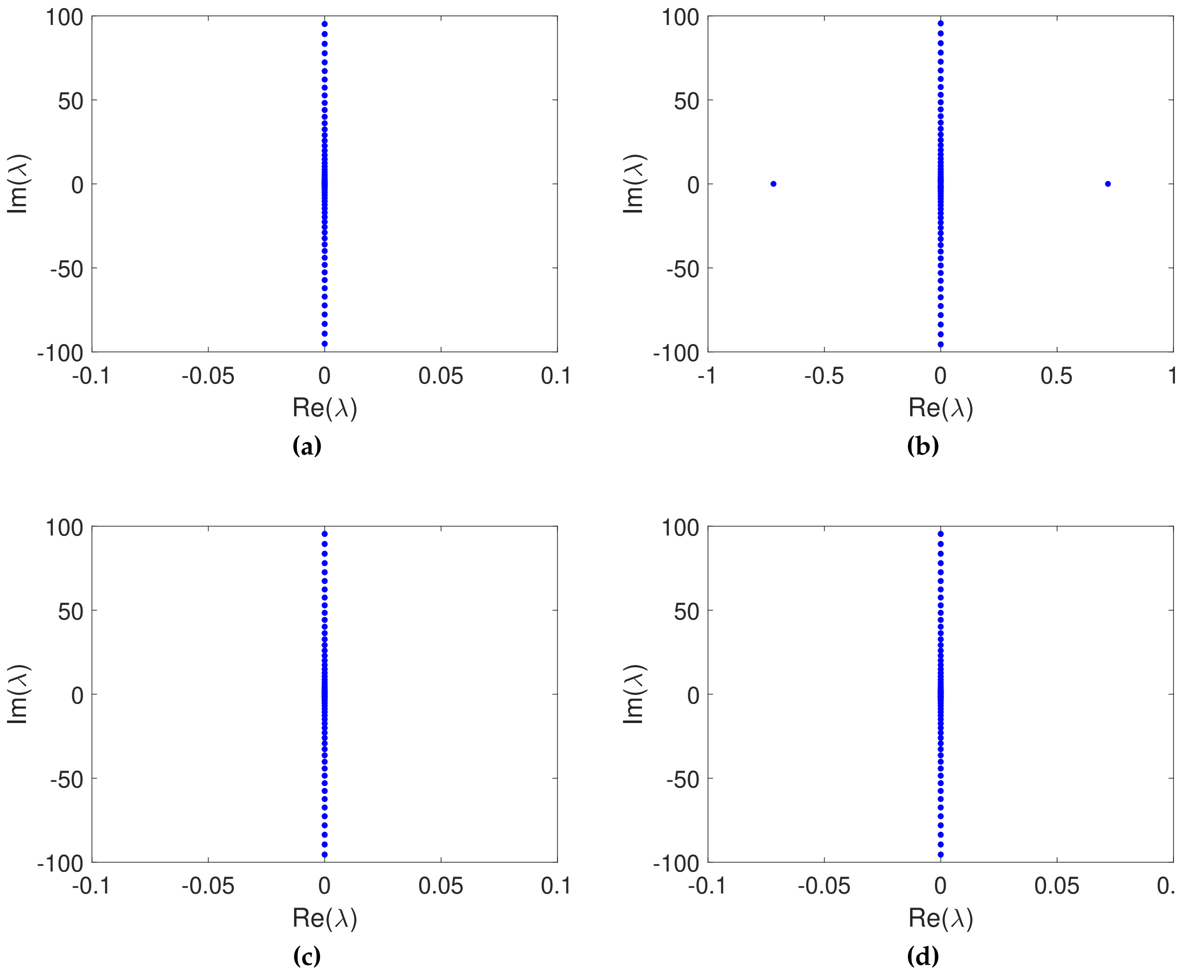

Figure 3.5. Spectrum in the complex plane of the solutions in Figure 3.2 in the same order. Panels (c) and (d) are exactly identical because the solutions are mirror symmetric to each other.

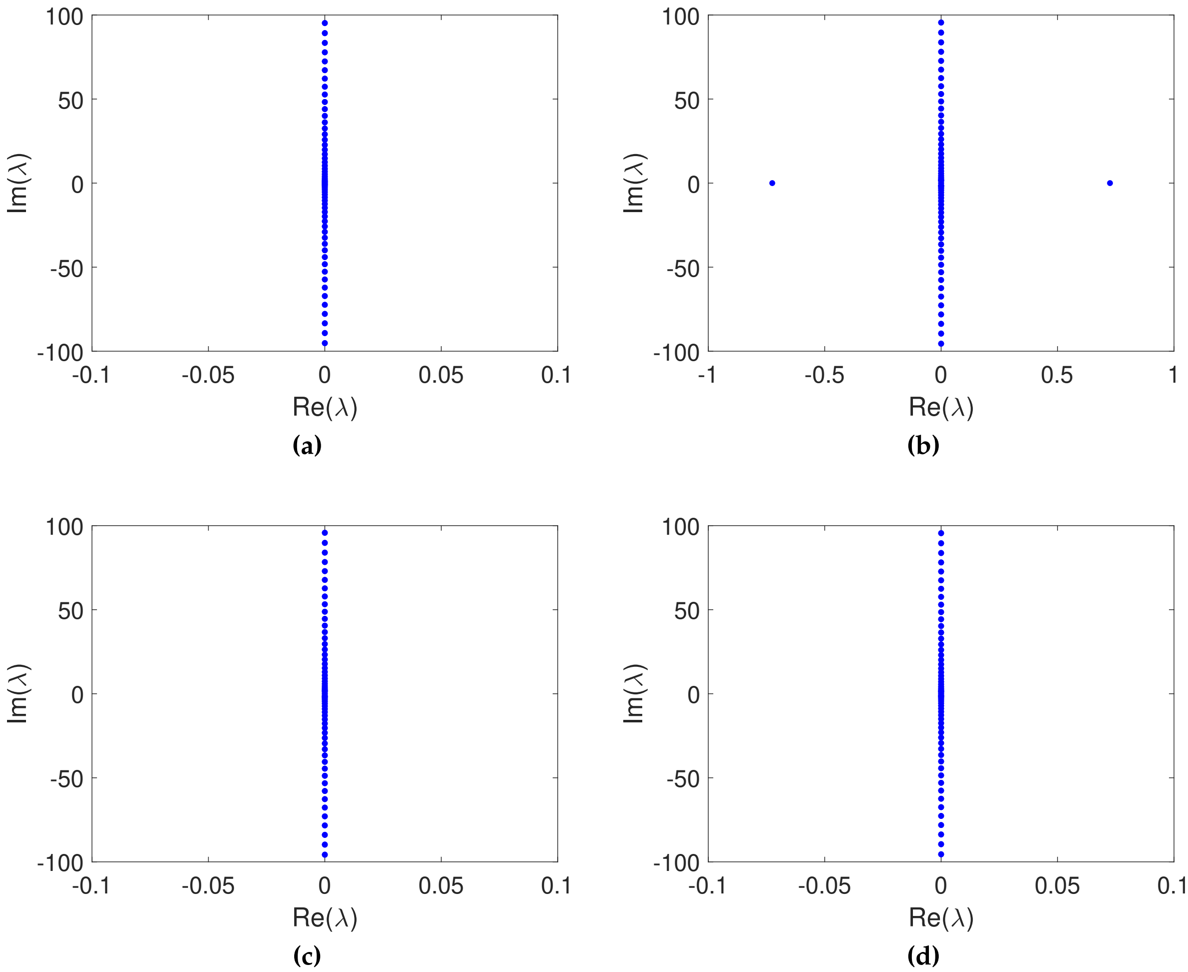

Figure 3.6. The same as Figure 3.5, but for the solitons in Figure 3.3.

this case $P \geq 2$. If $L_2 \leq \bar{L}_2$, **b** has a larger angle, then it does not give any additional crossing. The trajectories are labelled by R_5 in Figure 3.2 and Figure 3.3.

To summarise, we have the following results.

Theorem 3.4.2. *The positive definite homoclinic solutions of* (3.3)-(3.5) *with* $L_1 < \bar{L}_1$ *will have* $P \leq 1$. *If they have* $L_1 \geq \bar{L}_1$, *then there are two possible cases, i.e., either* $L_2 < \bar{L}_2$ *or* $L_2 \geq \bar{L}_2$. *The former case gives* $P \leq 1$, *while the latter yields* $P \geq 2$.

Using Theorem 3.4.1, the last case will give an unstable solution through a real eigenvalue. Solutions in Figures 3.2a, 3.2c, and 3.3c correspond to $L_1 < \bar{L}_1$. Solutions in Figures 3.2d, 3.3a and 3.3d correspond to $L_1 > \bar{L}_1$, but $L_2 < \bar{L}_2$. In those cases, we cannot determine their stability. Using numerics, our results in the next section show that they are stable. On the other hand, for the solutions in Figure 3.2b and 3.3b, $L_1 > \bar{L}_1$ and at the same time $L_2 > \bar{L}_2$. Hence, they are unstable.

3.5 Numerical results

We solved Equations (3.4) and (3.5) as well as Equation (3.22) numerically to study the localised standing waves and their stability, where a central finite difference is used to approximate the Laplacian with a relatively fine discretisation. While the results in Section 3.4 only tell us whether the solutions are unstable or not, here we present their spectrum obtained from solving the eigenvalue problem numerically.

We plot the spectrum of solutions in Figure 3.2 and 3.3 in Figure 3.5 and 3.6, respectively. We confirm the result of Section 3.4 that solutions plotted in panel (b) of Figure 3.2 and 3.3 are unstable. The instability is due to the presence of a pair of real eigenvalues.

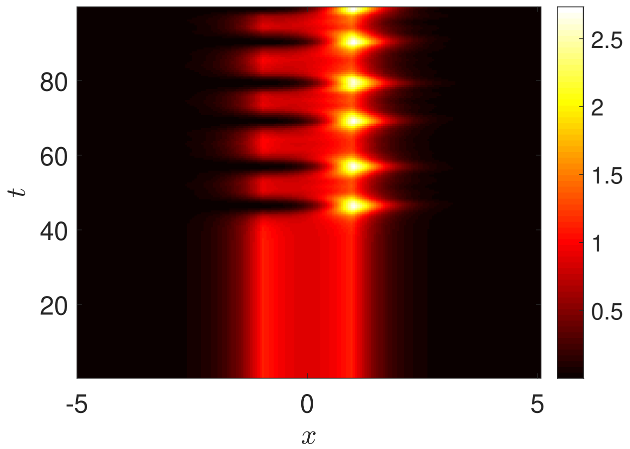

Figure 3.7. Time dynamics of the unstable solution in Figure 3.3b. The squared magnitude $|\Psi|^2$ is plotted against x and t with $L = 1$ and $\epsilon = 0.95$. Initially the standing wave is perturbed randomly.

When a solution is unstable, it is interesting to see its typical dynamics. To do so, we solve the governing equation (3.1) numerically where the Dirac delta potential is incorporated through the boundaries, see (3.5). While the spatial discretisation is still the same as before, the time derivative is integrated using the classic fourth-order Runge-Kutta method.

In Figure 3.7 we plot the temporal dynamics of the unstable solution shown in panel (b) of Figure 3.3. The time evolution is typical where the instability manifests in the form of periodic oscillations. The norm of the solution tends to be localised in one of the wells, which is the characteristics of the presence of symmetry breaking solutions [34, 49–51, 74].

3.6 Conclusion

In this chapter, we have considered broken symmetry breaking bifurcations, i.e. unfolded pitchfork bifurcations, in the NLS on the real line with an asymmetric double Dirac delta potential. By using a dynamical system approach, we presented the ground state solutions in the phase plane and their explicit expressions. We have shown that in contrast to the symmetric case where the bifurcation is of a pitchfork type, when the potential is asymmetric, the bifurcation is of a saddle node type. The linear instability of the corresponding solutions has been derived as well, using a geometrical approach developed by Jones [75]. Numerical computations have been presented illustrating the analytical results and simulations showing the typical dynamics of unstable solutions which have also been discussed.

Chapter 4

Dynamics of the nonlinear Schrödinger equations with delta potential on star graphs

In this chapter, we adventure into a new idea by considering the NLS equation on a three-edge star graph with a Dirac delta potential on each arm and study symmetry breaking bifurcation in the system. Star graph is a metric graph, i.e., a network-shaped structure of vertices connected by edges. The Schrödinger equation is suitably defined on the edges with boundary conditions describing the vertex. It can arise as a model for wave propagations in systems similar to a thin neighbourhood of a graph and has been growing in recent years due to their potentials of becoming a paradigm model for topological effects in nonlinear wave propagation, see [60] for a recent review.

A remarkable difference from the nonlinear Schrödinger equation on the line is that three-edge star graphs with Kirchhoff conditions at the vertex do not admit a unique 'trapped soliton' state as the ground state [78]. We report in this chapter another notable difference between symmetry breaking bifurcation in a double-well potential on the real line and on star-graphs. While the real line can be considered as a two-edge star graph with two-fold symmetry, three-edge star graphs have rotational symmetry of degree three. By introducing a linear Dirac delta potential on each arm, we obtain subcritical and supercritical-like symmetry breaking bifurcations emanating from the same threshold point. This is remarkably different from the standard symmetry breaking bifurcation, where only one of the two types is possible [79]. We call one of the pitchfork bifurcations supercritical-like because both the symmetric and asymmetric states are unstable, which has been shown to be possible for the nonlinear Schrödinger equation with generalised external potentials [80]. Not only that, we also observe a critical distance of the external potential minima from the vertex below which no symmetry breaking occurs. While our system can be seen as a Schrödinger equation with a triple-well potential, it is completely different from the case on the real line [14, 81, 82], where the presence of a third well causes all bifurcations to be of saddle-node type.

In Section 4.1, we introduce the model. In Section 4.2, we discuss the underlying linear states of the system, where we derive a transcendental equation determining the bifurcation points of eigenstates from the zero solution. In the same section, we discuss the existence and stability of standing localised solutions of the nonlinear equation by means of the coupled mode (i.e., Lyapunov-Schmidt) reduction method where it reduces the problem to a finite-dimensional dynamical system. Then, the stability of the states is analysed in Section 4.3, where we show that there is a threshold point at which symmetric states become unstable. The critical distance of the external potential minima from the vertex below which symmetric states are always stable is also discussed. In Section 4.4, we perform numerical simulations for typical dynamics of the standing waves when they are unstable. Finally, we summarise our work in Section 4.5.

4.1 Mathematical model

Our domain is a graph $\mathcal{G}$ constituted by three semi-infinite lines attached to a common vertex. The Schrödinger equation is then posed on the Hilbert space $L^2(\mathcal{G}) = \bigoplus_{k=1}^{3} L^2(\mathbb{R}^+)$. The wave function along each semi-infinite line is described by

$$i\Psi_t^{(k)} = -\Psi_{xx}^{(k)} - |\Psi^{(k)}|^2\Psi^{(k)} - \delta(x-a)\Psi^{(k)}, \tag{4.1}$$

where the upper indices $k = 1,2,3,$ label the different branches of the system and the subscripts indicate derivatives with respect to the variables, and ω is the propgation constant. At the meeting point between the three branches, i.e., $x = 0$, we have the free Kirchoff boundary conditions

$$\sum_{k=1}^{3} \Psi_x^{(k)}(0,t) = 0, \quad \Psi^{(1)}(0,t) = \Psi^{(2)}(0,t) = \Psi^{(3)}(0,t). \tag{4.2}$$

Representing $\vec{\Psi}(x,t) = \bigoplus_{k=1}^{3} \Psi^{(k)}(x,t)$, where $x,t \in \mathbb{R}^+$, the function lives in the Sobolev space $H^1(\mathcal{G}) = \bigoplus_{k=1}^{3} H^1(\mathbb{R}^+)$.

The system (4.1) with (4.2) conserves the squared L^2 norm $P = ||\vec{\Psi}||^2 = \langle \vec{\Psi}, \vec{\Psi} \rangle$, where the inner product is defined as

$$\langle \vec{\Psi}_i, \vec{\Psi}_j \rangle = \sum_{k=1}^{3} \int_0^\infty \Psi_i^{(k)} \Psi_j^{*(k)} dx. \tag{4.3}$$

The quantity P is known as the optical power in the nonlinear optics context, or the number of particles in the context of Bose-Einstein condensates.

The nonlinear bound states of (4.1) have the form $\Psi(x,t) = \psi(x)e^{i\omega t}$, where $\psi(x)$ satisfies

$$\psi_{xx}^{(k)} - \omega\psi^{(k)} + \left(\psi^{(k)}\right)^3 + \delta(x-a)\psi^{(k)} = 0. \tag{4.4}$$

Our aim is to study solutions of (4.4) and determine their stability. To do so, the idea is to use a coupled mode reduction method to (4.1) by exploiting the eigenstates of the linearised system. For the nonlinear Schrödinger equation on the line with a double-well potential, it has been established that on large but finite time scales, the dynamics are controlled by a finite dimensional dynamical system [49, 83]. In this work, we assume that the result of [49, 83] can be extended to our case (with a proof being left for future work).

4.2 Coupled mode approximations

In the following, we will derive a coupled mode approximation of the governing equation (4.1). We begin by determining the linear eigenstates of the system. We then explain how to find solutions of (4.1) as continuation of the obtained eigenstates.

4.2.1 Linear states

In the limit $\psi \to 0$, Equation (4.4) is reduced to the linear system

$$\psi_{xx}^{(k)} - \omega\psi^{(k)} + \delta(x-a)\psi^{(k)} = 0. \tag{4.5}$$

This is equivalent to the linear system $\psi_{xx}^{(k)} - \omega\psi^{(k)} = 0$ for $x \neq a$ with the matching conditions

$$\psi^{(k)}(a^+) = \psi^{(k)}(a^-), \quad \psi_x^{(k)}(a^+) - \psi_x^{(k)}(a^-) = -\psi^{(k)}(a). \tag{4.6}$$

Note as well that at $x = 0$, we still have the boundary conditions (4.2).

The general solution of (4.5) is given by

$$\psi^{(k)} = \begin{cases} A^{(k)} e^{-\sqrt{\omega}(x-a)}, & x > a, \\ B^{(k)} e^{-\sqrt{\omega}(x-a)} + C^{(k)} e^{\sqrt{\omega}(x-a)}, & x < a. \end{cases} \tag{4.7}$$

Using the matching and boundary conditions, we obtain the following linear system in $A^{(k)}, B^{(k)}, C^{(k)}$

$$
\begin{aligned}
A^{(k)} - B^{(k)} - C^{(k)} &= 0, \ k = 1,2,3, \\
\left(1 - \sqrt{\omega}\right)A^{(k)} + \sqrt{\omega}B^{(k)} - \sqrt{\omega}C^{(k)} &= 0, \ k = 1,2,3, \\
\sum_{k=1}^{3}\left(-\sqrt{\omega}e^{a\sqrt{\omega}}B^{(k)} + \sqrt{\omega}e^{-a\sqrt{\omega}}C^{(k)}\right) &= 0, \\
e^{a\sqrt{\omega}}B^{(1)} + e^{-a\sqrt{\omega}}C^{(1)} - e^{a\sqrt{\omega}}B^{(2)} - e^{-a\sqrt{\omega}}C^{(2)} &= 0, \\
e^{a\sqrt{\omega}}B^{(2)} + e^{-a\sqrt{\omega}}C^{(2)} - e^{a\sqrt{\omega}}B^{(3)} - e^{-a\sqrt{\omega}}C^{(3)} &= 0,
\end{aligned}
\tag{4.8}
$$

which has nonzero solutions if the determinant of its coefficient matrix is zero. It implies that the function (4.7) will be a solution of the linear system only if ω satisfies the transcendental relation

$$\left(1-\left(2\sqrt{\omega}-1\right)e^{2a\sqrt{\omega}}\right)\left(1+\left(2\sqrt{\omega}-1\right)e^{2a\sqrt{\omega}}\right)^2 = 0. \tag{4.9}$$

This equation determines bifurcation points of the linear states.

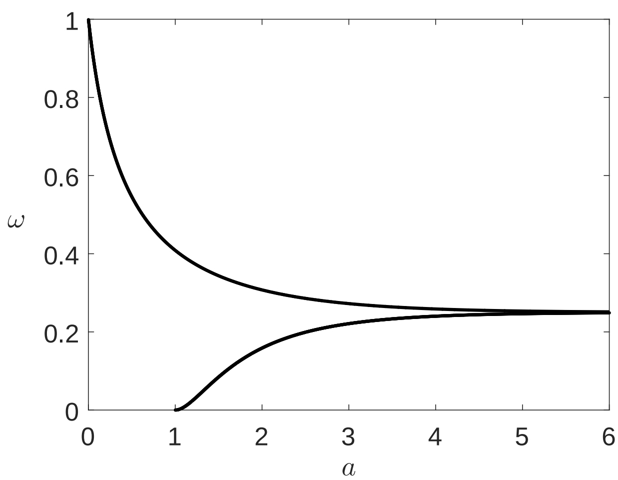

Figure 4.1. The eigenvalues as a function of a. The upper curve is ω_0.

Equation (4.9) gives us two eigenvalues ω_0 and ω_1 for $a \geq 1$ and one eigenvalue for $a < 1$. The eigenvalue ω_1 has multiplicity two, i.e.,

$$\begin{aligned} a &= -\ln\left(2\sqrt{\omega_0} - 1\right)/(2\sqrt{\omega_0}) \\ &\approx -\frac{1}{2}(\omega_0 - 1) + \frac{5}{8}(\omega_0 - 1)^2 - \frac{35}{48}(\omega_0 - 1)^3 + \cdots, \end{aligned} \tag{4.10}$$

and

$$\begin{aligned} a &= -\ln\left(1 - 2\sqrt{\omega_1}\right)/(2\sqrt{\omega_1}) \\ &\approx 1 + \sqrt{\omega_1} + \frac{4\omega_1}{3} + 2\omega_1^{3/2} + \cdots. \end{aligned} \tag{4.11}$$

We obtain that the eigenfunction with eigenvalue ω_0 exists for any a, while the other one only for $a \geq 1$. In the other limit $a \to \infty$, $\omega_0, \omega_1 \to 1/4$. The plot of (4.10) and (4.11) is given in Figure 4.1.

Let the corresponding eigenfunction to the eigenvalue ω_0 be denoted by $\psi_0(x)$, and the eigenspace corresponding to eigenvalue ω_1 be spanned by eigenfunctions $\psi_1(x)$ and $\psi_2(x)$. The eigenfunctions are given by

$$\psi_0^{(1)}(x) = \psi_0^{(2)}(x) = \psi_0^{(3)}(x) = \begin{cases} e^{-\sqrt{\omega_0}(x-a)}, & x > a, \\ -\frac{1-2\sqrt{\omega_0}}{2\sqrt{\omega_0}} e^{-\sqrt{\omega_0}(x-a)} + \frac{1}{2\sqrt{\omega_0}} e^{\sqrt{\omega_0}(x-a)}, & x < a, \end{cases} \tag{4.12a}$$

$$\begin{aligned} \psi_1^{(1)}(x) &= \begin{cases} e^{-\sqrt{\omega_1}(x-a)}, & x > a, \\ -\frac{1-2\sqrt{\omega_1}}{2\sqrt{\omega_1}} e^{-\sqrt{\omega_1}(x-a)} + \frac{1}{2\sqrt{\omega_1}} e^{\sqrt{\omega_1}(x-a)}, & x < a, \end{cases} \\ \psi_1^{(2)}(x) &= -\psi_1^{(1)}(x), \\ \psi_1^{(3)}(x) &= 0, \end{aligned} \tag{4.12b}$$

$$\psi_2^{(1)}(x) = \begin{cases} e^{-\sqrt{\omega_1}(x-a)}, & x > a, \\ -\frac{1-2\sqrt{\omega_1}}{2\sqrt{\omega_1}} e^{-\sqrt{\omega_1}(x-a)} + \frac{1}{2\sqrt{\omega_1}} e^{\sqrt{\omega_1}(x-a)}, & x < a, \end{cases}$$

$$\psi_2^{(2)}(x) = \psi_2^{(1)}(x),$$

$$\psi_2^{(3)}(x) = -2\psi_2^{(1)}(x). \tag{4.12c}$$

Using the inner product defined in (4.3), one can compute that ψ_0, ψ_1, and ψ_2 are orthogonal to each other. We plot the eigenfunctions in Figure 4.2. The positive definite mode ψ_0 is the ground state, while ψ_1 and ψ_2 are excited states.

4.2.2 Formulation of the finite dimensional system

In this subsection, we will derive a finite dimensional system of the governing equation (4.1) using a coupled mode reduction method that restricts the system to the bound state manifold. Let the ansatz for solutions of the nonlinear equation (4.1) be

$$\psi(x,t) = c_0(t)\psi_0(x) + c_1(t)\psi_1(x) + c_2(t)\psi_2(x), \tag{4.13}$$

where abusing the notation ψ_j, $j = 0,1,2$, is now the *normalised* eigenfunction from (4.12). Substituting the ansatz into (4.1), and considering that ψ_j satisfies the linear equation (4.5) with their corresponding eigenvalue ω_j ($\omega_2 = \omega_1$), we have

$$i(\dot{c}_0\psi_0 + \dot{c}_1\psi_1 + \dot{c}_2\psi_2) = (\omega - \omega_0)c_0\psi_0 + (\omega - \omega_1)c_1\psi_1 + (\omega - \omega_1)c_2\psi_2 \\ - (c_0\psi_0 + c_1\psi_1 + c_2\psi_2)^2 \left(c_0^*\psi_0 + c_1^*\psi_1 + c_2^*\psi_2\right),$$

where overdot denotes the time derivative. Projecting the equation onto the eigenstate ψ_j and denoting $g_{ijkl} = \langle \psi_i\psi_j\psi_k, \psi_l\rangle$, we obtain the finite dynamical system that we

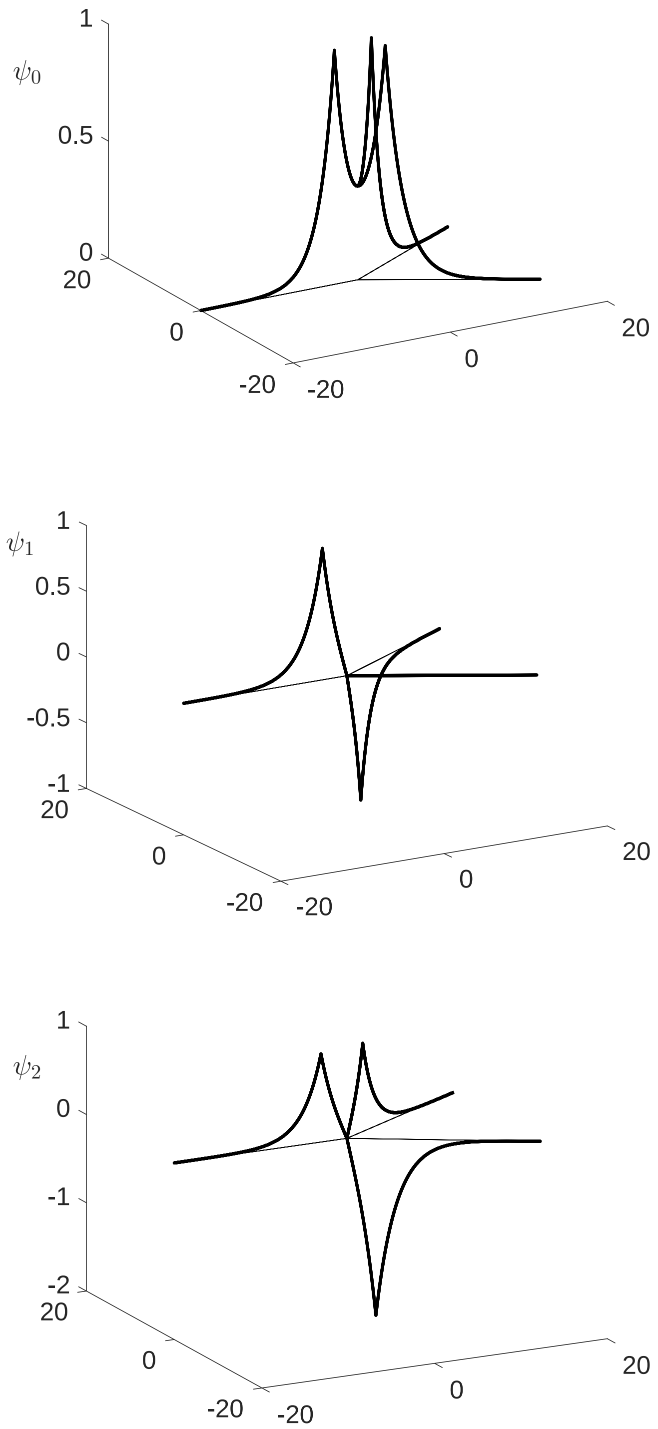

Figure 4.2. Plot of the eigenfunctions (4.12) for $a = 3$.

seek for

$$\begin{aligned}
i\dot{c}_0 &= (\omega-\omega_0)\,c_0 - g_{0000}|c_0|^2c_0 - g_{0110}\left(c_0^*c_1^2+2c_0|c_1|^2\right) - g_{1120}\left(2|c_1|^2c_2+c_1^2c_2^*\right)\\
&\quad - g_{0110}\left(c_0^*c_2^2+2c_0|c_2|^2\right)+g_{1120}|c_2|^2c_2,\\
i\dot{c}_1 &= (\omega-\omega_1)\,c_1 - g_{0110}\left(2|c_0|^2c_1+c_0^2c_1^*\right) - g_{1111}|c_1|^2c_1\\
&\quad - g_{1120}\left(2c_0^*c_1c_2+2c_0c_1^*c_2+2c_0c_1c_2^*\right) - g_{1221}\left(c_1^*c_2^2+2c_1|c_2|^2\right),\\
i\dot{c}_2 &= (\omega-\omega_1)\,c_2 - g_{1120}\left(c_0^*c_1^2+2c_0|c_1|^2\right) - g_{0110}\left(2|c_0|^2c_2+c_0^2c_2^*\right)\\
&\quad - g_{1221}\left(2|c_1|^2c_2+c_1^2c_2^*\right)+g_{1120}\left(c_0^*c_2^2+2c_0|c_2|^2\right)-g_{1111}|c_2|^2c_2.
\end{aligned}\tag{4.14}$$

Before we proceed with finding the equilibrium solution of (4.14), we will approximate the value of g_{ijkl}. For $a \gg 1$, we obtain that the coefficients are approximately related by

$$g_{0000} = g_{0110} = \sqrt{2}g_{1120} = \frac{2}{3}g_{1111} = 2g_{1221}. \tag{4.15}$$

The error made in this approximation is exponentially small for large a, yet it allows us a simpler analysis. Scaling the time as $t \to \Gamma t$, where $\Gamma = 1/g_{0000}$, Equations (4.14) become

$$\begin{aligned}
i\dot{c}_0 &= \Gamma(\omega-\omega_0)\,c_0 - |c_0|^2c_0 - \left(c_0^*c_1^2+2c_0|c_1|^2\right) - \frac{1}{\sqrt{2}}\left(2|c_1|^2c_2+c_1^2c_2^*\right)\\
&\quad - \left(c_0^*c_2^2+2c_0|c_2|^2\right)+\frac{1}{\sqrt{2}}|c_2|^2c_2,\\
i\dot{c}_1 &= \Gamma(\omega-\omega_1)\,c_1 - \left(2|c_0|^2c_1+c_0^2c_1^*\right) - \frac{3}{2}|c_1|^2c_1\\
&\quad - \sqrt{2}\left(c_0^*c_1c_2+c_0c_1^*c_2+c_0c_1c_2^*\right) - \frac{1}{2}\left(c_1^*c_2^2+2c_1|c_2|^2\right),\\
i\dot{c}_2 &= \Gamma(\omega-\omega_1)\,c_2 - \frac{1}{\sqrt{2}}\left(c_0^*c_1^2+2c_0|c_1|^2\right) - \left(2|c_0|^2c_2+c_0^2c_2^*\right)\\
&\quad - \frac{1}{2}\left(2|c_1|^2c_2+c_1^2c_2^*\right)+\frac{1}{\sqrt{2}}\left(c_0^*c_2^2+2c_0|c_2|^2\right)-\frac{3}{2}|c_2|^2c_2.
\end{aligned}\tag{4.16}$$

In the limit $a \to \infty, \Gamma = 12$. In the next section, we will analyse equilibrium solutions of (4.16).

4.2.3 Equilibrium solutions

Since the system (3.1) is gauge invariant, the equilibrium solutions of (4.16) satisfy

$$0 = \Gamma(\omega_0 - \omega)c_0 + c_0^3 + 3c_0c_1^2 + \frac{3}{\sqrt{2}}c_1^2c_2 + 3c_0c_2^2 - \frac{1}{\sqrt{2}}c_2^3, \tag{4.17a}$$

$$0 = \Gamma(\omega_1 - \omega)c_1 + 3c_0^2c_1 + \frac{3}{2}c_1^3 + \frac{6}{\sqrt{2}}c_0c_1c_2 + \frac{3}{2}c_1c_2^2, \tag{4.17b}$$

$$0 = \Gamma(\omega_1 - \omega)c_2 + \frac{3}{\sqrt{2}}c_0c_1^2 + 3c_0^2c_2 + \frac{3}{2}c_1^2c_2 - \frac{3}{\sqrt{2}}c_0c_2^2 + \frac{3}{2}c_2^3. \tag{4.17c}$$

In the following, we solve Equations (4.17) for c_0, c_1 and c_2. All possible solutions can be summarised in the following three cases. We illustrate the results in Figure 4.3 for $a = 3$. In the figure, we also describe their stability by plotting their eigenvalues in the complex plane that will be discussed in Section 4.3 later.

4.2.3.1 Case $c_0 = 0$

Here, we consider equilibria in the subspace spanned by ψ_1 and ψ_2. When $c_0 = 0$, Equations (4.17) reduce to the system

$$\frac{3c_1^2c_2}{\sqrt{2}} - \frac{c_2^3}{\sqrt{2}} = 0, \tag{4.18a}$$

$$\Gamma c_1(\omega_1 - \omega) + \frac{3c_1^3}{2} + \frac{3c_1c_2^2}{2} = 0, \tag{4.18b}$$

$$\Gamma c_2(\omega_1 - \omega) + \frac{3c_1^2c_2}{2} + \frac{3c_2^3}{2} = 0. \tag{4.18c}$$

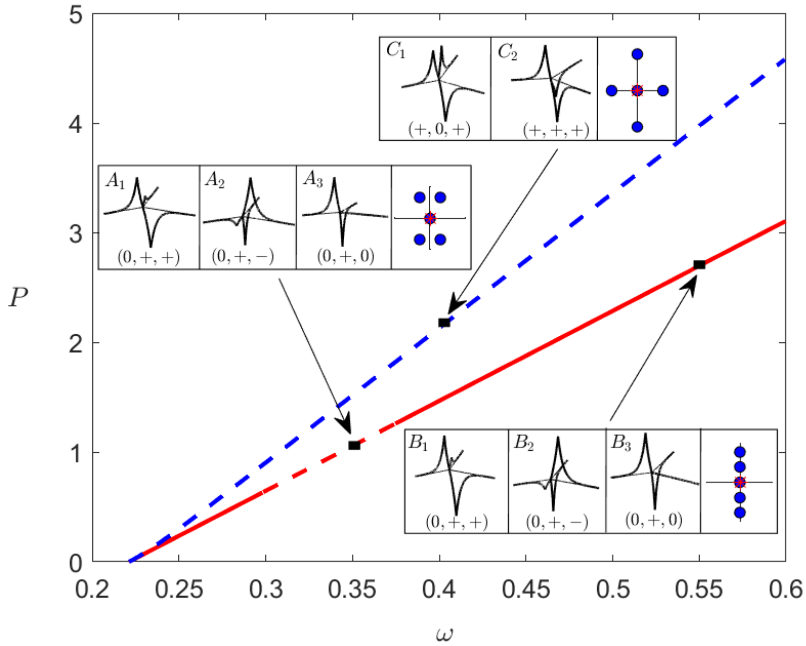

(a)

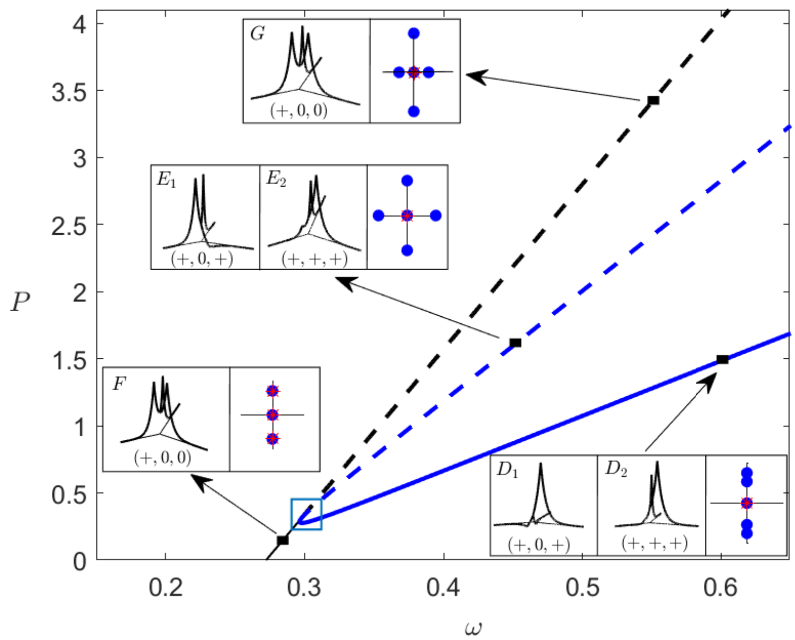

(b)

Figure 4.3. Bifurcation diagram of the various equilibrium solutions discussed in Section 4.2.3. Plotted are the solution norms squared as a function of ω for $a = 3$. The insets show the solution profiles and their corresponding spectrum in the complex plane.

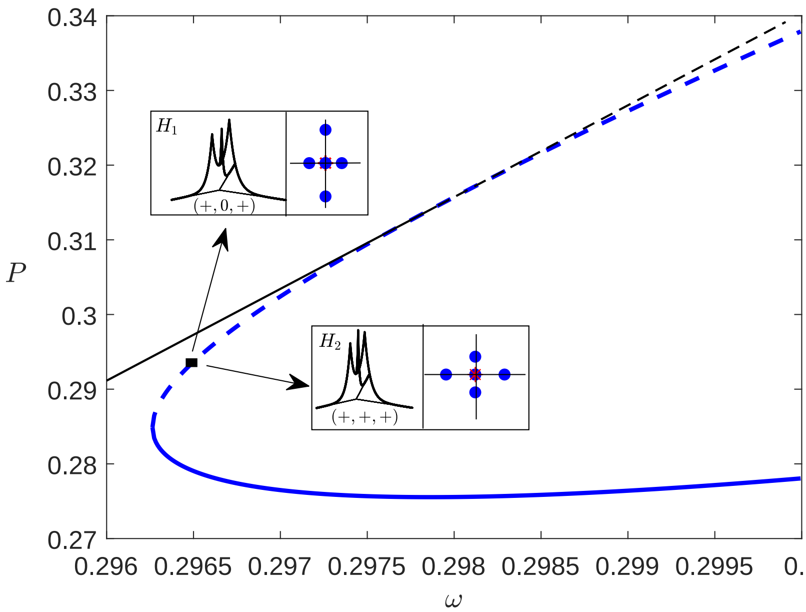

Figure 4.4. The zoom-in on the small square box in panel (b) in Figure 4.3b.

Solving (4.18a) for c_1, substituting into (4.18b) and (4.18c) will give us the solutions: $S_{1,2} = \left(0, \sqrt{\frac{1}{6}\Gamma(\omega-\omega_1)}, \pm\sqrt{\frac{1}{2}\Gamma(\omega-\omega_1)}\right)$, and $S_3 = (0, \sqrt{\frac{2}{3}\Gamma(\omega-\omega_1)}, 0)$. For $a = 3$, these solutions, represented in terms of their squared norms, are shown by the red curve in Figure 4.3a and labelled by $(0,+,\pm)$ and $(0,+,0)$.

4.2.3.2 Case $c_1 = 0$

When $c_1 = 0$, Equations (4.17) reduce to

$$c_0^3 + 3c_0c_2^2 - \frac{c_2^3}{\sqrt{2}} + c_0\Gamma(\omega-\omega_0) = 0, \tag{4.19a}$$

$$3c_0^2c_2 - \frac{3}{\sqrt{2}}c_0c_2^2 + \frac{3}{2}c_2^3 + c_2\Gamma(\omega-\omega_1) = 0. \tag{4.19b}$$

Solving (4.19b) for c_2, we have $c_2 = 0$ or $c_2 = \frac{1}{6}\left(3\sqrt{2}c_0 - \sqrt{6}\sqrt{4\Gamma\omega - 4\Gamma\omega_1 - 9c_0^2}\right)$. For $c_2 = 0$, we obtain $S_4 = (\sqrt{\Gamma(\omega-\omega_0)}, 0, 0)$. This is a continuation of ψ_0, which, as we will see later, experiences a symmetry breaking bifurcation. For $a = 3$, these solutions correspond to the black curve shown in Figure 4.3b labeled by (+, 0, 0).

As for the non-zero c_2, substituting it into (4.19a) yields

$$9\sqrt{3}c_0^2\sqrt{4\Gamma(\omega-\omega_1)-9c_0^2}+\sqrt{3}\Gamma(\omega_1-\omega)\sqrt{4\Gamma(\omega-\omega_1)-9c_0^2}-9\Gamma c_0(\omega_0-\omega_1)=0, \quad (4.20)$$

which can be re-written as the polynomial

$$729c_0^6-486\Gamma(\omega-\omega_1)c_0^4+27\Gamma^2\left(3\omega^2-2\omega_1(3\omega+\omega_0)+\omega_0^2+4\omega_1^2\right)c_0^2-4\Gamma^3(\omega-\omega_1)^3=0.$$

This is a cubic polynomial in c_0^2 and using Cardan's method [84], we can solve it to obtain the following roots.

(1) Within the interval $\omega_1 < \omega < \omega_{t_0}$, with $\omega_{t_0} = \sqrt{1+2/\sqrt{3}}(\omega_0-\omega_1)+\omega_1$, there is only one solution, $S_5 = \left(c_0, 0, \frac{1}{6}\left(3\sqrt{2}c_0-\sqrt{6}\sqrt{4\Gamma\omega-4\Gamma\omega_1-9c_0^2}\right)\right)$, with

$$c_0 = -\left(\frac{2}{9}\Gamma(\omega-\omega_1)+\frac{\sqrt[3]{-\sqrt{Y_1^2-h_1^2}-Y_1}+\sqrt[3]{\sqrt{Y_1^2-h_1^2}-Y_1}}{9\sqrt[3]{2}}\right)^{1/2},$$

where

$$Y_1 = -2\Gamma^3(\omega-\omega_1)\left(\omega^2-2\omega\omega_1-3\omega_0^2+6\omega_0\omega_1-2\omega_1^2\right)$$

$$h_1 = 2\left(\Gamma^2(\omega-\omega_0)(\omega+\omega_0-2\omega_1)\right)^{3/2}.$$

(2) Within the interval $\omega > \omega_{t_0}$, there are three solutions

$$c_0 = \frac{\sqrt{2\Gamma}}{3}\sqrt{\omega-\omega_1+G_1\cos(\theta_1)},$$

$$-\frac{\sqrt{2\Gamma}}{3}\sqrt{\omega-\omega_1-G_1\sin\left(\theta_1+\frac{\pi}{6}\right)}, \quad \frac{\sqrt{2\Gamma}}{3}\sqrt{\omega-\omega_1-G_1\sin\left(\frac{\pi}{6}-\theta_1\right)},$$

where

$$\cos(3\theta_1) = \frac{\Gamma^3(\omega-\omega_1)\left(\omega^2-2\omega\omega_1-3\omega_0^2+6\omega_0\omega_1-2\omega_1^2\right)}{\left(\Gamma^2(\omega-\omega_0)(\omega+\omega_0-2\omega_1)\right)^{3/2}},$$

and $G_1 = \sqrt{(\omega-\omega_0)(\omega+\omega_0-2\omega_1)}$. The three solutions are denoted by S_6, S_7, S_8, respectively.

For $a = 3$, the solution S_7 shown by the blue curve in Figure 4.3a and labelled by (+ 0 +) meets the curve of S_5 at ω_{t_0}, while those correspond to S_6 and S_8 shown by the blue curves bifurcate from the ones that correspond to S_4 in Figure 4.3b and are labelled by (+, 0, +).

4.2.3.3 Case $c_0, c_1, c_2 \neq 0$

Solving (4.17b) for c_0 gives us

$$c_0 = \frac{1}{6}\left(\sqrt{6}\sqrt{2\Gamma(\omega-\omega_1)-3c_1^2}-3\sqrt{2}c_2\right).$$

Substituting this to (4.17a) and (4.17c) yields

$$81c_2^3+18\Gamma c_2(\omega_0-\omega_1)-27c_2^2K+2\Gamma(2\omega-3\omega_0+\omega_1)K+3c_1^2(-5K-9c_2)=0,$$

$$\left(c_1^2-3c_2^2\right)(K-3c_2)=0,$$

where $K = \sqrt{6\Gamma(\omega-\omega_1)-9c_1^2}$. We only consider the case when $c_1^2 = 3c_2^2$ since the case with $K-3c_2 = 0$ yields solutions that have been obtained in Subsection 4.2.3.1, i.e., the case $c_0 = 0$. We obtain

$$\Gamma(2\omega-3\omega_0+\omega_1)\sqrt{6\Gamma(\omega-\omega_1)-27c_2^2}-36c_2^2\sqrt{6\Gamma(\omega-\omega_1)-27c_2^2}+9\Gamma c_2(\omega_0-\omega_1)=0. \tag{4.21}$$

Using a similar procedure as in the Subsection 4.2.3.2, we obtain c_2 satisfying (4.21) are as follows:

(1) Within the interval $\omega_1 < \omega < \omega_{t_0}$, there is only one solution,

$$c_2 = \left(\frac{1}{18}\Gamma(2\omega - \omega_0 - \omega_1) + \frac{\sqrt[3]{-\sqrt{Y_2^2 - h_2^2} - Y_2} + \sqrt[3]{\sqrt{Y_2^2 - h_2^2} - Y_2}}{18\sqrt[3]{2}} \right)^{1/2},$$

where

$$Y_2 = -\Gamma^3\left(2\omega^3 - 3\omega_1\left(3\omega^2 + 2\omega\omega_0 + \omega_0^2\right) + 3\omega^2\omega_0 + 6\omega_1^2(2\omega + \omega_0) + \omega_0^3 - 6\omega_1^3\right)$$

$$h_2 = 2\left(\Gamma^2(\omega - \omega_1)(\omega + \omega_0 - 2\omega_1)\right)^{3/2}.$$

(2) Within the interval $\omega > \omega_{t_0}$,

$$c_2 = \frac{\sqrt{\Gamma}}{3\sqrt{2}}\sqrt{2\omega - \omega_0 - \omega_1 + G_2\cos(\theta_2)}, -\frac{\sqrt{2\Gamma}}{3}\sqrt{2\omega - \omega_0 - \omega_1 - G_2\sin\left(\theta_2 + \frac{\pi}{6}\right)},$$
$$\frac{\sqrt{2\Gamma}}{3}\sqrt{2\omega - \omega_0 - \omega_1 - G_2\sin\left(\frac{\pi}{6} - \theta_2\right)},$$

where

$$\cos(3\theta_2) = \frac{\Gamma^3\left(2\omega^3 - 3\omega_1\left(3\omega^2 + 2\omega\omega_0 + \omega_0^2\right) + 3\omega^2\omega_0 + 6\omega_1^2(2\omega + \omega_0) + \omega_0^3 - 6\omega_1^3\right)}{2\left(\Gamma^2(\omega - \omega_1)(\omega + \omega_0 - 2\omega_1)\right)^{3/2}},$$

and $G_2 = 2\sqrt{(\omega - \omega_1)(\omega + \omega_0 - 2\omega_1)}$. For $a = 3$, it turns out that the squared norms of the solutions are the same as ones in the Subsection 4.2.3.2. They are represented by the blue curve shown in Figure 4.3 and labelled by $(+,+,+)$.

4.3 Stability and dynamics near the nonlinear bound states

After we obtain all the equilibrium solutions of (4.16), we will now discuss their stability by solving the corresponding linear eigenvalue problems. Using the linearisation ansatz $c_j(t) = \tilde{c}_j + \delta(x_j + iy_j)e^{\lambda t}, j = 0,1,2$, with $\lambda \in \mathbb{C}$, $\delta \ll 1$, and $\tilde{c}_j$ the equilibrium solution obtained in Subsection 4.2.3, and substituting it into (4.16), we will have an eigenvalue problem

$$\lambda x = Mx,$$

where $x = (x_0, y_0, x_1, y_1, x_2, y_2)^T$, and $M = (m_{jk}), j,k = 1,2,\cdots,6$, is the coefficient matrix with components given by

$$m_{12} = \Gamma(\omega-\omega_0) - \tilde{c}_0^2 - \tilde{c}_1^2 - \tilde{c}_2^2, \qquad m_{14} = -2\tilde{c}_0\tilde{c}_1 - \sqrt{2}\tilde{c}_1\tilde{c}_2,$$

$$m_{16} = -2\tilde{c}_0\tilde{c}_2 - \frac{\tilde{c}_1^2}{\sqrt{2}} + \frac{\tilde{c}_2^2}{\sqrt{2}}, \qquad m_{21} = -\Gamma(\omega-\omega_0) + 3\tilde{c}_0^2 + 3\tilde{c}_1^2 + 3\tilde{c}_2^2,$$

$$m_{23} = -3m_{14}, \qquad m_{25} = -3m_{16},$$

$$m_{32} = m_{14}, \qquad m_{34} = \Gamma(\omega-\omega_1) - \tilde{c}_0^2 - \sqrt{2}\tilde{c}_0\tilde{c}_2 - \frac{3\tilde{c}_1^2}{2} - \frac{\tilde{c}_2^2}{2},$$

$$m_{36} = \frac{1}{\sqrt{2}}m_{14}, \qquad m_{41} = -3m_{14},$$

$$m_{43} = \Gamma(\omega-\omega_1) - 3\tilde{c}_0^2 - 3\sqrt{2}\tilde{c}_0\tilde{c}_2 - \frac{9\tilde{c}_1^2}{2} - \frac{3\tilde{c}_2^2}{2}, \qquad m_{45} = -\frac{3}{\sqrt{2}}m_{14},$$

$$m_{52} = m_{16}, \qquad m_{54} = \frac{1}{\sqrt{2}}m_{14},$$

$$m_{56} = \Gamma(\omega-\omega_1) - \tilde{c}_0^2 + \sqrt{2}\tilde{c}_0\tilde{c}_2 - \frac{\tilde{c}_1^2}{2} - \frac{3\tilde{c}_2^2}{2}, \qquad m_{61} = -3m_{16},$$

$$m_{63} = -\frac{3}{\sqrt{2}}m_{14}, \qquad m_{65} = \Gamma(\omega-\omega_1) - 3\tilde{c}_0^2 + 3\sqrt{2}\tilde{c}_0\tilde{c}_2 - \frac{3\tilde{c}_1^2}{2} - \frac{9\tilde{c}_2^2}{2},$$

and zero elsewhere. A solution is unstable when $\mathrm{Re}(\lambda) > 0$ for some λ and linearly stable otherwise.

In the following, we will discuss the stability of each solution obtained in Subsection 4.2.3. We discuss briefly the eigenvalues for each of three cases that were explained in Subsection 4.2.3.

4.3.1 Case $c_0 = 0$

For any of the equilibria in this case, the characteristic equation of M is

$$\frac{1}{3}\lambda^2\left(\gamma+\beta^2\lambda^2+3\lambda^4\right)=0, \tag{4.22}$$

where

$$\beta=\Gamma^2\left(3\omega^2-8\omega_1(\omega+\omega_0)+2\omega\omega_0+3\omega_0^2+8\omega_1^2\right),\ \gamma=4\Gamma^4(\omega-\omega_1)^3(\omega_0-\omega_1),$$

Equation (4.22) can be solved for the nonzero eigenvalue, λ,

$$\lambda^2=\frac{-\beta\pm\sqrt{\beta^2-12\gamma}}{12}.$$

There is a change of stability as shown by the red-dashed line in Figure 4.3a, in the interval $\omega_{t_1}<\omega<\omega_{t_2}$, with

$$\begin{aligned}\omega_{t_1}&=\frac{1}{9}\left(2\left(\sqrt[3]{3\left(\sqrt{57}+9\right)}+\sqrt[3]{27-3\sqrt{57}}\right)\sqrt[3]{(\omega_0-\omega_1)^3}+3(\omega_0+2\omega_1)\right),\\ \omega_{t_2}&=3\omega_0-2\omega_1,\end{aligned} \tag{4.23}$$

in which the solution is unstable.

4.3.2 Case $c_1 = 0$

For the equilibrium $(\sqrt{\Gamma(\omega-\omega_0)}, 0, 0)$, the eigenvalues of M are: $0, \pm\Gamma\sqrt{\omega_0-\omega_1}\sqrt{2\omega-3\omega_0+\omega_1}$. Since $\omega_0 > \omega_1$, there is a change of stability of the equilibrium from stable to unstable, for $\omega > \omega_{t_3}$ with

$$\omega_{t_3} = \frac{3\omega_0 - \omega_1}{2}, \tag{4.24}$$

the solution is unstable and shown by the black-dashed line in Figure 4.3b.

For the case where $c_0, c_2 \neq 0$, from (4.19) we obtain $\Gamma(\omega-\omega_0)$ and $\Gamma(\omega-\omega_1)$ in terms of $\tilde{c}_j$. Substituting these into the coefficient matrix M, we obtain the eigenvalues

$$\begin{aligned}\lambda =& 0, \pm\frac{3\sqrt{2\sqrt{2}\tilde{c}_0^5\tilde{c}_2 - 5\tilde{c}_0^4\tilde{c}_2^2 + \sqrt{2}\tilde{c}_0^3\tilde{c}_2^3}}{\sqrt{2}\tilde{c}_0},\\ &\pm\frac{\sqrt{-6\sqrt{2}\tilde{c}_0^5\tilde{c}_2 - 25\tilde{c}_0^4\tilde{c}_2^2 + 19\sqrt{2}\tilde{c}_0^3\tilde{c}_2^3 - 6\tilde{c}_0^2\tilde{c}_2^4 + 2\sqrt{2}\tilde{c}_0\tilde{c}_2^5 - \tilde{c}_2^6}}{\sqrt{2}\tilde{c}_0}.\end{aligned}$$

Within the interval $\omega_1 < \omega < \sqrt{1+2/\sqrt{3}}(\omega_0 - \omega_1) + \omega_1$, the solution is unstable, while for $\omega > \sqrt{1+2/\sqrt{3}}(\omega_0-\omega_1)+\omega_1$, we have two unstable solutions and one stable solution. They are shown by the solid and dashed blue line, respectively, in Figure 4.3.

4.3.3 Case $c_0, c_1, c_2 \neq 0$

Using a similar procedure, substituting $\Gamma(\omega-\omega_0)$ and $\Gamma(\omega-\omega_1)$ that are obtained from (4.19) yields the eigenvalues

$$\lambda = 0, \pm \frac{3\sqrt{2}\sqrt{\left(-\sqrt{2}\right)\tilde{c}_0^5\tilde{c}_2 - 5\tilde{c}_0^4\tilde{c}_2^2 - 2\sqrt{2}\tilde{c}_0^3\tilde{c}_2^3}}{\tilde{c}_0},$$
$$\pm \frac{\sqrt{2}\sqrt{3\sqrt{2}\tilde{c}_0^5\tilde{c}_2 - 25\tilde{c}_0^4\tilde{c}_2^2 - 38\sqrt{2}\tilde{c}_0^3\tilde{c}_2^3 - 24\tilde{c}_0^2\tilde{c}_2^4 - 16\sqrt{2}\tilde{c}_0\tilde{c}_2^5 - 16\tilde{c}_2^6}}{\tilde{c}_0}.$$

As we can see, the eigenvalues can be written in terms of $\tilde{c}_0$ and $\tilde{c}_2$. We found that these yield the same eigenvalues with those in Subsection 4.3.2. This result implies that not only the solutions have the same squared norms with the solutions obtained for the case in Subsection 4.3.2, but they also have the same stability i.e., there are two unstable solutions and one stable solution shown by the blue line in Figure 4.3.

4.4 Discussion

Figure 4.3 now provides a complete picture of the bifurcations of standing waves from the linear states (see Figure 4.2) for $a \gg 1$. The red curve in Figure 4.3a shows bifurcations of a family of three nonlinear states from the eigenfrequency ω_1. They have the same norm. The solution denoted by $(0, +, 0)$ is the continuation of the linear state ψ_1. Not only they share the same norm, the solutions also have the same stability. For the parameter ω close to the bifurcation point, all three solutions are stable. As ω varies, there is an interval of ω in which the solution is unstable due to a Hamiltonian-Hopf bifurcation. In this interval, there are two pairs of eigenvalues with non-zero real parts, i.e., oscillatory instability.

When a solution is unstable, we are also interested in its typical dynamics. To do so, we have solved the coupled mode equations (4.16) numerically using a fourth-order Runge-Kutta method. The initial condition is an unstable equilibrium perturbed by small disturbances. To present the simulation results, we substituted the time-evolution of c_j into Equation (4.13) and plotted the resulting function.

We have considered the unstable solution denoted by point A_2 in Figure 4.3a. We depict its dynamics in the left panels in Figure 4.5. Around $t \approx 50$, we see the oscillatory nature of the instability that seemingly later leads to chaotic dynamics. We have simulated the instability of the other two solutions where we also observed a potential chaotic dynamics. Of course, we need to check further the dynamics, for example, using Lyapunov exponents.

The other curve in Figure 4.3a (blue-dashed curve) shows bifurcations to another family of solutions from ω_1. One of the bifurcating solutions denoted by $(+,0,+)$ can be seen as the continuation of the linear state ψ_2. Our analysis reveals that the nonlinear continuation is always unstable in its region of existence. The instability is due to a pair of real eigenvalues, i.e., exponential instability. We have also simulated the unstable solutions denoted by points C_1 and C_2, where we obtained that the long-time dynamics are also seemingly chaotic. We depict the dynamics of C_2 in the right panels in Figure 4.5. The only difference visually with the oscillatory instability of C_2 is at the initial dynamics when the instability starts to kick in, i.e., instead of oscillatory, in this case we obtain a continuous increase/decrease of the fields.

Figure 4.3b is considerably the main result of the work, which is the bifurcation of the ground state ψ_0. Near the bifurcation point ω_0, the nonlinear state is stable. As ω is increased further, there is a threshold value ω_{t_3} (4.24) where the symmetric

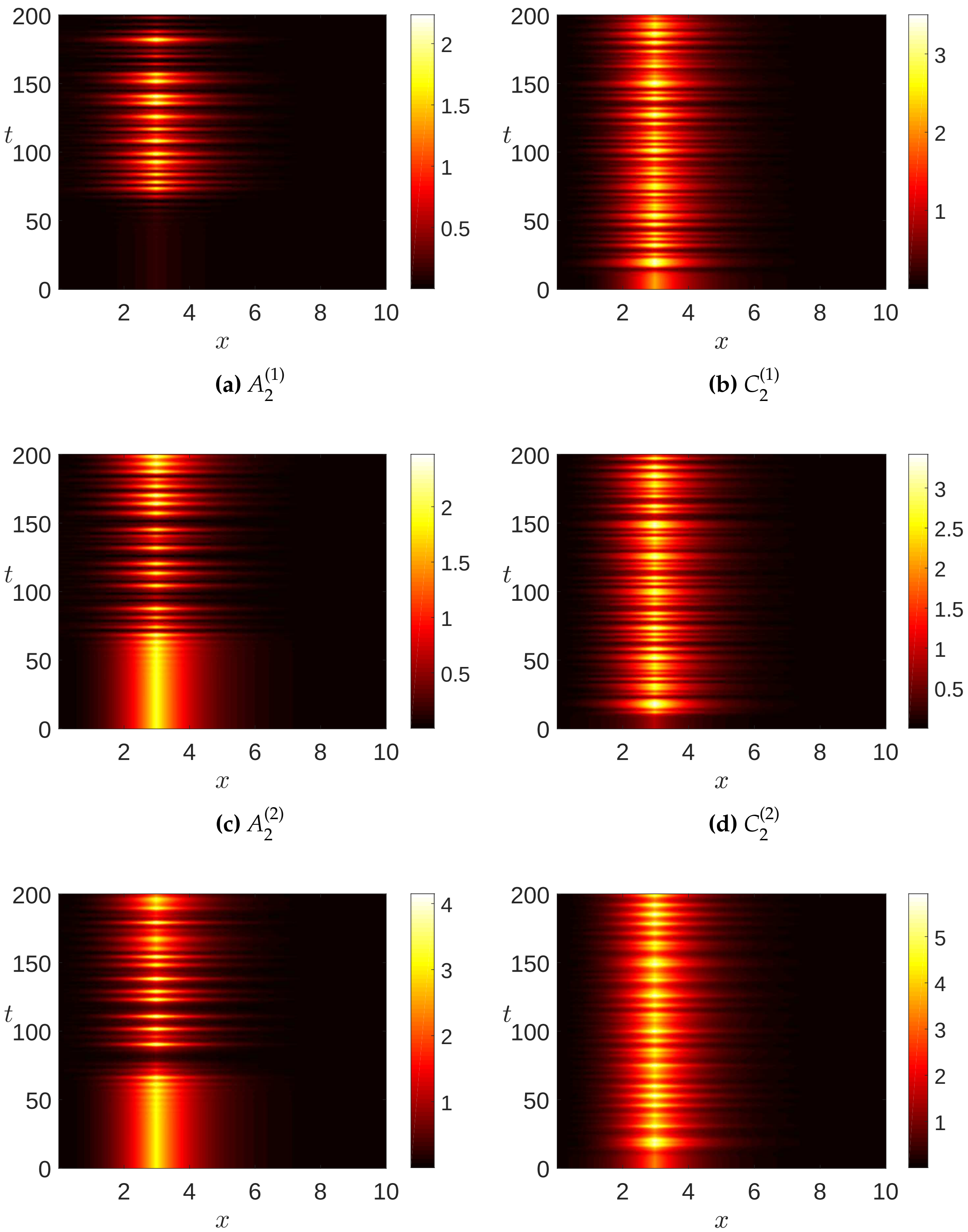

(a) $A_2^{(1)}$ **(b)** $C_2^{(1)}$

(c) $A_2^{(2)}$ **(d)** $C_2^{(2)}$

(e) $A_2^{(3)}$ **(f)** $C_2^{(3)}$

Figure 4.5. Time dynamics of the unstable solution at point (a,c,e) A_2 and (b,d,f) C_2 in Figure 4.3a. Shown are $|\psi^{(k)}|^2$, $j = 1, 2, 3$.

state becomes (exponentially) unstable. At this point we obtain a bifurcation of two asymmetric states in a supercritical-like manner for $\omega > \omega_{t_3}$, but the bifurcating solution is also unstable, and another two asymmetric ones in a subcritical manner for $\omega < \omega_{t_3}$. Figure 4.4 zooms in on the area about the subcritical bifurcation. Near ω_{t_3} the asymmetric solutions are due to the interaction of the modes ψ_0 with ψ_1 and ψ_2.

We have also simulated the unstable solution denoted by point H_1 in Figure 4.6. Unlike the previous dynamics, here we obtain that as t increases the solution is approaching a periodic solution. The same typical dynamics is also obtained for point H_2 shown in Figure 4.6.

As a final remark, we need to mention that the symmetry breaking bifurcation reported above is clearly due to the interaction of several modes, see the ansatz (4.13). Such an ansatz is only possible for $a > 1$, see Figure 4.1. When $a < 1$, only the linear state ψ_0 exists. In that case, the ground state is the symmetric state. In the limit $a \to 0$, our observation here may be related to the result of [26], where a symmetric trapped soliton at the vertex with a δ-interaction is the ground state for any solution norm.

4.5 Conclusion and future work

In this chapter, we have considered bifurcations of nonlinear states from the linear counterparts and their stability. By deriving a finite dimensional dynamical system approximation using the coupled mode reduction method, we presented novel

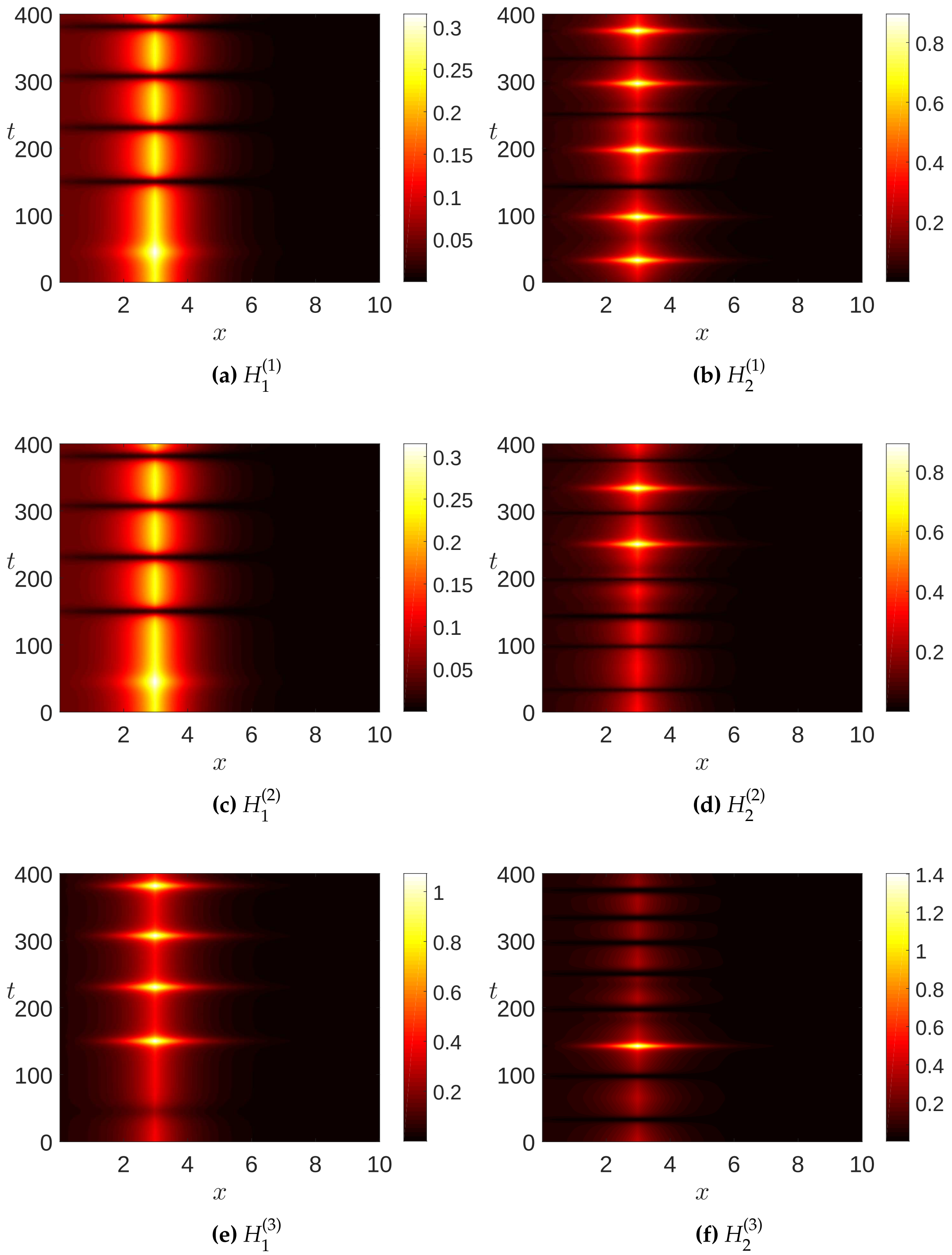

(a) $H_1^{(1)}$ **(b)** $H_2^{(1)}$

(c) $H_1^{(2)}$ **(d)** $H_2^{(2)}$

(e) $H_1^{(3)}$ **(f)** $H_2^{(3)}$

Figure 4.6. The same with Figure 4.6, but for the unstable solution denoted by point (a, c, e) H_1 and (b, d, f) H_2 in Figure 4.3a.

results on the degenerate symmetry breaking bifurcations of the positive definite solutions which are the ground states. The bifurcating asymmetric states were shown to be unstable, even though one of them regained stability after a turning point. Continuations of excited states have been discussed in detail as well.

We also presented typical time dynamics of the unstable solutions, where in general we obtained either chaotic dynamics or periodic states. It will be particularly interesting to address the origin of the two behaviours, following the study of, e.g., [14, 82] for triple-well potentials in the real line. This is addressed in future work. Another important problem is the extension of the present work to many-edge star graphs and study the general picture of the symmetry breaking bifurcations in such systems. This will also be reported in the future.

Chapter 5

Variational approximations using Gaussian ansatz, false instability, and its remedy in nonlinear Schrödinger lattices

In the previous two chapters, our study was focused on the NLS with external potential where we transformed our problem from PDEs into ODEs using two different approaches, namely, phase plane analysis and the coupled mode reduction method. In this chapter, we present the study of existence and stability of soliton solutions in the DNLS equation using another variational method which is called Variational Approximations (VA).

As a nonintegrable system, the DNLS equation has no explicit solution in terms of elementary functions. Scott and MacNeil [85] were the first to study the equation systematically and to report stationary soliton solutions. There is a vast literature on approximate solutions to the DNLS equation and their stability [65, 86–88]. Studies of discrete solitons in the DNLS equation use an exponential function as the standard VA ansatz, see, e.g., [63–65, 89] and references therein. The exponential function is chosen because it captures the tail behaviour and at the same time provides an effective Lagrangian with a closed form expression. Its validity is presented in [89], where it is shown that the ansatz captures the dynamics of the original infinite dimensional system for small coupling between lattices.

On the other hand, when the coupling is strong, i.e., the continuum limit, one uses a sech ansatz that may yield an exact solution [90, 91] or a Gaussian function [19, 92]. A natural question then emerges: can we apply an ansatz that works for all coupling constant? The sech or Gaussian function will yield an intractable effective Lagrangian. However, one may employ numerical approximations to yield a semianalytical method.

Here, we consider a variational method based on a Gaussian ansatz to the 1-D DNLS equation. Even though the infinite summation in the Lagrangian cannot be evaluated to yield a closed form expression, we may approximate it using only several dominating terms in the strongly discrete case, or using an integral approximation in the large coupling case.

In this chapter, we report two important findings: 1) there is an interval of coupling constant in which the on-site (i.e., bond-centered) soliton is unstable, in apparent contradiction with established results [64, 65, 93], i.e. a false instability; 2) by introducing a multiple Gaussian ansatz, we provide a remedy to the false instability. False instabilities of the variational technique perhaps were first reported in [94]. The stability issue reported here, however, is novel as it does not belong to the case analysed in [95], that explained false instabilities to be caused by coupling between modes. Kaup and Vogel [96] studied that the Gaussian ansatz is not good only when one is interested in soliton interactions. Using the Vakhitov-Kolokolov criterion, we conclude that our instability is due to the shape of the ansatz.

In Section 5.1, we apply the VA method and present approximate solutions of on-site (i.e., bond-centered) and inter-site (i.e., site-centered) solitons. In Section 5.2, we discuss the presence of false instability and the comparison between the analytical result and the numerical computation. In Section 5.3, we propose a remedy for the false instability by considering a multiple Gausian ansatz and finally, in Section 5.4, we summarise the work.

5.1 Approximation based on Gaussian ansatz

The one dimensional DNLS we consider is

$$i\frac{d\Psi_n}{dt} = c\Delta\Psi_n - \omega\Psi + |\Psi_n|^2\Psi_n, \quad n \in \mathbb{Z}, \tag{5.1}$$

where $\Delta \boxdot_n = \boxdot_{n+1} - 2\boxdot_n + \boxdot_{n-1}$, Ψ_n is a complex-valued function of time t at site n, c is the strength of the coupling between adjacent sites which is also called the dispersion coefficient, and ω is the propagation constant.

To study discrete solitons of the governing equation using VA, we use the ansatz

$$\psi_n = Ae^{-a(n-n_0)^2} e^{i\left(\alpha+\beta(n-n_0)+\frac{\gamma}{2}(n-n_0)^2\right)}, \tag{5.2}$$

where the set of parameters $X = (x_k) = (A, a, \alpha, \beta, \gamma, n_0)^T$ are functions of t. On-site and inter-site solitons correspond to $n_0 = 0, 1/2$, respectively. The variational equations for the dynamics of the parameters are given by (see Equation (2.31) in 2.3.2)

$$\mathrm{Re}\left[\sum_{n=-\infty}^{\infty}\left(i\dot{\psi}_n\right)\left(\frac{\partial \psi_n^*}{\partial x_j}\right)\right] = \mathrm{Re}\left[\sum_{n=-\infty}^{\infty}\left(-\omega\psi_n - c\Delta\psi_n - |\psi_n|^2\psi_n\right)\left(\frac{\partial \psi_n^*}{\partial x_j}\right)\right]. \tag{5.3}$$

Explicit computations will yield the system of nonlinear differential equations

$$M\frac{dX}{dt} = F(X), \tag{5.4}$$

where $M = (m_{jk})$, $j,k = 1,2,\cdots,6$, is the coefficient matrix and $F(X) = (F_j)$ is a vector of nonlinear functions of the variational parameters. We write equation (5.4) explicitly. Writing

$$\varphi_s = \sum_{n=-\infty}^{\infty} (n-n_0)^s e^{-2a(n-n_0)^2},$$
$$\phi_s = \sum_{n=-\infty}^{\infty} (n-n_0)^s e^{-4a(n-n_0)^2},$$
$$\chi_s = \sum_{n=-\infty}^{\infty} (n-n_0)^s \left(e^{-i\beta} e^{-2a(n-n_0)-i\gamma(n-n_0)-2a(n-n_0)^2} + e^{i\beta} e^{2a(n-n_0)+i\gamma_1(n-n_0)-2a(n-n_0)^2}\right),$$

the matrix M is given by

$$M = \begin{pmatrix} 0 & 0 & -A\varphi_0 & 0 & -\frac{1}{2}A\varphi_2 & A(\beta\varphi_0+\gamma\varphi_1) \\ 0 & 0 & A^2\varphi_2 & A^2\varphi_3 & \frac{1}{2}A^2\varphi_4 & -A^2(\beta\varphi_2+\gamma\varphi_3) \\ A\varphi_0 & -A^2\varphi_2 & 0 & 0 & 0 & 2A^2a\varphi_1 \\ 0 & -A^2\varphi_3 & 0 & 0 & 0 & 2aA^2\varphi_2 \\ \frac{1}{2}A\varphi_2 & -\frac{1}{2}A^2\varphi_4 & 0 & 0 & 0 & A^2a\varphi_3 \\ -A(\beta\varphi_0+\gamma\varphi_1) & A^2(\beta\varphi_2+\gamma\varphi_3) & -2A^2a\varphi_1 & -2A^2a\varphi_2 & -A^2a\varphi_3 & 0 \end{pmatrix},$$

while the vector function F is

$$F = \begin{pmatrix} A^3\phi_0 + Ac\chi_0 - A(\omega+2c)\varphi_0 \\ -A^4\phi_2 - A^2c\chi_2 + A^2(\omega+2c)\varphi_2 \\ \mathrm{Re}(-iA^2ce^{-a+\frac{i\gamma}{2}}\chi_0) \\ \mathrm{Re}(-iA^2ce^{-a+\frac{i\gamma}{2}}\chi_1) \\ \mathrm{Re}\left(-\frac{1}{2}iA^2ce^{-a+\frac{i\gamma}{2}}\chi_2\right) \\ 2A^2a(A^2\phi_1-(\omega+2c)\varphi_1)+\mathrm{Re}(iA^2c\beta_1e^{-a+\frac{i\gamma}{2}}\chi_0+A^2(2a+i\gamma)ce^{-a+\frac{i\gamma}{2}}\chi_1) \end{pmatrix}.$$

5.1.1 Time independent solution and stability

The nonlinear differential equation (5.4) is not trivial to be solved completely. In this subsection, we deal with a particular solution, called a time independent solution, or known also as steady state solution. It is a solution which is constant in time t and corresponds to $\alpha = \beta = \gamma = 0$. The variables A and a satisfying

$$\begin{aligned} A^2\phi_0 - (\omega + 2c)\varphi_0 + ce^{-a}\chi_0 = 0, \\ A^2\phi_2 - (\omega + 2c)\varphi_2 + ce^{-a}\chi_2 = 0, \end{aligned} \tag{5.5}$$

where ϕ_k, φ_k, and χ_k, $k = 0, 2$, evaluated at the equilibrium $X^{(0)}$. Exact solutions of Equation (5.5) can be obtained numerically using a fixed point iteration.

After a solution is obtained, we can discuss its stability. Introducing the linearisation ansatz $X = X^{(0)} + \delta X^{(1)} e^{\lambda t}$, with $\lambda \in \mathbb{C}$, and $\delta \ll 1$, taking a Taylor series expansion and keeping only the linear term in δ yield the generalized eigenvalue problem

$$\lambda \tilde{M} X^{(1)} = B X^{(1)}, \tag{5.6}$$

where

$$B = (b_{jk}), \quad b_{jk} = \left.\frac{\partial F_j(X)}{\partial x_k}\right|_{X^{(0)}}.$$

By defining

$$\zeta_s = \sum_{n=-\infty}^{\infty} (n - n_0)^s \left(e^{-2a_1(n-n_0) - 2a_1(n-n_0)^2} - e^{2a(n-n_0) - 2a(n-n_0)^2} \right),$$

the explicit expressions of the matrix component b_{jk} in (5.6) are given by

$$\begin{aligned} b_{11} &= 3A^2\phi_0 - (\omega + 2c)\varphi_0 + ce^{-a}\chi_0, & b_{12} &= -Ace^{-a}\chi_0 - 2Ace^{-a}\zeta_1 - 4A^3\phi_2 \\ & & &\quad + 2A(\omega + 2c)\varphi_2 - 2Ace^{-a}\chi_2 \\ b_{13} &= 0, & b_{14} &= 0 \\ b_{15} &= 0, & b_{16} &= 2aAce^{-a}\zeta_0 \end{aligned}$$

$$b_{21} = -4A^3\phi_2 + 2A(\omega+2c)\varphi_2 - 2Ace^{-a}\chi_2, \qquad b_{22} = A^2ce^{-a}\chi_2 + 2A^2ce^{-a}\zeta_3 + 4A^4\phi_4 - 2A^2(\omega+2c)\varphi_4 + 2A^2ce^{-a}\chi_4$$

$$b_{23} = 0, \qquad b_{24} = 0$$

$$b_{25} = 0, \qquad b_{26} = -2aA^2ce^{-a}\zeta_2 - 4aA^2ce^{-a}\chi_3$$

$$b_{31} = 0, \qquad b_{32} = 0$$

$$b_{33} = 0, \qquad b_{34} = A^2ce^{-a}\zeta_0$$

$$b_{35} = \frac{1}{2}A^2ce^{-a}\chi_0 + A^2c\zeta_1, \qquad b_{36} = 0$$

$$b_{41} = 0, \qquad b_{42} = 0$$

$$b_{43} = 0, \qquad b_{44} = A^2ce^{-a}\zeta_1$$

$$b_{45} = A^2ce^{-a}\zeta_2, \qquad b_{46} = 0$$

$$b_{51} = 0, \qquad b_{52} = 0$$

$$b_{53} = 0, \qquad b_{54} = \frac{1}{2}A^2ce^{-a}\zeta_2$$

$$b_{55} = \frac{1}{4}A^2ce^{-a}\chi_2 + \frac{1}{2}A^2ce^{-a}\zeta_3, \qquad b_{56} = 0$$

$$b_{61} = 0, \qquad b_{62} = -4aA^2ce^{-a}\zeta_2 - 4aA^2ce^{-a}\chi_3$$

$$b_{63} = 0, \qquad b_{64} = 0$$

$$b_{65} = 0, \qquad b_{66} = -2aA^4\phi_0 + 2aA^2(\omega+2c)\varphi_0 - 2aA^2ce^{-a_1}\chi_0 + 16a^2A^4\phi_2 - 8a^2A^2(\omega+2c)\varphi_2 + 4a^2A^2ce^{-a}(2\chi_2+\zeta_1).$$

The matrix $\tilde{M}$ is

$$\tilde{M} = \left.\begin{pmatrix} 0 & 0 & -A\varphi_0 & 0 & -\frac{1}{2}A\varphi_2 & 0 \\ 0 & 0 & A^2\varphi_2 & 0 & \frac{1}{2}A^2\varphi_4 & 0 \\ A\varphi_0 & -A^2\varphi_2 & 0 & 0 & 0 & 0 \\ 0 & 0 & 0 & 0 & 0 & 2aA^2\varphi_2 \\ \frac{1}{2}A\varphi_2 & -\frac{1}{2}A^2\varphi_4 & 0 & 0 & 0 & 0 \\ 0 & 0 & 0 & -2A^2a\varphi_2 & 0 & 0 \end{pmatrix}\right|_{X=X^{(0)}}.$$

A solution is stable when $\mathrm{Re}\,(\lambda) < 0$ for all λ.

5.1.2 Approximate solution and eigenvalue of (5.5) and (5.6)

To obtain an approximate solution of Equation (5.5), we need to approximate analytically the factors ϕ_k, φ_k, and χ_k, $k = 0, 2$. Consider, e.g.,

$$\phi_0 = \sum_{n=-\infty}^{\infty} e^{-4an^2} = \theta_3(0, e^{-4a}), \tag{5.7}$$

where θ_3 is a theta function defined as [97]

$$\theta_3(u, q) = 1 + 2\sum_{n=1}^{\infty} q^{n^2}\cos(2nu). \tag{5.8}$$

For large a, the function e^{-4an^2} converges to zero very rapidly as $|n|$ increases. Therefore, we may approximate ϕ_0 using the first few terms only, e.g., for the on-site solitons we take $n = -2..2$,

$$\phi_0 \approx y_1 = 1 + 2e^{-4a_1} + 2e^{-16a_1}. \tag{5.9}$$

On the other hand, because $f(n) = \int_{-\infty}^{\infty} f(x)\delta(x-n)\,dx$, then for $c \gg \omega$, i.e., $a \to 0$, we use the identity

$$\sum_{n=-\infty}^{\infty} f(n) = \int_{-\infty}^{\infty} f(x) \sum_{n=-\infty}^{\infty} \delta(x-n)dx, \tag{5.10}$$

where $\delta(x)$ is Dirac delta function. Using Fourier series, the Dirac comb can be written as

$$\sum_{-\infty}^{\infty} \delta(x-n) = 1 + 2\sum_{k=1}^{\infty} \cos(2k\pi x). \tag{5.11}$$

Taking only the first harmonic $k = 1$, the function ϕ_0 can be approximated by

$$\phi_0 \approx y_2 = \frac{\sqrt{\pi}\left(1 + 2e^{-\frac{\pi^2}{4a}}\right)}{2\sqrt{a}}. \tag{5.12}$$

Figure 5.1 shows the comparison between ϕ_0, y_1, and y_2, where we observe that y_1 is indeed good for large a, while y_2 is good for small a.

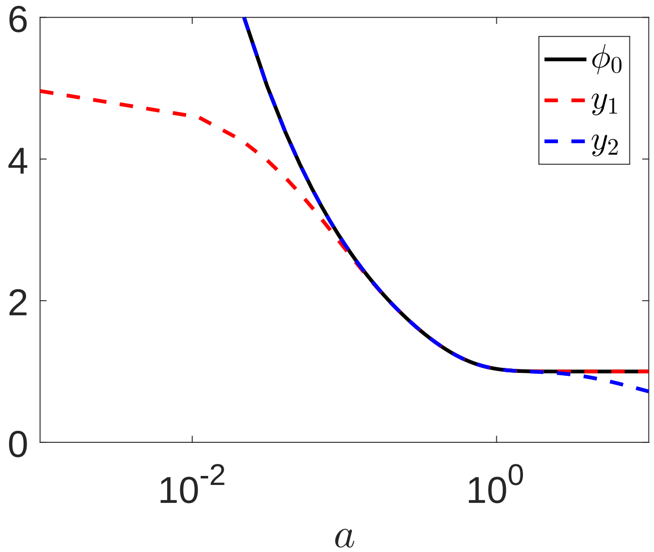

Figure 5.1. Plot of ϕ_0 and its approximations y_1 and y_2 given by equations (5.9) and (5.12), respectively.

After performing the same approximations to the remaining factors, for the on-site solitons ($n_0 = 0$), system (5.5) reduces to

$$\begin{aligned} A^2(1+2e^{-4a}+2e^{-16a})-(\omega+2c)(1+2e^{-2a}+2e^{-8a})+ce^{-a}(4+4e^{-4a}+2e^{-12a}) &= 0 \\ A^2(2e^{-4a}+8e^{-16a})-(\omega+2c)(2e^{-2a}+8e^{-8a})+ce^{-a}(2+10e^{-4a}+8e^{-12a}) &= 0, \end{aligned} \tag{5.13}$$

and for large a (which holds for $c \ll \omega$)

$$\begin{aligned} A &\approx \frac{\sqrt{(2c+\omega)(4e^{-7a}+e^{-a})-4e^{-12a}c-5e^{-4a}c-c}}{\sqrt{e^{-15a}\left(e^{12a}+4\right)}}, \\ c &\approx \frac{3\omega}{\kappa+5\sinh(a)-3\sinh(3a)+\cosh(a)+3\cosh(3a)-6}, \end{aligned} \tag{5.14}$$

where

$$\kappa = \frac{e^a\left(20e^{2a}-4e^{4a}+26e^{6a}+9e^{10a}+5e^{12a}+14\right)}{10e^{2a}+10e^{4a}+4e^{6a}+4e^{8a}+e^{14a}+6}. \tag{5.15}$$

At the leading order, when $a \gg 1$, $\kappa \approx 5e^{-a}$ and $c \approx \omega e^{-a}$, which implies that A is well defined. For inter-site solitons ($n_0 = 1/2$), we take $n = -1..2$ and system (5.5) reduces to

$$\begin{aligned} A^2(e^{-a}+e^{-9a})-(\omega+2c)(e^{-a/2}+e^{-9a/2})+ce^{-a}(e^{a/2}+2e^{-3a/2}+e^{-15a/2}) &= 0 \\ A^2(e^{-a}+9e^{-9a})-(\omega+2c)(e^{-a/2}+9e^{-9a/2})+ce^{-a}(e^{a/2}+10e^{-3a/2}+9e^{-15a/2}) &= 0, \end{aligned} \tag{5.16}$$

and we obtain the approximation for large a

$$A \approx \frac{16\sqrt[4]{2}c^{19/8}\sqrt[4]{\omega}\left(2c^4\left(5T+9\sqrt{\omega}\right)+S_+\right)^{1/2}}{\left(T+\sqrt{\omega}\right)^{17/4}\left(2c^4\left(5T-41\sqrt{\omega}\right)+9S_-\right)^{1/2}}, \qquad a \approx \operatorname{arcsinh}\left(\frac{\sqrt{\omega}}{2\sqrt{c}}\right), \tag{5.17}$$

where

$$T = \sqrt{4c+\omega},$$

$$S_{\pm} = 10c^3\omega\left(T \pm 3\sqrt{\omega}\right) + 3c^2\left(5T\omega^2 \pm 9\omega^{5/2}\right) + c\left(7T\omega^3 \pm 9\omega^{7/2}\right) + \omega^4\left(T \pm \sqrt{\omega}\right).$$

The approximate solutions of (5.5) for small a can also be obtained similarly, but we will not present them here.

Next, we analyse the stability of the solitons in the framework of the VA, i.e., by obtaining their approximate eigenvalue from solving Equation (5.6).

For the on-site case, substituting (5.14) into (5.6), we obtain a pair of critical eigenvalues as functions of A, a and c

$$\lambda = \pm\frac{\sqrt{c}\left(e^{3a}\left(cR_1 - 2e^{5a}\omega R_2\right) + 2A^2R_3\right)^{1/2}}{e^{19a/2}\left(16e^{2a} + e^{8a} + 18\right)}, \tag{5.18}$$

where

$$\begin{aligned} R_1 = {} & -576e^{2a} - 480e^{5a} - 1984e^{6a} + 1152e^{7a} - 1608e^{8a} - 908e^{10a} + 1688e^{11a} + 88e^{12a} \\ & + 3552e^{13a} + 1572e^{14a} + 704e^{15a} - 780e^{16a} - 72e^{17a} - 316e^{18a} - 652e^{19a} + 28e^{20a} \\ & - 1504e^{21a} - 28e^{22a} - 648e^{23a} + 532e^{24a} - 104e^{25a} + 189e^{26a} - 100e^{27a} + 24e^{28a} \\ & - 28e^{29a} + 30e^{30a} - 4e^{31a} - 4e^{32a} - 4e^{33a} + e^{34a} + 240 \\ R_2 = {} & -288e^{2a} - 422e^{6a} - 888e^{8a} - 176e^{10a} + 18e^{12a} + 163e^{14a} + 376e^{16a} + 162e^{18a} \\ & + 26e^{20a} + 25e^{22a} + 7e^{24a} + e^{26a} + e^{28a} + 120 \\ R_3 = {} & -288e^{2a} - 1082e^{6a} - 1824e^{8a} - 640e^{10a} + 104e^{12a} + 1230e^{14a} + 684e^{16a} + 860e^{18a} \\ & - 48e^{20a} - 221e^{22a} + 200e^{24a} - 42e^{26a} + 24e^{28a} + 43e^{30a} + 5e^{34a} + 120 \end{aligned}$$

The other eigenvalues are zero or purely imaginary.

For the inter-site case, evaluating the generalised eigenvalue problem (5.6) at the time independent solution (5.17) yields a pair of critical eigenvalues

$$\lambda = \pm \frac{2\sqrt{L_1^8 + 2L_1^6 - 3}\,\sqrt{c^2 L_2 + cL_3}}{L_1^4\left(L_1^4 + 9\right)\sqrt{L_1^8 + 9}\,\sqrt{\ln(L_1)}}, \tag{5.19}$$

where

$$L_1 = \sqrt{\frac{1}{4c} + 1} + \frac{1}{2\sqrt{c}}$$

$$L_2 = 8L_1^6\left(L_1^2 - 1\right)^2\left(L_1^4 - 1\right) - 6\left(2L_1^6 - 3L_1^4 + 1\right)\left(L_1^8 + 9\right)\ln(L_1)$$

$$L_3 = L_1^4\left(L_1^4 + 9\right)\left(L_1^8 + 9\right)\omega\ln(L_1) - 8L_1^8\left(L_1^4 - 1\right)\omega.$$

The other eigenvalues are also zero or purely imaginary.

5.2 Numerical comparison and false instability

To check the validity of the VA, we calculate time independent discrete solitons of (5.1) by solving the system numerically. We used Newton's iteration method. After a discrete soliton, let us say $\tilde{\psi}_n$, is obtained, we determine its stability by solving the eigenvalue problem using a linearisation ansatz $\Psi_n(t) = \tilde{\psi}_n + \delta\epsilon_n(t)$, $\delta \ll 1$. By writing $\epsilon_n = (\eta_n + i\xi_n)e^{\lambda t}$, we obtain the eigenvalue problem

$$\begin{pmatrix} 0 & \omega - c\Delta - \tilde{\psi}_n^2 \\ -\omega + c\Delta + 3\tilde{\psi}_n^2 & 0 \end{pmatrix}\begin{pmatrix} \xi_n \\ \eta_n \end{pmatrix} = \lambda\begin{pmatrix} \xi_n \\ \eta_n \end{pmatrix}. \tag{5.20}$$

In the following, unless mentioned otherwise, we set $\omega = 1$.

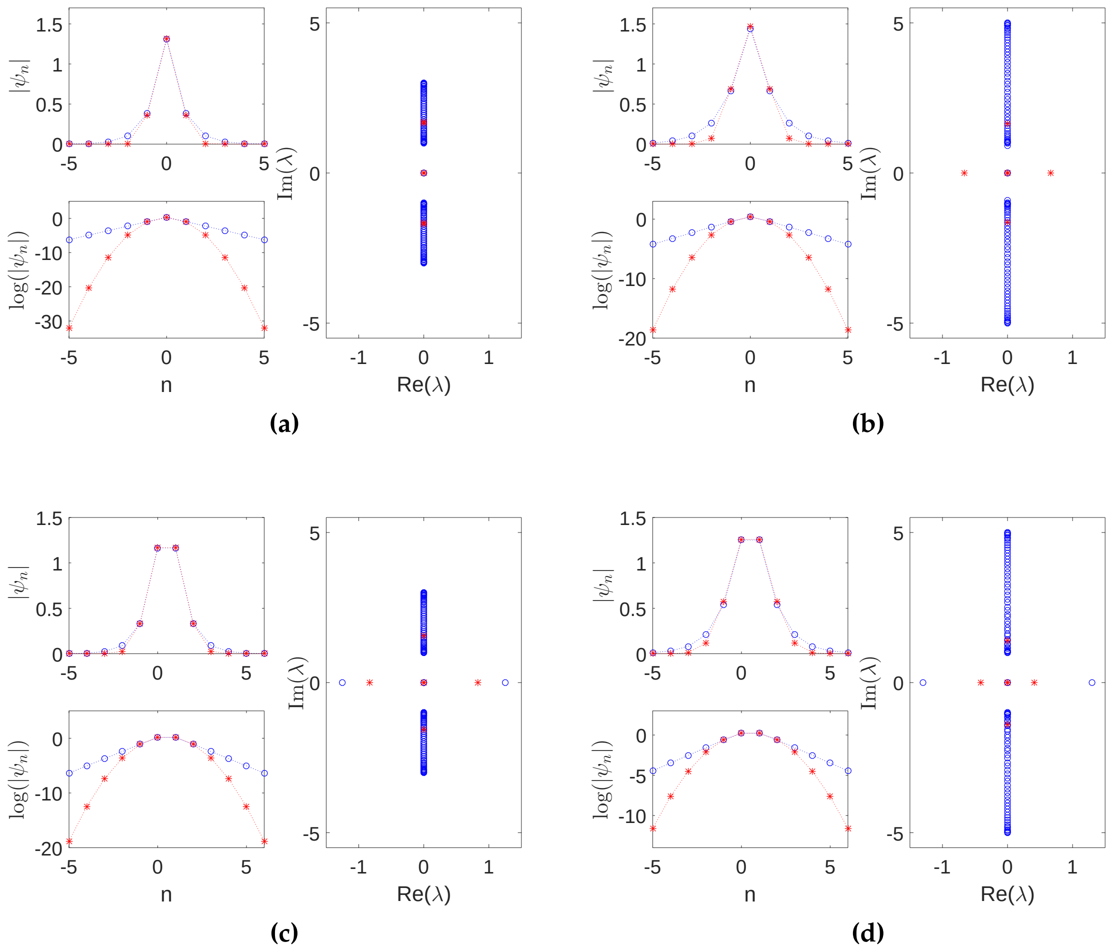

Figure 5.2. Comparison between the numerically obtained on-site (a,b) and inter-site (c,d) solutions of (5.1) and Gaussian VA (5.2) and (5.5) for $\omega = 1$ and (a, c) $c = 0.5$, (b, d) $c = 1$. Corresponding spectrum of the solution profile is in the right panel of each figure. Blue circle-dashed and red star-dashed lines indicate numerical and Gaussian VA results, respectively. Observe the false unstable spectrum in panel (b).

Figures 5.2a and 5.2b show the profiles of the time independent on-site soliton and its corresponding spectrum for $c = 0.5$ and $c = 1$, respectively. The profiles and spectrum of inter-site solitons are shown in Figures 5.2c and 5.2d. Results from the original discrete equation (5.1) and (5.6) are shown in blue circle-dashed lines. We also have solved Equation (5.5) and the eigenvalue problem (5.6) numerically. Substituting the results into the ansatz (5.2), we plot the VA in Figure 5.2 in red star-dashed lines. As expected, one can observe that the ansatz is not good in capturing the soliton tails. We have also plotted the eigenvalues from the VA (5.6).

In general, VA captures the qualitative stability of the discrete solitons, i.e., on-site and inter-site solitons are stable and unstable, respectively, due to the presence of an eigenvalue with positive real part. However, it is important to note that we found an unexpected result where according to VA the on-site soliton in Figure 5.2b is unstable. This finding is in contrast with the established result, that on-site solitons are always stable for any coupling constant. We therefore observe a false instability. In the following, we will study the emergence of this unstable eigenvalue from our VA.

In Figure 5.3, we plot the eigenvalues of (5.6) obtained numerically for varying coupling constant c. The results are shown in blue-solid lines. In Figure 5.3a and 5.3b we plot the real and the imaginary parts of the eigenvalues, respectively. From the figures, we conclude that one of the eigenvalues move along the imaginary axis towards the origin and then bifurcates into the real axis, creating a false instability. The unstable eigenvalue exists within a finite interval of coupling constant c. In

Figure 5.3a, we also plot our analytical approximation (5.18) as the red-dashed line, where good agreement is obtained.

Similarly for the inter-site case, we plot in Figures 5.3c and 5.3d the real and imaginary parts of the eigenvalues obtained from solving (5.6) numerically as blue-solid lines. We also display our approximation (5.19) as red-dashed line, where we again obtain good agreement. As a comparison, we also plot as black-dotted curve the critical eigenvalue of inter-site solitons obtained from solving the eigenvalue problem from the original system (5.20).

The false instability of on-site solitons is believed to be caused by the shape of the ansatz (i.e., the tail error). To show this, we consider the dependence of the soliton power defined as

$$P(\omega) = \sum_{n=-\infty}^{\infty} |\psi_n|^2, \tag{5.21}$$

on the propagation constant ω. According to the Vakhitov-Kolokolov criterion [72], the soliton is unstable when $\frac{dP}{d\omega} < 0$. Figure 5.4 shows P for varying ω when $c = 1$ for the on-site solitons based on the VA ansatz (5.2) and (5.5). Indeed we obtain a negative slope about $\omega = 1$. This confirms our finding that the false instability is due to the Gaussian ansatz (5.2).

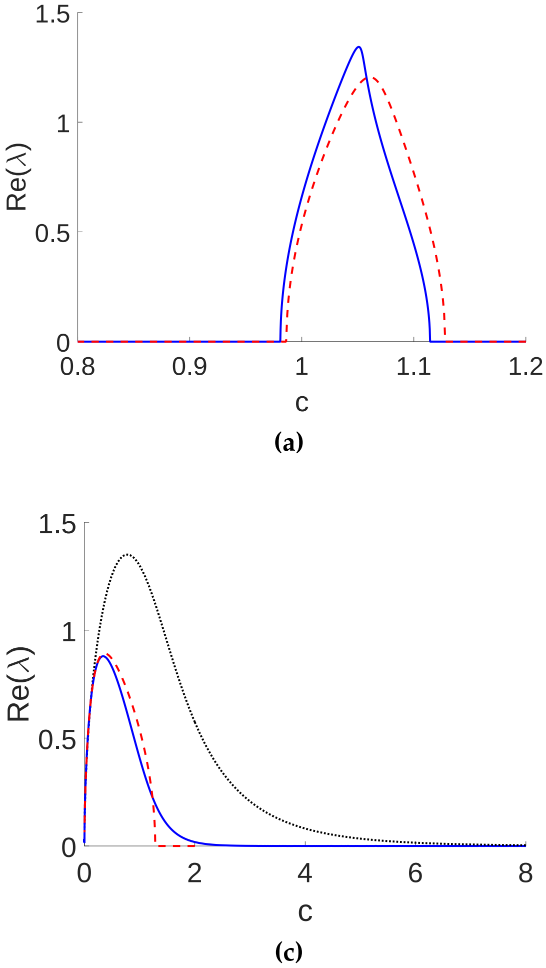

Figure 5.3. Critical eigenvalues calculated using VA of on-site solitons (a,b) and inter-site solitons (c,d) for varying c. Red-dashed lines in panels (a,b) are equation (5.18) with A and a using (5.14), while those in (c,d) are from equation (5.19). Blue-solid lines are obtained from solving (5.6) numerically. In panel (c), the black-dotted line shows the critical eigenvalue obtained from solving (5.20).

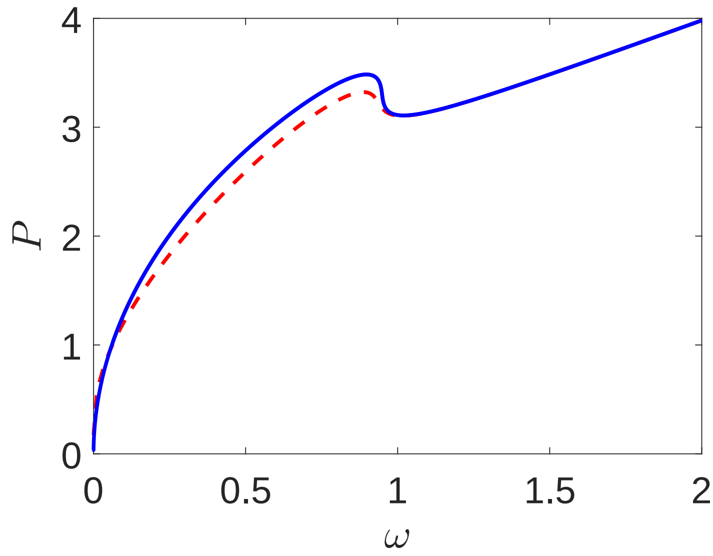

Figure 5.4. Power of on-site soliton approximated by Gaussian ansatz, as a function of ω for $c = 1$. Red-dashed and blue-solid lines correspond to the soliton amplitude A and width a computed in (5.14) and from (5.5), respectively.

5.3 Multiple Gaussian ansatz

We will solve the DNLS (5.1) using VA as in Section 5.1, but now using an ansatz containing multiple Gaussian functions,

$$\psi_n = \sum_{j=1}^{N} A_j e^{-a_j(n-n_0)^2} e^{i\left(\alpha_j+\beta_j(n-n_0)+\frac{\gamma_j}{2}(n-n_0)^2\right)}. \tag{5.22}$$

We have $(5N+1)$ parameters, i.e., $A_j, a_j, \alpha_j, \beta_j, \gamma_j, j = 1,2,\ldots,N$ and n_0, being functions of t. We will show that it gives a remedy to the false instability reported above. The idea of using several Gaussian functions in concert here has been proposed and used before in the context of spatially continuous linear or nonlinear Schrödinger equations [68, 92, 98, 99]. However, applying the idea in the context of spatially

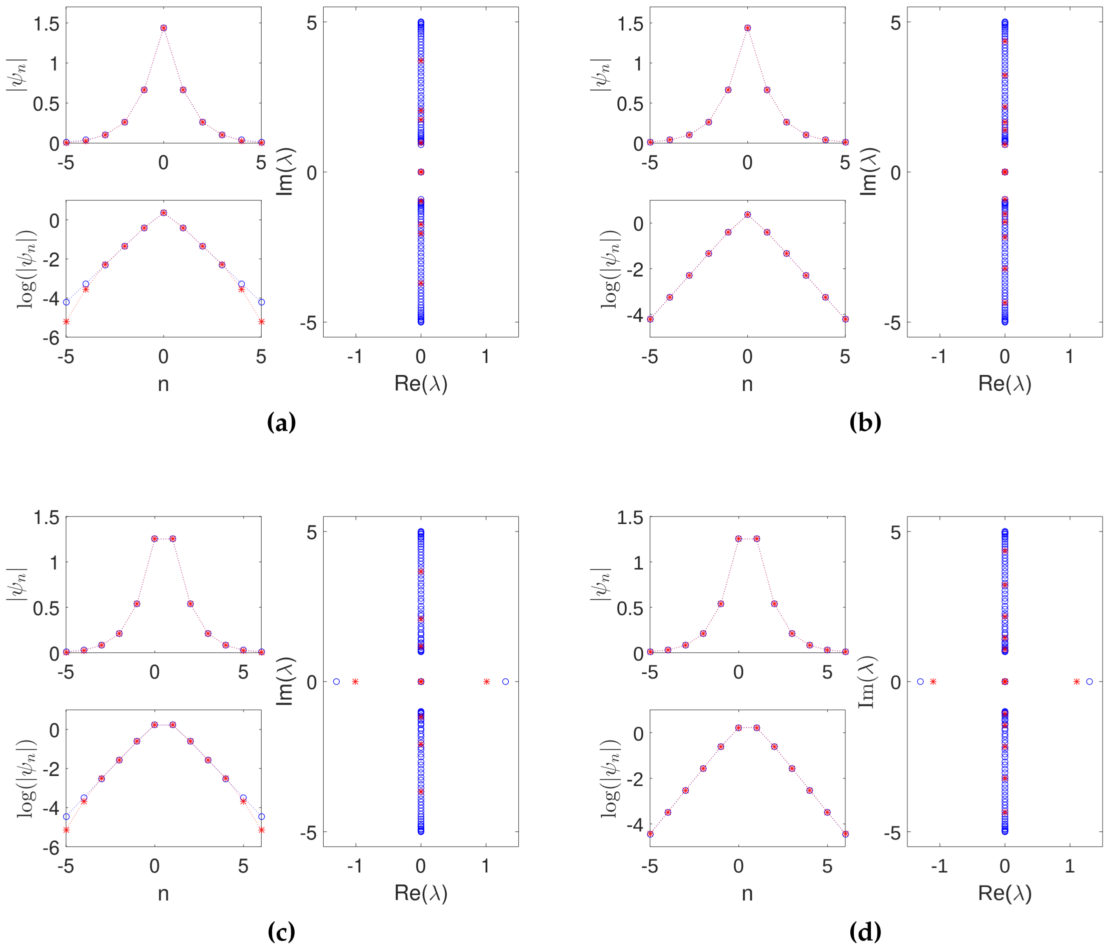

Figure 5.5. Comparison between the numerically obtained on-site (a,b) and inter-site (c,d) solutions of (5.1) and Gaussian VA (5.22) and (5.5) for $\omega = 1, c = 1$ and (a, c) $N = 2$, (b, d) $N = 3$. Corresponding spectrum of the solution profile is in the right panel of each figure. Blue circle-dashed and red star-dashed lines indicate numerical and Gaussian VA results, respectively.

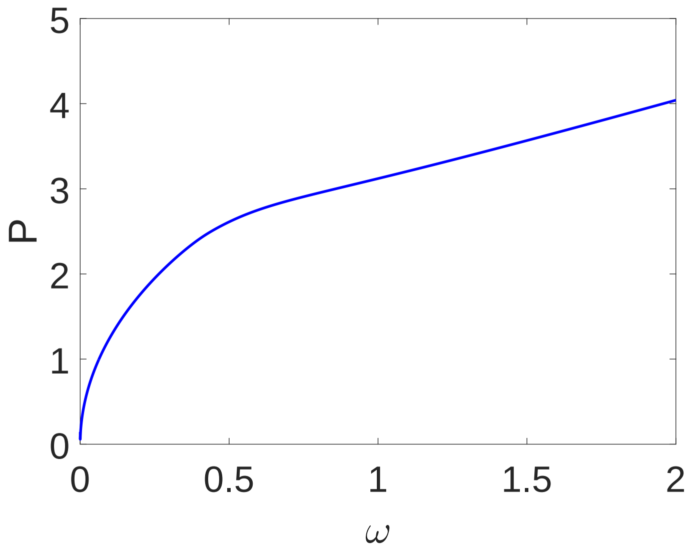

Figure 5.6. Power of on-site solitons as a function of ω for $c = 1$ and $N = 2$.

discrete equations is novel. In the following we will present the results of applying multiple Gaussian ansatz using the similar approach discussed in Section 5.1.

Figure 5.5 depicts the comparison of on-site and intersite solutions obtained from the numeric of time-independent DNLS (5.1) and multiple Gaussian VA for $c = 1$. The results shown are for $N = 2$ and $N = 3$, where we can see that the solution profile is getting closer to the numerical result. The results also show that by increasing the number of Gaussian functions used in the VA, the approximation provides a better capture to the soliton amplitude and tail. The error of the approximation can be seen in Figure 5.7c and 5.7d. We also show in Figure 5.5 the corresponding spectrum of the on-site and inter-site solitons. We can see that for on-site cases, the false instability no longer exists. Figure 5.7 shows the approximation errors for other values of coupling constant, $c = 0.5$ and $c = 1.5$ where we can see that increasing the number of Gaussian function also gives the smaller error.

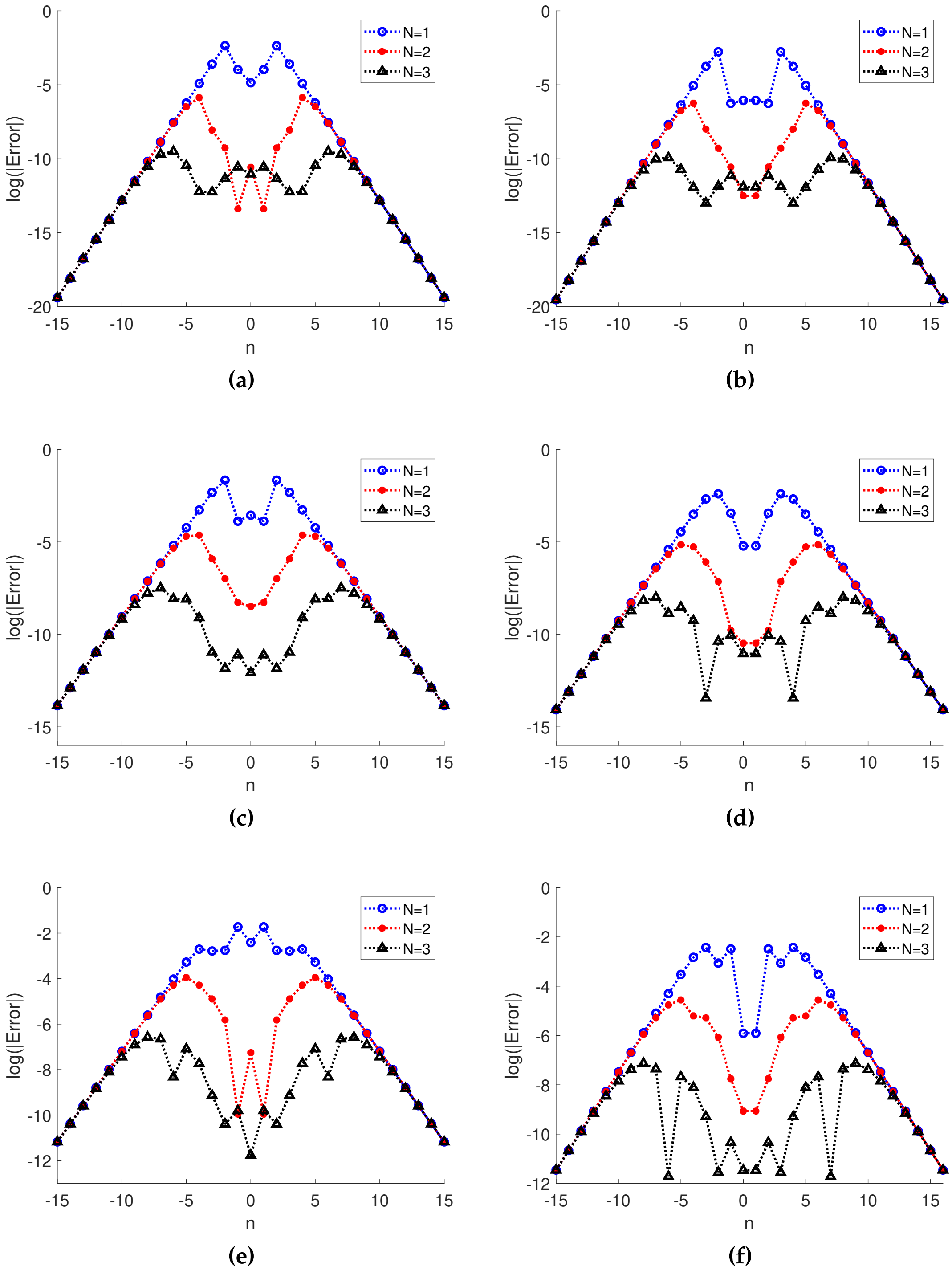

Figure 5.7. The approximation error of on-site (a,c,e) and inter-site (b,d,f) solutions of Gaussian VA (5.22) and (5.5) for $\omega = 1$ and (a, b) $c = 0.5$, (c, d) $c = 1$, (e, f) $c = 1.5$.

We can also see the remedy of the false instability using Vakhitov-Kolokolov criterion for $N = 2$. Figure 5.6 shows the plot of P for $c = 1$ and $N = 2$, where we can see that the on-site soliton is now stable for any value of ω, i.e., there is no negative slope that existed in the case of $N = 1$ shown in Figure 5.4.

5.4 Conclusions

We have studied time independent solutions of DNLS equation and their stability by using the VA method. We have employed the ansatz that contains single and multiple Gaussian functions. We have shown that the method can be used to approximate the solution of DNLS and to analyse their stability. Analytically, we have approximated the solution using a single Gaussian function, and found that for the on-site case, there is a false instability. A remedy has been provided by increasing the number of Gaussian functions used in the ansatz, confirming the fact that the instability is caused by the shape of the ansatz, which has not been reported elsewhere.

Chapter 6

Conclusions

Our aim, in this thesis, was to investigate analytically and numerically the solitary waves in three inhomogeneous systems of the NLS-type equations. Two of the systems are continuous, namely, the NLS equation on the real line with an asymmetric double Dirac delta potential and the NLS equation with delta potential on star graphs, and another one is discrete nonlinear Schrödinger equation. Some novel observations have been found in the study. First, we found an unfolded symmetry breaking in the NLS equation with asymmetric double Dirac delta potential. Second, we obtained a degenerate spontaneous symmetry bifurcation in the NLS equation with delta potential on star graphs. Last, we found a false instability when using a Gaussian ansatz which is remedied by using a multiple Gaussians ansatz.

6.1 Summary

Now, we summarise the work and main results obtained in this thesis as follows: In Chapter 3, we considered the NLS equation with asymmetric double Dirac delta potential. Using a dynamical system approach, we showed the existence of the ground state solutions and presented their solutions in the phase plane and their explicit expressions which are of the form of Jacobi elliptic functions. We also showed that there exists an unfolded symmetry breaking of the ground states. In contrast with the symmetric potential case, which is a pitchfork, interestingly we obtained a saddle-node type bifurcation. We found a threshold value of solution norm at which an asymmetric ground state bifurcates from the symmetric one. Using linear stability and an approach based on geometric analysis we studied the stability of the solutions and obtained the condition for the stability, which is related to the 'time' threshold value between two defects. To confirm the analytical results, we solved the stationary equation and the eigenvalue problem numerically using central finite differences. We also presented the typical dynamics of the unstable solutions where the instability led to periodic solutions.

Next, in Chapter 4 we considered the NLS equation on a three-edge star graph with a Dirac delta potential on each arm. First, we discussed the linear eigenstates of the system and then using a coupled mode reduction method we obtained the nonlinear bound states as a continuation of the linear states. By reducing the problem to a finite dimensional dynamical system, we analysed the existence and stability of the nonlinear states and surprisingly, it gave us the explicit expressions for all approximate solutions. We found novel results on symmetry breaking bifurcations of nonlinear bound states which are degenerate. There exists subcritical and supercritical-like symmetry breaking bifurcations emanating from the same threshold point at which symmetric states become unstable.

Finally, in Chapter 5, we applied the VA method to investigate the existence and the stability of stationary solutions of the DNLS equation. First, we approximated the discrete solitons using a single Gaussian ansatz and found analytically a false instability for the on-site solitons. We found an interval of coupling constants where the on-site solitons are unstable which contradicted with the established results. By increasing the number of Gaussian functions used, we obtained the remedy for the false instability and confirmed that the instability was caused by the shape of the ansatz. We compared the analytical results to numerical computations to confirm the validity of VA method used. We solved for the time independent discrete solitons using Newton's iteration method.

6.2 Future work

The process and findings in the present work have arised some new interesting ideas and problems to be proposed as future work. One interesting problem that can be addressed is applying the approach on geometric analysis discussed in Chapter 3 to study the stability of localised standing waves in the following governing system of differential equations

$$iu_t = u_{xx} + |u|^2 u, \;\; |x| > L,$$

$$iu_t = u_{xx} + |u|^4 u, \;\; |x| < L.$$

We would also like to expand the work to obtain the bifurcation of twisted mode that has not been addressed in the present work in Chapter 3.

As mentioned in Chapter 4 about the dynamics of the NLS equations with delta potential on three-edge star graph, we would like to investigate the origin of the typical time dynamics of the unstable solutions following the study of, e.g., [14, 82] for triple-well potentials in the real line. We would also like to study the bifurcations when the delta potential on each arm is located at different distance from the origin. Another interesting problem is to extend the work to many-edge star graphs and study the general picture of the symmetry breaking bifurcations in such systems.

Bibliography

[1] National Oceanic and Atmospheric Administration. What is a tsunami? national ocean service website. https://oceanservice.noaa.gov/facts/tsunami.html, 2019. [Online; accessed 10-September-2019].

[2] J. Yang. *Nonlinear Waves in Integrable and Nonintegrable Systems*, volume 16. SIAM, 2010.

[3] G. B. Whitham. *Linear and Nonlinear Waves*, volume 42. John Wiley & Sons, 2011.

[4] N. J. Zabusky and M. D. Kruskal. Interaction of "solitons" in a collisionless plasma and the recurrence of initial states. *Physical Review Letters*, 15(6):240, 1965.

[5] J. S. Russell. Report on waves. In *14th meeting of the British Association for the Advancement of Science*, pages 311–390. John Murray, London, 1844.

[6] M. J. Ablowitz. *Nonlinear Dispersive Waves: Asymptotic Analysis and Solitons*, volume 47. Cambridge University Press, 2011.

[7] C. Sulem and P. Sulem. *The Nonlinear Schrödinger Equation: Self-focusing and Wave Collapse*, volume 139. Springer Science & Business Media, 2007.

[8] M. Remoissenet. *Waves Called Solitons: Concepts and Experiments*. Springer Science & Business Media, 2013.

[9] M. Haragus. Stability and instability of nonlinear waves: Introduction. http://depts.washington.edu//bdecon/workshop2012/a_stability.pdf, 2006. [Online; accessed 10-September-2019].

[10] M. I. Weinstein. Lyapunov stability of ground states of nonlinear dispersive evolution equations. *Communications on Pure and Applied Mathematics*, 39(1):51–67, 1986.

[11] J. P. Boyd. *Weakly Nonlocal Solitary Waves and Beyond-All-Orders Asymptotics: Generalized Solitons and Hyperasymptotic Perturbation Theory*, volume 442. Springer Science & Business Media, 2012.

[12] R. K. Jackson and M. I. Weinstein. Geometric analysis of bifurcation and symmetry breaking in a Gross-Pitaevskii equation. *Journal of Statistical Physics*, 116(1-4):881–905, 2004.

[13] R. W. Boyd. *Nonlinear Optics*. Elsevier, 2003.

[14] R. Goodman. Hamiltonian Hopf bifurcations and dynamics of NLS/GP standing-wave modes. *Journal of Physics A: Mathematical and Theoretical*, 44(42):425101, 2011.

[15] R. Carretero-González, D. J. Frantzeskakis, and P. G. Kevrekidis. Nonlinear waves in Bose–Einstein condensates: physical relevance and mathematical techniques. *Nonlinearity*, 21(7):R139, 2008.

[16] J. Chris Eilbeck and M. Johansson. The discrete nonlinear Schrödinger equation-20 years on. In *Localization and Energy Transfer in Nonlinear Systems*, pages 44–67. World Scientific, 2003.

[17] P. G. Kevrekidis. *The Discrete Nonlinear Schrödinger Equation: Mathematical Analysis, Numerical Computations and Physical Perspectives*, volume 232. Springer Science & Business Media, 2009.

[18] P. G. Kevrekidis, K. Ø. Rasmussen, and A. R. Bishop. The discrete nonlinear Schrödinger equation: a survey of recent results. *International Journal of Modern Physics B*, 15(21):2833–2900, 2001.

[19] D. Anderson. Variational approach to nonlinear pulse propagation in optical fibers. *Physical Review A*, 27(6):3135, 1983.

[20] M. J. Ablowitz, B. Prinari, and A. D. Trubatch. *Discrete and Continuous Nonlinear Schrödinger Systems*, volume 302. Cambridge University Press, 2004.

[21] D. N. Christodoulides, F. Lederer, and Y. Silberberg. Discretizing light behaviour in linear and nonlinear waveguide lattices. *Nature*, 424(6950):817–823, 2003.

[22] M. J. Ablowitz and Z. H. Musslimani. Integrable nonlocal nonlinear Schrödinger equation. *Physical Review Letters*, 110(6):064105, 2013.

[23] M. J. Ablowitz and Z. H. Musslimani. Inverse scattering transform for the integrable nonlocal nonlinear Schrödinger equation. *Nonlinearity*, 29(3):915, 2016.

[24] M. J. Ablowitz and Z. H. Musslimani. Integrable nonlocal nonlinear equations. *Studies in Applied Mathematics*, 139(1):7–59, 2017.

[25] V. S. Gerdjikov and A. Saxena. Complete integrability of nonlocal nonlinear Schrödinger equation. *Journal of Mathematical Physics*, 58(1):013502, 2017.

[26] R. Adami, C. Cacciapuoti, D. Finco, and D. Noja. Stationary states of NLS on star graphs. *EPL (Europhysics Letters)*, 100(1):10003, 2012.

[27] E. B. Davies. Symmetry breaking for a non-linear Schrödinger equation. *Communications in Mathematical Physics*, 64(3):191–210, 1979.

[28] J. C. Eilbeck, P. S. Lomdahl, and A. C. Scott. The discrete self-trapping equation. *Physica D: Nonlinear Phenomena*, 16(3):318–338, 1985.

[29] T. W. B. Kibble. Spontaneous symmetry breaking in gauge theories. *Philosophical Transactions of the Royal Society A: Mathematical, Physical and Engineering Sciences*, 373(2032):20140033, 2015.

[30] M. Albiez, R. Gati, J. Fölling, S. Hunsmann, M. Cristiani, and M. K. Oberthaler. Direct observation of tunneling and nonlinear self-trapping in a single bosonic Josephson junction. *Physical Review Letters*, 95(1):010402, 2005.

[31] T. Zibold, E. Nicklas, C. Gross, and M. K. Oberthaler. Classical bifurcation at the transition from Rabi to Josephson dynamics. *Physical Review Letters*, 105(20):204101, 2010.

[32] M. Liu, D. A. Powell, I. V. Shadrivov, M. Lapine, and Y. S. Kivshar. Spontaneous chiral symmetry breaking in metamaterials. *Nature Communications*, 5:4441, 2014.

[33] C. Green, G. B. Mindlin, E. J. D'Angelo, H. G. Solari, and J. R. Tredicce. Spontaneous symmetry breaking in a laser: the experimental side. *Physical Review Letters*, 65(25):3124, 1990.

[34] P. G. Kevrekidis, Z. Chen, B. A. Malomed, D. J. Frantzeskakis, and M. I. Weinstein. Spontaneous symmetry breaking in photonic lattices: Theory and experiment. *Physics Letters A*, 340(1-4):275–280, 2005.

[35] S. Sawai, Y. Maeda, and Y. Sawada. Spontaneous symmetry breaking turing-type pattern formation in a confined dictyostelium cell mass. *Physical Review Letters*, 85(10):2212, 2000.

[36] T. Heil, I. Fischer, W. Elsässer, J. Mulet, and C. R. Mirasso. Chaos synchronization and spontaneous symmetry-breaking in symmetrically delay-coupled semiconductor lasers. *Physical Review Letters*, 86(5):795, 2001.

[37] P. Hamel, S. Haddadi, F. Raineri, P. Monnier, G. Beaudoin, I. Sagnes, A. Levenson, and A. M. Yacomotti. Spontaneous mirror-symmetry breaking in coupled photonic-crystal nanolasers. *Nature Photonics*, 9(5):311, 2015.

[38] E. M. Wright, G. I. Stegeman, and S. Wabnitz. Solitary-wave decay and symmetry-breaking instabilities in two-mode fibers. *Physical Review A*, 40(8):4455, 1989.

[39] C. Paré and M. Florjańczyk. Approximate model of soliton dynamics in all-optical couplers. *Physical Review A*, 41(11):6287, 1990.

[40] A. I. Maĭmistov. Propagation of a light pulse in nonlinear tunnel-coupled optical waveguides. *Soviet Journal of Quantum Electronics*, 21(6):687, 1991.

[41] N. Akhmediev and A. Ankiewicz. Novel soliton states and bifurcation phenomena in nonlinear fiber couplers. *Physical Review Letters*, 70(16):2395, 1993.

[42] B. A. Malomed, I. M. Skinner, P. L. Chu, and G. D. Peng. Symmetric and asymmetric solitons in twin-core nonlinear optical fibers. *Physical Review E*, 53(4):4084, 1996.

[43] M. I. Qadir, H. Susanto, and P. C. Matthews. Fluxon analogues and dark solitons in linearly coupled Bose-Einstein condensates. *Journal of Physics B: Atomic, Molecular and Optical Physics*, 45(3):035004, 2012.

[44] S. Su, S. Gou, A. Bradley, O. Fialko, and J. Brand. Kibble-Zurek scaling and its breakdown for spontaneous generation of Josephson vortices in Bose-Einstein condensates. *Physical Review Letters*, 110(21):215302, 2013.

[45] M. I. Qadir, H. Susanto, and P. C. Matthews. Multiple fluxon analogues and dark solitons in linearly coupled Bose-Einstein condensates. *Spontaneous Symmetry Breaking, Self-Trapping, and Josephson Oscillations*, 1:485, 2014.

[46] L. Salasnich and B. A. Malomed. Spontaneous symmetry breaking in linearly coupled disk-shaped Bose-Einstein condensates. *Molecular Physics*, 109(23-24):2737–2745, 2011.

[47] Z. Chen, Y. Li, B. A. Malomed, and L. Salasnich. Spontaneous symmetry breaking of fundamental states, vortices, and dipoles in two-and one-dimensional linearly coupled traps with cubic self-attraction. *Physical Review A*, 96(3):033621, 2017.

[48] K. W. Mahmud, J. N. Kutz, and W. P. Reinhardt. Bose-Einstein condensates in a one-dimensional double square well: Analytical solutions of the nonlinear Schrödinger equation. *Physical Review A*, 66(6):063607, 2002.

[49] J. L. Marzuola and M. I. Weinstein. Long time dynamics near the symmetry breaking bifurcation for nonlinear Schrödinger/Gross-Pitaevskii equations. *Discrete & Continuous Dynamical Systems-A*, 28(4):1505–1554, 2010.

[50] H. Susanto, J. Cuevas, and P. Krüger. Josephson tunnelling of dark solitons in a double-well potential. *Journal of Physics B: Atomic, Molecular and Optical Physics*, 44(9):095003, 2011.

[51] H. Susanto and J. Cuevas. Josephson tunneling of excited states in a double-well potential. In *Spontaneous Symmetry Breaking, Self-Trapping, and Josephson Oscillations*, pages 583–599. Springer, 2012.

[52] B. A. Malomed. *Spontaneous Symmetry Breaking, Self-Trapping, and Josephson Oscillations*. Springer, 2013.

[53] S. Le Coz, R. Fukuizumi, G. Fibich, B. Ksherim, and Y. Sivan. Instability of bound states of a nonlinear Schrödinger equation with a Dirac potential. *Physica D: Nonlinear Phenomena*, 237(8):1103–1128, 2008.

[54] R. H. Goodman, P. J. Holmes, and M. I. Weinstein. Strong NLS soliton–defect interactions. *Physica D: Nonlinear Phenomena*, 192(3-4):215–248, 2004.

[55] J. Holmer, J. Marzuola, and M. Zworski. Soliton splitting by external delta potentials. *Journal of Nonlinear Science*, 17(4):349–367, 2007.

[56] T. Kapitula and K. Promislow. *Spectral and Dynamical Stability of Nonlinear Waves*, volume 457. Springer, 2013.

[57] A. Scott. *Encyclopedia of Nonlinear Science*. Routledge, 2006.

[58] G. Fibich. *The Nonlinear Schrödinger Equation*. Springer, 2015.

[59] R. Haberman. *Applied Partial Differential Equations: with Fourier Series and Boundary Value Problems*, volume 5. Pearson Prentice Hall Upper Saddle River, 2013.

[60] D. Noja. Nonlinear Schrödinger equation on graphs: recent results and open problems. *Philosophical Transactions of the Royal Society A: Mathematical, Physical and Engineering Sciences*, 372(2007):20130002, 2014.

[61] Y. Li, F. Li, and J. Shi. Ground states of nonlinear Schrödinger equation on star metric graphs. *Journal of Mathematical Analysis and Applications*, 459(2):661–685, 2018.

[62] R. Adami, C. Cacciapuoti, D. Finco, and D. Noja. Fast solitons on star graphs. *Reviews in Mathematical Physics*, 23(04):409–451, 2011.

[63] B.A. Malomed and M. I. Weinstein. Soliton dynamics in the discrete nonlinear Schrödinger equation. *Physics Letters A*, 220(1-3):91–96, 1996.

[64] D. J. Kaup. Variational solutions for the discrete nonlinear Schrödinger equation. *Mathematics and Computers in Simulation*, 69(3-4):322–333, 2005.

[65] J. Cuevas, G. James, P. G. Kevrekidis, B. A. Malomed, and B. Sanchez-Rey. Approximation of solitons in the discrete NLS equation. *Journal of Nonlinear Mathematical Physics*, 15(sup3):124–136, 2008.

[66] J. H. P. Dawes and H. Susanto. Variational approximation and the use of collective coordinates. *Physical Review E*, 87(6):063202, 2013.

[67] A. D. McLachlan. A variational solution of the time-dependent Schrödinger equation. *Molecular Physics*, 8(1):39–44, 1964.

[68] E. J. Heller. Time dependent variational approach to semiclassical dynamics. *The Journal of Chemical Physics*, 64(1):63–73, 1976.

[69] C. Lubich. On variational approximations in quantum molecular dynamics. *Mathematics of Computation*, 74(250):765–779, 2005.

[70] E. Faou and C. Lubich. A Poisson integrator for Gaussian wavepacket dynamics. *Computing and Visualization in Science*, 9(2):45–55, 2006.

[71] S. Le Coz. Standing waves in nonlinear Schrödinger equations. *Analytical and Numerical Aspects of Partial Differential Equations*, pages 151–192, 2009.

[72] N. G. Vakhitov and A. A. Kolokolov. Stationary solutions of the wave equation in a medium with nonlinearity saturation. *Radiophysics and Quantum Electronics*, 16(7):783–789, 1973.

[73] S. H. Strogatz. *Nonlinear dynamics and chaos with student solutions manual: With applications to physics, biology, chemistry, and engineering*. CRC press, 2014.

[74] G. Theocharis, P. G. Kevrekidis, D. J. Frantzeskakis, and P. Schmelcher. Symmetry breaking in symmetric and asymmetric double-well potentials. *Physical Review E*, 74(5):056608, 2006.

[75] C. K. R. T. Jones. Instability of standing waves for non-linear Schrödinger-type equations. *Ergodic Theory and Dynamical Systems*, 8(8*):119–138, 1988.

[76] R. Marangell, C. K. R. T. Jones, and H. Susanto. Localized standing waves in inhomogeneous Schrödinger equations. *Nonlinearity*, 23(9):2059, 2010.

[77] R. Marangell, H. Susanto, and C. K. R. T. Jones. Unstable gap solitons in inhomogeneous nonlinear Schrödinger equations. *Journal of Differential Equations*, 253(4):1191–1205, 2012.

[78] R. Adami, C. Cacciapuoti, D. Finco, and D. Noja. On the structure of critical energy levels for the cubic focusing NLS on star graphs. *Journal of Physics A: Mathematical and Theoretical*, 45(19):192001, 2012.

[79] A. W. Snyder, D. J. Mitchell, L. Poladian, D. R. Rowland, and Y. Chen. Physics of nonlinear fiber couplers. *JOSA B*, 8(10):2102–2118, 1991.

[80] J. Yang. Stability analysis for pitchfork bifurcations of solitary waves in generalized nonlinear Schrödinger equations. *Physica D: Nonlinear Phenomena*, 244(1):50–67, 2013.

[81] T. Kapitula, P. G. Kevrekidis, and Z. Chen. Three is a crowd: Solitary waves in photorefractive media with three potential wells. *SIAM Journal on Applied Dynamical Systems*, 5(4):598–633, 2006.

[82] R. H. Goodman. Bifurcations of relative periodic orbits in NLS/GP with a triple-well potential. *Physica D: Nonlinear Phenomena*, 359:39–59, 2017.

[83] R. H. Goodman, J. L. Marzuola, and M. I. Weinstein. Self-trapping and Josephson tunneling solutions to the nonlinear Schrödinger/Gross-Pitaevskii equation. *Discrete & Continuous Dynamical Systems-A*, 35(1):225–246, 2015.

[84] R. W. D. Nickalls. A new approach to solving the cubic: Cardan's solution revealed. *The Mathematical Gazette*, 77(480):354–359, 1993.

[85] A. C. Scott and L. Macneil. Binding energy versus nonlinearity for a "small" stationary soliton. *Physics Letters A*, 98(3):87–88, 1983.

[86] D. E. Pelinovsky, P. G. Kevrekidis, and D. J. Frantzeskakis. Stability of discrete solitons in nonlinear Schrödinger lattices. *Physica D: Nonlinear Phenomena*, 212(1):1–19, 2005.

[87] D. E. Pelinovsky and P. G. Kevrekidis. Stability of discrete dark solitons in nonlinear Schrödinger lattices. *Journal of Physics A: Mathematical and Theoretical*, 41(18):185206, 2008.

[88] M. I. Weinstein. Excitation thresholds for nonlinear localized modes on lattices. *Nonlinearity*, 12(3):673, 1999.

[89] C. Chong, D. E Pelinovsky, and G. Schneider. On the validity of the variational approximation in discrete nonlinear Schrödinger equations. *Physica D: Nonlinear Phenomena*, 241(2):115–124, 2012.

[90] D. Anderson, A. Bondeson, and M. Lisak. A variational approach to perturbed soliton equations. *Physics Letters A*, 67(5-6):331–334, 1978.

[91] B. A. Malomed. Variational methods in nonlinear fiber optics and related fields. *Progress in Optics*, 43:71–194, 2002.

[92] T. Ilg, R. Tschüter, A. Junginger, J. Main, and G. Wunner. Dynamics of solitons in the one-dimensional nonlinear Schrödinger equation. *The European Physical Journal D*, 70(11):232, 2016.

[93] C. Chong and D. Pelinovsky. Variational approximations of bifurcations of asymmetric solitons in cubic-quintic nonlinear Schrödinger lattices. *Discrete & Continuous Dynamical Systems-S*, 4(5):1019–1031, 2011.

[94] B. A. Malomed and R. S. Tasgal. Vibration modes of a gap soliton in a nonlinear optical medium. *Physical Review E*, 49(6):5787, 1994.

[95] D. J. Kaup and T. I. Lakoba. Variational method: how it can generate false instabilities. *Journal of Mathematical Physics*, 37(7):3442–3462, 1996.

[96] D. J. Kaup and T. K. Vogel. Quantitative measurement of variational approximations. *Physics Letters A*, 362(4):289–297, 2007.

[97] E. T. Whittaker and G. N. Watson. *A Course of Modern Analysis*. Cambridge University Press, 1996.

[98] E. J. Heller. Time-dependent approach to semiclassical dynamics. *The Journal of Chemical Physics*, 62(4):1544–1555, 1975.

[99] E. J. Heller. Frozen Gaussians: A very simple semiclassical approximation. *The Journal of Chemical Physics*, 75(6):2923–2931, 1981.

[100] P. S. Landa. *Regular and Chaotic Oscillations*. Springer Science & Business Media, 2001.

Appendix A

Cardan's method for solving a cubic equation

The result in this appendix is taken from paper [84]. Cardan's method is used to solve the general cubic equation. In this section, we only present explicit expressions of the results and skip the derivation. See [84] for the details. Consider the cubic equation

$$y = f(x) = ax^3 + bx^2 + cx + d, \tag{A.1}$$

and let α, β, and γ be the roots of $f(x) = 0$. Let δ, h, x_N, and y_N be parameters that are defined by $\delta^2 = \frac{b^2-3ac}{9a^2}, h = 2a\delta^3, x_N = -\frac{b}{3a}$, and $y_N = f(x_N)$. Then,

1. if $y_N^2 > h^2$, then there is only one real root α with

$$\alpha = x_N + \sqrt[3]{\frac{1}{2a}\left(-y_N + \sqrt{y_N^2 - h^2}\right)} + \sqrt[3]{\frac{1}{2a}\left(-y_N - \sqrt{y_N^2 - h^2}\right)}$$

and two complex roots

$$\beta = -\frac{\alpha}{2} + \frac{\sqrt{3}}{2}\sqrt{\alpha^2 - 4\delta^2}i,$$
$$\gamma = -\frac{\alpha}{2} - \frac{\sqrt{3}}{2}\sqrt{\alpha^2 - 4\delta^2}i.$$

2. if $y_N^2 < h^2$, there are three distinct roots,

$$\alpha = x_N + 2\delta\cos\theta,$$

$$\beta = x_N + 2\delta\cos(2\pi/3 + \theta),$$

$$\gamma = x_N + 2\delta\cos(4\pi/3 + \theta),$$

   where $\cos(3\theta) = -y_N/h$.

3. if $y_N^2 = h^2$, there are 3 real roots (two or three equal roots), $\alpha = \beta = x_N + \delta$, and $\gamma = x_N - 2\delta$. If $y_N = h = 0$, then $\delta = \sqrt[3]{y_N/(2a)} = 0$ and there are three equal roots.

Appendix B

Duffing equation

Here, we present a method to solve the time independent NLS equation (2.5). Such an equation, when x is considered as time, is known as Duffing equation (See [100] for details).

$$\psi_{xx} + a\psi + b\psi^3 = 0, \tag{B.1}$$

This second order linear ordinary differential equation describes natural oscillations of an oscillator. The sign of a and b determines the type of oscillation. Equation (B.1) can be written as first order ODEs by setting $u = \psi$, $y = \psi_x$,

$$\begin{aligned} u_x &= y, \\ y_x &= -au - bu^3. \end{aligned} \tag{B.2}$$

The trajectories or the vector field in the phase plane are obtained from

$$\frac{dy}{du} = \frac{y_x}{u_x} = \frac{-au - bu^3}{y}. \tag{B.3}$$

So, we have that the equation of the phase trajectories is

$$y^2 + au^2 + \frac{1}{2}bu^4 = E. \tag{B.4}$$

Solving (B.4) for y gives

$$y = \pm\sqrt{E - au^2 - \frac{1}{2}bu^4}$$

or

$$x = \int \frac{1}{\pm\sqrt{E - au^2 - \frac{1}{2}bu^4}}\,du.$$

This is an elliptic integral of the first kind.

B.1 Case $a, b > 0$

The system has an equilibrium point, $u = 0$ of centre type. The trajectories (B.4) are closed as shown in Figure B.1a. The explicit solution of (B.1) can be written as Jacobi elliptic cosine

$$u(x) = A\,\mathrm{cn}(\omega x, k), \tag{B.5}$$

where A is the oscillations amplitude, $\omega = \sqrt{a + bA^2} = 4\mathbf{K}(k)/T$, T is the oscillations period, $\mathbf{K}(k)$ is the full elliptic integral of the first kind, $k = \sqrt{b/2}A/\omega$ is the modulus of the Jacobi ellliptic function.

B.2 Case $a > 0, b < 0$

In this case, there are three equilibrium points, namely $u = 0$ which is of center type and $u = \pm\sqrt{a/|b|}$ which are saddle nodes. The phase trajectories are closed for $E < \frac{a^2}{2|b|}$ and nonclosed for $E > \frac{a^2}{2|b|}$. For $E = \frac{a^2}{2|b|}$, the orbit is connecting the saddle points and called heteroclinic orbit, which corresponds to solution $u(x) = \pm\sqrt{a/|b|}\tanh(\sqrt{a/2}x)$.

The explicit expression of the general solution of (B.1) is in terms of Jacobi elliptic sine

$$u(x) = A\,\mathrm{sn}(\omega x, k), \tag{B.6}$$

where $\omega = \sqrt{a - |b|A^2/2}$, and $k = \sqrt{|b|/2}A/\omega$. The solution (B.6) is valid for $k \leq 1$.

B.3 Case $a < 0, b > 0$

For $E \in \left(\frac{-a^2}{2b}, 0\right)$, there are two closed orbits in the phase plane, each enclosing one of the equilibrium points $u = \sqrt{|a|/b}$ and $u = -\sqrt{|a|/b}$. The points enclosed are of center type. Another equilibrium point, $u = 0$ is a saddle node and the orbit that passes through the origin is called homoclinic and corresponds to $E = 0$. For $E > 0$, the trajectories are closed and surround the homoclinic orbits.

The explicit solution of (B.1) can be written as

$$u(x) = \begin{cases} \pm A\,\mathrm{dn}(\omega_1 x, k_1) & \text{for} \quad \frac{-a^2}{2b} < E < 0, \\ A\,\mathrm{cn}\,(\omega_2 x, k_2) & \text{for} \quad E > 0, \end{cases} \tag{B.7}$$

where $\omega_1 = \sqrt{b/2}A$, $\omega_2 = \sqrt{bA^2 - |a|}$, $k_1 = \omega_2/\omega_1$, $k_2 = \omega_1^2/\omega_2^2$. Note that for $E = 0$, the solution is the homoclinic orbit, $u(x) = \pm\sqrt{2|a|/b}\,\mathrm{sech}(\sqrt{|a|}x)$.

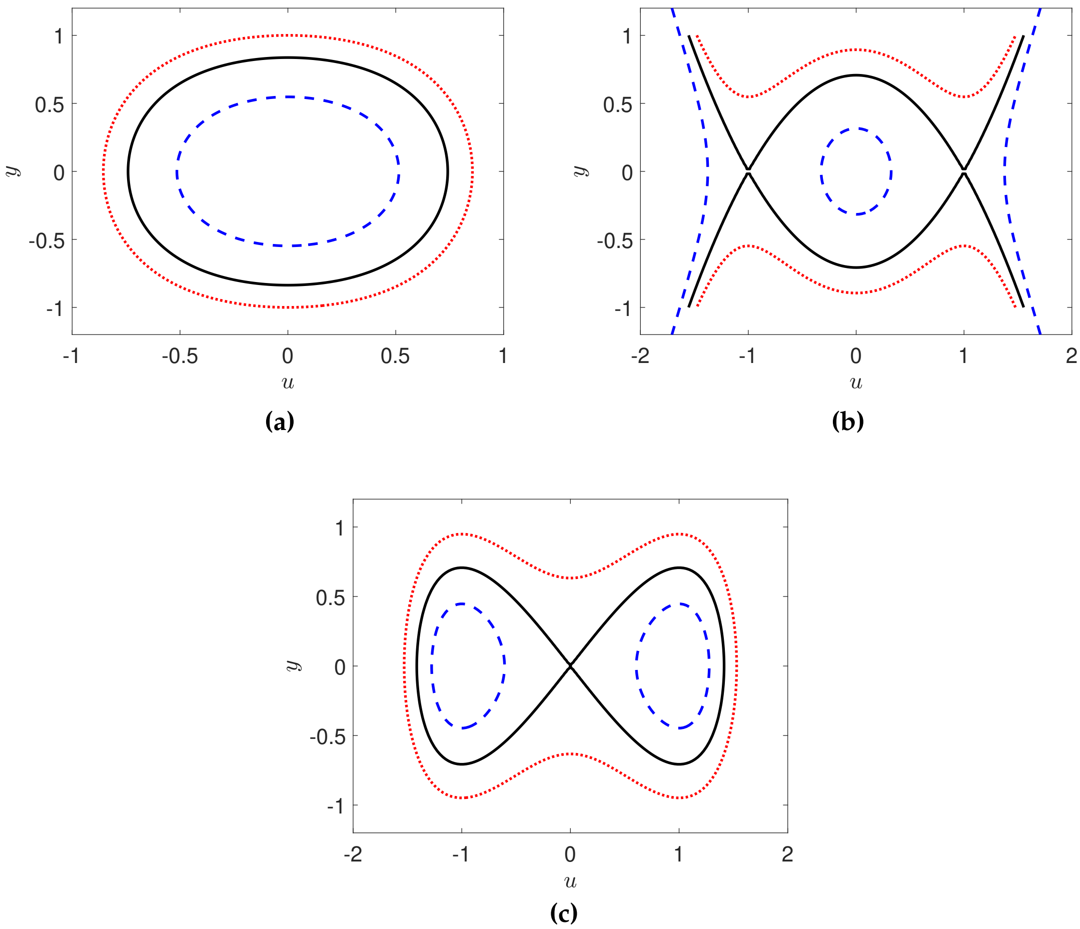

Figure B.1. Orbit of (B.1) for (a) $a = 1, b = 1$, (b) $a = 1, b = -1$, and (c) $a = -1, b = 1$. Blue dashed, black solid and red dotted lines correspond to orbit with (a) $E = 0.3, 0.7$, and $E = 1$, (b) $E = 0.1, 0.5$, and $E = 0.8$, (c) $E = -0.3, 0$, and $E = 0.4$, respectively.